

國立交通大學  
電機與控制工程學系  
博士論文

禪坐之腦部非線性動態研究  
Towards the Brain Dynamics under Chan  
Meditation Based on EEG Nonlinear  
Analysis



研究生：黃瑄詠

指導教授：羅佩禎 博士

中華民國九十七年十一月

禪坐之腦部非線性動態研究

Towards the Brain Dynamics under Chan Meditation Based on  
EEG Nonlinear Analysis

研究生：黃瑄詠  
指導教授：羅佩禎

Student : Hsuan-Yung Huang  
Advisor : Pei-Chen Lo

國立交通大學

電機與控制工程學系



A Dissertation

Submitted to Department of Electrical and Control Engineering  
College of Electrical and Computer Engineering  
National Chiao Tung University  
In Partial Fulfillment of the Requirements  
For the Degree of  
Doctor of Philosophy  
in  
Electrical and Control Engineering  
November 2008  
Hsinchu, Taiwan, Republic of China

中華民國九十七年十一月

# 禪坐之腦部非線性動態研究

研究生：黃瑄詠

指導教授：羅佩禎 博士

國立交通大學 電機與控制工程研究所

## 摘要

儘管禪定帶給人類多方面身心的益處，然而相關的電生理研究卻非常的少。本篇論文以非線性動態系統的觀點，研究禪坐對於中樞神經系統的影響。主要研究的主题是禪定腦電波訊號，同時輔以另類互補醫學儀器-ARDK 的測量。ARDK 量測方便，因此可以就禪坐對身體健康的影響提供一個大致的輪廓。實驗結果顯示禪坐的確可以全面促進健康狀況，尤其是在”身體能量”以及”筋骨系統”等指數。由這些結果可推論出禪坐對身體健康有長期的影響與助益。

在禪定對腦電波的影響方面，我們基於非線性動態理論發展了兩個分析參數：平均複雜度指標( $\bar{\delta}$ )以及相似度指標( $S$ )。此外，也使用傳統的線性參數：頻譜分析及相關性分析，來量化禪坐對於腦電波的影響以作為比較。我們首先分析實驗組禪定以及控制組在閉眼放鬆休息狀態，其長時間腦電波的劇本變化。藉由快數演算法，連續 $\bar{\delta}$ 可以反映出腦部隨著不同的意識狀態之變化。結果顯示在深度禪定時，腦部動態系統呈現較高的複雜度指標。另外透過連續 $\bar{\delta}$ ，禪坐過程中的三種不同的階段特性也得以顯示出來。

由初步的研究結果得知，資深的禪定者比起初修者較容易進入深定，禪定品質較好，伴隨有更顯著的身心變化。因此我們接著選取了 23 位資深的禪定者，與 23 位無禪定經驗者做進一步的研究。我們分別對於實驗組(禪坐)與控制組(閉眼放鬆)錄製 40 分鐘的腦電波，並選取在禪坐(放鬆)的前中後各 5 分鐘的錄製結果做 $\bar{\delta}$ 以及頻譜分析。我們的實驗結果顯示，在禪坐的過程中前腦的 alpha-1

(8-10Hz)以及後腦的 beta 成分的振幅較控制組增加，而閉眼放鬆的控制組則是 theta 增加。至於腦部動態參數 $\bar{\delta}$ 則與 beta 有高度相關，也隨著禪坐過程而增加；至於控制組的 $\bar{\delta}$ 則無顯著的變化。對照禪定者的口述推測：深定狀態時伴隨著內在光的出現，此時 beta 成分會增加，這種現象可以被 $\bar{\delta}$ 參數有效的反映出來。我們的結果證實，長期禪定訓練的確可以使禪定者在禪定時引發大腦皮質層的電訊號變化。

本論文接著以非線性多變數分析，探討禪坐時腦電波之空間交互作用的特性。我們以相似數指標(S)量化不同錄製點間的非對稱交互影響的強度。對於 12 位資深禪定者分別錄製閉眼放鬆(R)、40 分鐘的禪定實(M)、以及 5 分鐘的守禪心輪(Z)的腦電波。在多數大腦區域，禪坐者整體上在 M 及 Z 狀態都呈現比 R 狀態較強的交互影響。而這種強化的趨勢尤以處於意識放空又覺知的 M 狀態更為顯著。至於在高頻的交互影響方面 (>13Hz)，整體而言，兩種禪坐狀態都較閉眼放鬆有較強的耦合效果。然而，這種增強的交互影響尤以處於內觀而精神統一的 Z 狀態更為顯著，並以後腦最為顯著。此外在 Z 狀態只有很少數對的電極彼此的相互影響是非對等的。這種強度相仿的結果顯示，在禪定時不同部位的大腦皮質彼此密集的交互作用及增強的相互影響，此特徵尤其以高頻的 Z 狀態最為顯著。我們的實驗結果證實了隨著不同的禪定階段，引起不同的大腦動態變化，這種現象可以以非線性指標得到良好的量化結果。

# Towards the Brain Dynamics under Chan Meditation Based on EEG Nonlinear Analysis

Student : Hsuan-Yung Huang

Advisor : Dr. Pei-Chen Lo

Institute of Electrical and Control Engineering  
National Chiao Tung University

## Abstract

Orthodox Chan-Buddhist meditation brings multiform benefits to human beings but little has yet been disclosed regarding the electrophysiological characteristics of the CNS. This dissertation reports the effects of Chan meditation on CNS electrophysiological behaviors in the aspect of nonlinear brain dynamics. This work was mainly focused on the meditation electroencephalogram (EEG) signals, with the reference of a CAM instrument, ARDK. The ARDK measure might provide a feasible index for the effects of Chan meditation on the health. The results showed that Chan meditation could lead a better performance in the overall Health Condition Ratio especially in Body Energy and Musculoskeletal System. The observation allows us to infer that Chan meditation may cause a long-term effect on the practitioner to have a better health condition.

Based on the nonlinear dynamical modeling, this study developed two analyzing schemes, the averaged complexity index ( $\bar{\delta}$ ) and the similarity index ( $S$ ), to investigate the effects and phenomena of meditation EEGs. In addition, the popular power spectral analysis and coherence evaluation were applied to meditation EEGs for comparison. EEG investigation started with the exploration of long-time records

for both experimental (n=17) and control groups (n=16) to obtain the meditation EEG schema. Using an efficient algorithm of averaged complexity index, running  $\bar{\delta}$  measures may reflect how the brain dynamics switches between various states of consciousness. The results showed that brain dynamics exhibited high  $\bar{\delta}$  in deep meditation. Three different meditation scenarios have been identified from the running  $\bar{\delta}$  chart.

According to the preliminary findings of meditation scenarios, our study accordingly investigated the experienced Chan-meditation practitioners because, compared with novices, advanced practitioners might experience different physiological, cognitive, and psychological states and traits. Changes in the EEG characteristics in experienced Chan-Meditation practitioners (n = 23) during 40-minute of meditation were compared with those in the matched controls (n = 23) taking a rest for 40 minutes.  $\bar{\delta}$  evaluation and spectral analysis were measured in three intervals, the first-, mid- and the last-5min sessions of Chan meditation or relaxing rest, each lasting for 5 minutes. Significant increase in frontal alpha-1 (8-10Hz) and occipital beta power was found during meditation as compared with the EEG under the rest, whereas an average increase of theta power was observed in the controls. In meditation, brain dynamics exhibited high  $\bar{\delta}$  which correlated with more beta activity. Control subjects showed no significant change in  $\bar{\delta}$  level. Deeper meditation state has been reported as implications of increased beta power which might probably correlate with a particular state of consciousness involving the inner-light perception. This can be more prominent by the approach of  $\bar{\delta}$  estimation. Our results substantiate that long-term training with Chan-meditation does induce changes in the electro-cortical activity of the brain that are distinguishable from those observed for normal relaxation.

This dissertation further presents our study on the brain interactions of experienced Chan-meditation practitioners ( $n = 12$ ) varying with the meditation stages based on the nonlinear multivariate analysis. This method of similarity index ( $S$ ) was used to measure the degree of possibly asymmetric coupling among multi-recording sites. Brain interactions were compared among three phases - 40-minute meditation (M), 5-minute Chakra-focusing practice (Z) and rest with closed eyes (R). Meditators exhibited, overall, stronger interactions among multiple cortical areas in meditation stages M and Z than in the R state. This enhancement was greater in the M stage when the meditator was accompanied by a thought-free and fully consciousness state. In the high-frequency band ( $>13\text{Hz}$ ), the overall interdependence was also higher in both meditation stages than at baseline rest. However, the interaction strength, especially in the posterior regions, was greatest in the Z stage, which involved internal attention. Few electrode pairs were observed with significant pair-wise asymmetry in the Z state. The similarity is a possible characteristic of dense reciprocal and strong mutual interactions between multiple cortical areas during meditation - especially in the Z state in the high-frequency band. Results of this study demonstrate that profound Chan meditation induces various dynamic states in different phases of meditation, possibly reflected by nonlinear interdependence measure.

## 誌 謝

我人生中的一個重要階段—博士學位求學期間，終於告一個段落了。

當論文口試結束的那一剎那，心中無限感恩，能完成這篇論文要感謝的人太多了！首先感謝指導教授羅佩禎老師，羅老師不管是在學術上指導我，在日常生活上老師的身教言教更令我獲益良多，她對於學術源源不絕的創意、熱情，尤其令我敬佩！也感謝老師一路以來，在我遭遇學業與人生困境的時候，在旁支持我、協助我。

感謝口試委員謝仁俊、蔡敦仁、許晉銓、林進燈、楊谷洋老師，老師們對於論文的不吝指導，讓我見識到專業的深度與廣度，令我獲益匪淺。

特別感謝博士班的剛鳴、適達、權毅與憲正；剛鳴的積極帶動是我學習的典範；最常麻煩的是適達，芝麻綠豆小事他都願意幫忙；還有權毅與憲正給予我的協助。在這條漫長的求學路上大家相互扶持，箇中的酸甜苦辣因為有你們的同行與砥礪，阻力化為助力，讓我得以順利的完成學業。

感謝實驗室的學長：勇哥、清泉、政勳，你們的指導與經驗，指引了我的研究方向。感謝實驗室前前後後的成員：致豪、仕揚、威助、致亨，小波波、進忠、啟宏、仁隆、維廷、哲賢、小逸屏、清文、政恩、昶毅、恩榮、小胖胖、Bono、宏彥，有你們的歡樂與活力，讓我們的實驗室充滿了歡笑與光彩。

感謝室友欣瑩這幾年來的互勉與照顧，也感謝禪宗佛教會師姐師兄一路同行，更感恩 師父開啟了我的視野，照亮我的生命。禪的世界浩瀚無邊，非常禪愧只能用我極淺薄的知識試圖研究它，感恩有這樣的機會完成我博士學位的心願。

最重要的是，感謝我的父母及妹妹們，父母總是在我身旁默默的支持，妹妹們讓我在經濟、家庭上無後顧之憂，我才能自由自在的投入這條研究的道路；謝謝你們無怨無悔的付出與耐心的等待，對我無限的疼愛與包容，只有以我微薄的智慧與能力回報你們，我永遠愛你們。

要感謝的人太多，千言萬語，只有感恩再感恩！



# Contents

摘要	i
Abstract	iii
致謝	vi
Contents	vii
List of Tables	x
List of Figures	xi
Chapter I INTRODUCTION	1
I-1 Backgrounds	1
I-2 Introduction of Chan-Buddhist Meditation	3
I-3 Introduction of Nonlinear EEG Analysis	5
I-4 Aims of This Work	8
Chapter II EVALUATION OF CHAN MEDITATION BASED ON TCM PRINCIPLE	12
II-1 Introduction of Meridian Energy: ARDK Estimation	13
II-2 Methods and Materials	18
II-3 Results	19
II-4 Discussion	25
Chapter III MATERIALS and SUBJECTS	28
III -1 Introduction of EEG	28
III -2 Spatiotemporal Characteristics of Chan Meditation EEG	31
III -2-1 Subjects	31
III -2-2 Procedures and materials	32
III -3 Synchronization in Different Meditating Phases	33

III -3-1 Subjects -----	33
III -3-2 Procedures and materials -----	34
Chapter IV METHODS -----	35
IV-1 EEG Investigation Based on Nonlinear Time Series Analyses -----	36
IV-2 Embedding: Reconstruction of System Dynamics from Observations-----	40
IV-3 Univariate Analysis: Complexity Index -----	42
III -3-1 Definition and estimation -----	43
III -3-2 Efficient method for estimation-----	43
III -3-3 Applications to meditation EEG-----	44
IV-4 Multivariate Analysis: Nonlinear Interdependence Measure -----	45
IV-4-1 Definition and estimation -----	45
IV-4-2 Asymmetric property of interdependence measure -----	47
IV-4-3 Applications to meditation EEG -----	48
IV-5 EEG Investigation Based on Spectral Power Analysis and Coherence Function Analysis -----	49
IV-5-1 Estimation of spectral power -----	50
IV-5-2 Estimation of coherence function-----	50
IV-6 Statistical Analysis -----	53
IV-6-1 Spatiotemporal characteristics of Chan meditation EEG-----	53
IV-6-2 Synchronization in different meditating phases -----	54
Chapter V RESULTS -----	55
V-1 Spatiotemporal Characteristics of Chan Meditation EEG -----	55
V-1-1 Meditation EEG features -----	55
V-1-2 Chan Meditation EEG Scenarios -----	61
V-1-3 Spatio-temporal resolution of experienced meditators -----	66

V-2 Synchronization in Different Meditative Phases -----	72
V-2-1 Coherence function analysis -----	72
V-2-2 Interdependence measure analysis -----	77
 Chapter VI DISCUSSION and CONCLUSION-----	 87
VI-1 Spatiotemporal Characteristics of Chan Meditation EEG -----	87
VI-2 Synchronization in different meditative phases -----	92
VI-3 Conclusion -----	99
 Appendix A Complexity Index -----	 102
REFERENCES -----	104
Vita and Publication List -----	116



## List of Tables

Table 2-1 The items of Health Condition Ratio .....	17
Table 2-2 The items of System Reports .....	18
Table 2-3 Mean, standard deviation and the number of subjects whose 5 health condition parameters are within the range of normal values .....	20
Table 2-4 Mean (standard deviation) and the number of subjects whose parameters of system reports are within the range of normal values .....	24
Table 5-1 The statistical results of complexity index ( $\bar{\delta}$ ) and relative powers in different frequency bands of characteristic EEG features collected from 23 meditators (mean $\pm$ std for each group); implementing parameters applied: $n=15$ , $\tau=5$ samples, epoch length: 5 seconds (1000 samples), $20 \leq K \leq 35$ . .....	61
Table 5-2 Characteristics of EEGs and the range of more than 70% of $\bar{\delta}$ for the control group and three experimental groups .....	64
Table 5-3 ANOVA Results of Spectral Powers .....	69
Table 5-4 Regional mean coherence ( $\pm$ standard deviation) in different frequency bands for the free meditation (M), guarding Zen Chakra (Z) and the eye-closed rest (R) sessions (A: anterior; P: posterior; P-A: posterior to anterior; A-P: anterior to posterior; R-L: right to left) .....	75
Table 5-5 Regional mean $S$ ( $\pm$ standard deviation) for the M, Z and R stages (A: anterior; P: posterior; P $\rightarrow$ A: posterior to anterior; A $\rightarrow$ P: anterior to posterior; R-L: right vs left ). * $p < 0.05$ , ** $p < 0.01$ .....	84

## List of Figures

Fig. 1-1	Locations of the Zen Chakra, Dharma-Eye Chakra, and Wisdom Chakra ----4	
Fig. 2-1	The measurement probe (left) and the measurement window (right) of ARDK -----	15
Fig. 2-2	The measurement points of ARDK (The left side is analogous to the right side) -----	15
Fig. 2-3	The meridian chart shows the energy value of 24 acupoints -----	16
Fig. 2-4	The value of Body Energy (a), Musculoskeletal System (b) and Autonomic Nervous System (c) for every subject during the two states -----	21
Fig. 2-5	Mean value of the items of health condition that showed between- and within-group changes -----	22
Fig. 2-6	The mean of System reports for both groups before and after the meditation or rest. * $P < 0.05$ , ** $P < 0.01$ -----	25
Fig. 3-1	Illustration of 10-20 system: profile view (a) and top view (b). Each region has a letter to identify the lobe location (c). Note that there exists no central lobe and the "C" letter is only used for identification purposes only -----	30
Fig. 3-2	The 30-channel electrode placement-----	30
Fig. 4-1	Block diagram illustrating the entire scheme employed in this study (a) analysis of spatiotemporal characteristics (b) synchronization of different meditating phases. -----	35
Fig. 4-2	Schematic illustration of time delay embedding. A short segment of a time series is shown in (a), and its corresponding phase space trajectory shown in	

(b)----- 41

Fig. 4-3 Recording sites for ‘local’ and ‘far’ coherences (a) local anterior and posterior coherences (dotted line) (b) antero-to-posterior and postero-to-anterior directions (dotted line) ----- 53

Fig. 5-1 Meditation EEG characteristics (a) The 5-sec EEG segments demonstrate six major prototypes observed during meditation (from top downwards): flat beta, high-frequency beta, alpha, alpha-1, theta and delta activities. (b) Fourier magnitude spectra of meditation EEG prototypes in (a), with baseline and low frequency components removed. (c) The 2D phase trajectories and (d) complexity indexes ( $\delta$ ) varying with  $k$  (number of nearest neighbors) for meditation EEG prototypes in (a). Range of  $k$  (20~35) used to estimate  $\bar{\delta}$  is shown by two dashed lines ----- 56

Fig. 5-2 The dependence of  $\delta$  on values of  $K$  when analyzing the complexity index of the  $\Delta$  rhythmic activity. ----- 59

Fig. 5-3 The 25-minute running  $\bar{\delta}$  charts (channel O2) for the representatives in the control group (C1) and experimental groups (M1, M2, and M3) ----- 64

Fig. 5-4 The brain mappings of  $\bar{\delta}$  averaged over one minute for the control group C1 and the experimental groups M1, M2, and M3. The  $\bar{\delta}$  mappings for the first and the last five minutes are shown. ----- 65

Fig. 5-5 Brain mappings of  $\bar{\delta}$ ’s (leftmost column) and power spectra  $Pr()$ ’s for meditators (M, top) and control subjects (C, bottom), with EEG signals selected from the mid-5min segments of main 40min meditation/relaxation sessions---65

Fig. 5-6 Percentage of power differences between sessions derived by: (top) subtracting the first-5min  $Pr(\theta)$  from the mid-5min’s; (middle) subtracting the mid-5min  $Pr(\theta)$  from the last-5min’s and (bottom) subtracting the first-5min  $Pr(\beta)$  from the

	mid-5min's. ....	68
Fig. 5-7	The percent time during which $\bar{\delta} > 8.3$ was present within each 5-min recording period for the meditation group (M) and the control group (C)-----	71
Fig. 5-8	Differences of coherence ( $d$ -values) for meditation (M) and Zen chakra (Z) stages in compared with baseline rest (R ) .....	73
Fig. 5-9	Significant probability mapping showing the comparison between (a) M and R states and (b) Z and R states. It is evident that Z and M states showed significantly higher synchronization over multiple cortical areas as compared with baseline rest. ....	74
Fig. 5-10	Percentage of regional and far coherence change between stages-----	76
Fig. 5-11	Example for a 19x19 $S$ -matrix of a 9-year meditator recorded during Z stage. For example, the leftmost bottom pixel represents $S(\text{Fp1} \text{O2})$ .....	77
Fig. 5-12	A significant change of interdependence measure ( $P < 0.01$ or better) with respect to the baseline condition is mapped by a connection between the two electrodes of a pair, for the M state (a) and Z state (b). An arrow represents a sink site. For better visual clarity, intra- and inter-hemispheric connections are displayed separately. Solid line indicates an increase and dashed line indicates a decrease of $S$ measure. ....	78
Fig. 5-13	The overall topographic differences of $S$ ( $d$ -values) when the selected electrode was considered as a sink (left) and as a source (right) ( $d > 1.80, P < 0.05$ ). The upper row shows the differences between Z state and baseline R state and the bottom row shows the changes for the M state versus R state. ....	81
Fig. 5-14	The same expressions as Fig. 5-13 but for high frequency EEG data-----	81
Fig. 5-15	The same expressions as Fig. 5-12 but for high frequency EEG data-----	82
Fig. 5-16	Percentage of regional and far interdependence change between stages -----	84
Fig. 6-1	Topographic maps of relative power (upper row of each panel) and coherence	

(lower row) for different frequency bands during R, M and Z stages. Only 35 electrode pairs with the highest coherences were showed ----- 95





# Chapter I

## INTRODUCTION

### I-1 Backgrounds

As complementary and alternative medicine (CAM) became more appealing to the public in 1980's, researchers began taking a more serious attitude toward this oriental approach for health maintenance and promotion. In 1998, National Center for Complementary and Alternative Medicine (NCCAM), one component of the National Institutes of Health within the U.S. Department of Health and Human Services, was established for promoting scientific researches on the complementary and alternative medicine. CAM is defined as a group of diverse medical and health care systems or practices that are out of the cope of conventional medicine. According to the World Health Organization, there has already been about 65% to 80% world population relying on traditional or "alternative" medicine (Elizabeth, 2003). In the United States, 36% of adults are using some form of CAM, according to the 2002 edition of the National Center for Health Statistics' National Health Interview Survey (NHIS). Mind-body medicine, one of the five major domains of CAM, has become one of the research fields being extensively studied in medicine and clinical applications because of the growing population of users (53%) in resent years. Meditation, the main aim of this dissertation, is one of the most common mind-body interventions and is also one of the 10 most commonly used CAM therapies. (From the 2002 edition of NHIS)

For many centuries, eastern religious and secular groups, such as the Buddhists, Taoist traditionalists, and the Indian Yogis, have been practicing meditation in order to achieve certain physical, mental and spiritual ends. Meditation is a conscious mental process that induces a set of integrated physiological changes. Although diverse types of meditation

exist, most practitioners are able to experience relaxed and so-called tranquil awareness. This state has been given various descriptions such as “Satori,” “enlightenment,” “samadhi,” or “pure consciousness.”

Although individuals in the East have been practicing various forms of meditation throughout history, scientific study of meditation did not begin until it was becoming popular in the West. With the introduction of Transcendental Meditation (TM) in the late 1960's, meditation extended from a solely mystic process of spiritual quest and religious practice to a complementary effective method in several health situations in the last years. Scientific studies began with the focus of physiological alterations induced by the process (Bagchi & Wenger, 1957; Das & Gastaut, 1957; Anand *et al.*, 1961; Kasamatsu & Hirai, 1966. For reviews, see Jevning *et al.*, 1992); gradually, meditation came to deserve attentions from journals and researchers, giving place to its assessment in different indications. For several decades, scientific exploration has corroborated the effectiveness of meditation practice on the health promotion, improved cardiovascular functions and immunity, hormone-level regulation, positive emotional states, stress manipulation, anxiety reduction, depression relief, etc. (Yu *et al.*, 2003; Newell & Sanson-Fisher, 2000; Coker, 1999; MacLean *et al.*, 1997; Tooley *et al.*, 2000; Lester, 1999; Shapiro *et al.*, 1999; Aftanas & Golocheikine, 2001; Travis & Pearson, 2000).

Among many divergent methods, the research for physical and psychological correlates of meditation has centered mostly on: Yoga from India, Transcendental Meditation (TM) in the United States, and comparatively less Buddhism of Zen meditation in Japan and Tibetan Buddhism (for a review, see Cahn & Polich, 2006). Up to the present, little has yet been disclosed regarding the phenomena of Chan meditation (Kasamatsu & Hirai, 1966; Murata *et al.*, 1994). In the past decade, orthodox Chan-Buddhist meditation (or simply “Chan meditation”), as an unconventional therapy, has proved efficacious for many chronic diseases, infections, and even some malignant tumors. Consequently, more

people began to practice orthodox Chan-Buddhist meditation in Taiwan. It aroused our attention to the physiological investigation on the Chan-Buddhist disciples since 1998. New findings have been continuously observed and reported (Lo et al., 2003). This thesis is mainly devoted to the electroencephalograph (EEG) signals, of orthodox Chan-Buddhist practitioners.

## **I-2 Introduction of Chan-Buddhist Meditation**

Chan meditation originating more than 2,500 years ago has been proved to benefit the health while on the way toward the ultimate Buddhahood state (Lo *et al.*, 2003; Chang & Lo, 2005). In the preaching history of Chan-Buddhism, Buddha Shakyamuni found the eternal truth, the supreme wisdom, the noumenal energy, and the natural powers of the universe in meditation under a linden tree. The orthodox Chan Buddhism originated when Buddha Shakyamuni transmitted this light of wisdom to the Great Kashiyapa some 2,500 years ago. The same path towards perfect enlightenment (Buddhahood) was promulgated in mainland China in 527 by Bodhidharma, the 28<sup>th</sup> patriarch. The current patriarch is Chan master Wu Chueh Miao Tien (or simply “Miao Tien”), the 85<sup>th</sup> patriarch of the orthodox Chan-Buddhism Sect since the Great Kashiyapa. In orthodox Chan-Buddhist practice, very few disciples were able to catch the quintessence since it cannot be taught in any form of lectures. Written material and spoken words cannot promulgate the true message of Chan, which can only be preached by a master who has achieved the Buddhahood.

In the course of meditation, meditators experience various states of consciousness. According to their subjective narration, their mentality transcends the physiological (the fifth), mental (the sixth), subconscious (the seventh), and Alaya (the eighth) conscious state. The practice of Chan meditation itself is much more highly standardized than is a wide diversity of various Yogic meditation techniques. Chan meditation is practiced in the lotus

or half-lotus position with eye closed. Two major techniques for a beginner to get into good-quality meditation are: 1) switching the breathing habit from chest to abdominal breathing so that the breathing becomes smooth and quite, and 2) guarding some important *apertures* like the Zen Chakra (inside the third ventricle), the Wisdom Chakra (corpora quadrigemina), and the Dharma-eye Chakra (hypophysis). (refer to *Introduction of Chan Meditation*, lectured by Master Wu Chueh Miao Tien, published by Zen Cosmos, 2004). Fig. 1-1 illustrates the locations of these Chakras. Gradually, meditation releases their minds from thoughts and mental activities in both conscious and subconscious realms. The practitioners experience a state of thoughtless awareness and finally free from the interference of the subconscious. By transcending the physiological, mental, subconscious, and Alaya conscious states, the human life system is immersed in the inner energy and enters a unique status in harmony with the nature and the universe (called “the unification of heaven, earth, and human”). Through meditation, a practitioner attain the enlightened state of complete mental quiescence and subliminal consciousness tranquil.

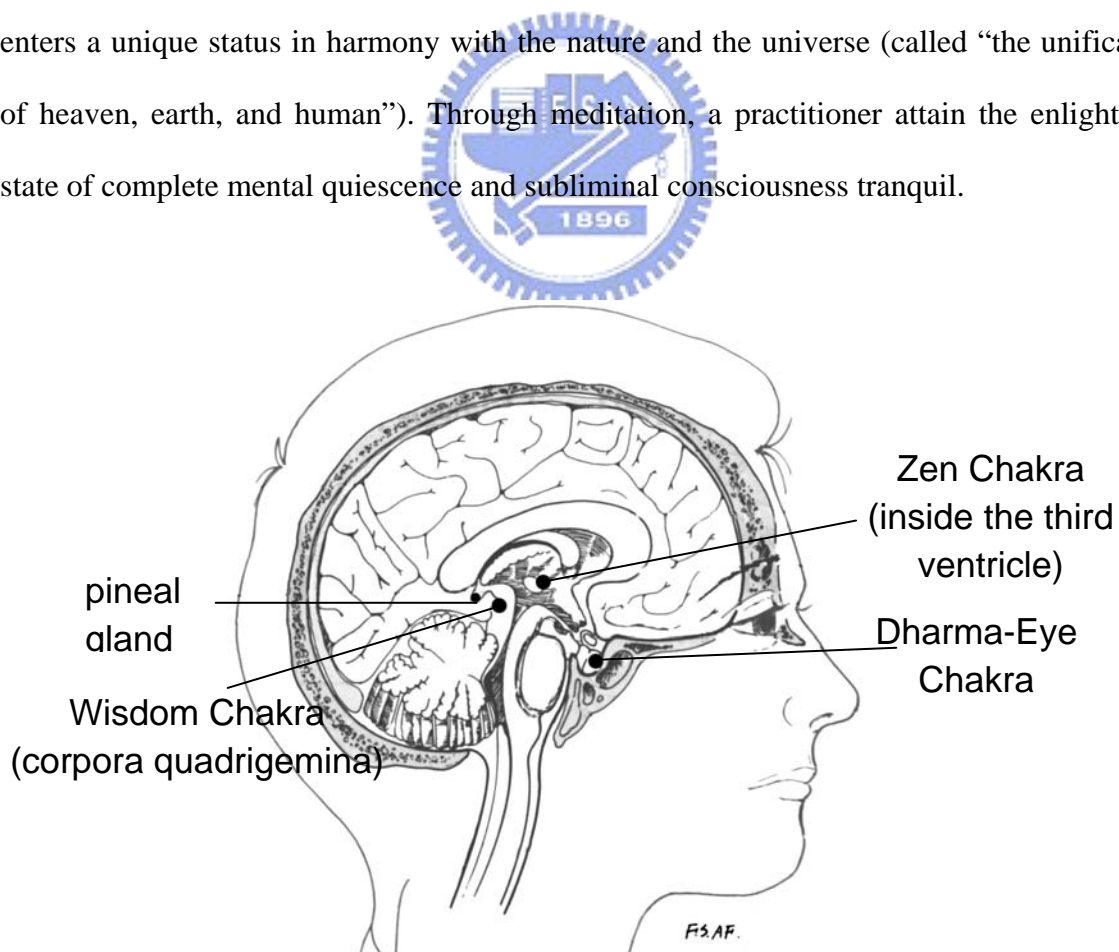


Fig. 1-1 Locations of the Zen Chakra, Dharma-Eye Chakra, and Wisdom Chakra

### **I-3 Introduction of Nonlinear EEG Analysis**

In regard to an unknown system such as the brain, researchers have developed the approaches for probing the system characteristics by analyzing its output or response recordable (e.g., Galka, 2000). As in most cases multi-channel neurophysiological signals are simultaneously recorded, univariate analysis alone cannot accomplish the assessment of the interdependence among channels. Therefore, it is necessary to make use of the multivariate analysis giving more insights into the brain dynamical mechanisms. Despite their capability of approaching specific aims, univariate and multivariate time-series analysis are mostly based on the widely-used, conventional time-domain and frequency-domain approaches (see, e.g., Bendat and Piersol, 2000). Unfortunately, these methods based on linear assumption cannot give any information about the nonlinear features of the signal.

Neurons are highly nonlinear, moreover, have been demonstrated to exhibit chaotic behavior (Matsumoto and Tsuda, 1988). Due to the intrinsic nonlinearity of neuronal activities, their integrative activities constituting the brain functions are nonlinear based on a sound hypothesis. Thus, other techniques based on the nonlinear dynamic theory have been introduced and been proved useful in EEG analysis (van Gils *et al.*, 1997). These methods have been used to quantify underlying brain dynamics and evaluate EEG spatio-temporal complexity since two decades ago (Babloyantz *et al.*, 1985; Babloyantz and Destexhe, 1986; Lo and Principe, 1989; Rapp *et al.*, 1989; Pijn *et al.*, 1991; van Putten, 2001). First encouraging results claimed that EEG signals showed chaotic structure (Babloyantz *et al.*, 1985), but further studies did not find any strong evidence of chaos in EEG (Pijn, 1990, Theiler *et al.*, 1992 and Theiler and Rapp, 1996). In the recent years, it is accepted that EEG signals are, at least in a general sense, not (low-dimensionally) chaotic (Lehnertz *et al.*, 2000). In spite of that, nonlinear chaotic measures are still used for a more

practical goal even if there is no sign of chaos. Invariant quantities from the representation of the signals in the phase space may reveal nonlinear structures which are inaccessible by standard linear approaches (Stam, 2005).

Methods for univariate nonlinear time series analysis were originally applied to neurophysiological data about two decades ago (Babloyantz et al., 1985). Most popular tools from nonlinear dynamical theory used for EEG analysis are dimensional computation. Complexity measure reflecting the dimensionality of underlying CNS dynamics provides a macroscopic view and thus the first measurand for quantifying an unknown system. Thereby, this parameter denotes the number of state variables required to describe the temporal dynamics of the EEG signal (Grassberger & Procaccia, 1983) and provides an index that has been roughly interpreted as a measure of the irregularity or complexity of EEG dynamics. A number of studies have reported the fruitful results of characterizing the dynamic behavior of the CNS (central nervous system) under various physiological or mental states (for recent surveys: Elbert et al., 1994; Korn & Faure, 2003; Segundo, 2001; Stam, 2005). It is well known that the dimensional complexity of the human EEG increases during various types of stimulation such as imagery (Schupp *et al.*, 1994) and mental activity (Rapp *et al.*, 1989; Mölle *et al.*, 1999). Many studies also investigated the relationship between “brain complexity” and different states of consciousness. For example, correlation dimension has been useful in sleep-wake research (Pereda et al., 1998; Pradhan et al., 1995) and in studies of the depth of anesthesia (van den Broek et al., 2005; Widman et al., 2000).

Although univariate nonlinear method, such as correlation dimension, furnishes important information about the CNS characteristics, they mostly suffer from the problems of indirect estimation, computational inefficiency and bias from implementing parameters (Lo and Principe, 1989; Yaylali, 1996; Lo and Chung, 2000). To deal with the problems, we introduced the method “complexity index ( $\delta$ )” (Lo and Chung, 2000; Lo and Chung, 2001)

with an efficient algorithm into long-term EEG analysis. Details of the algorithm are illustrated in Chapter IV.

In the past few years, researchers in engineering and medicine began employing several nonlinear multivariate techniques in neurophysiology. A number of studies have proposed the viewpoint of considering brain dynamics as a large ensemble of coupled nonlinear dynamical subsystems. Accordingly, significant nonlinear synchronization has been detected on the macroscopic scales of EEG channels in healthy subjects (Breakspear & Terry, 2000a, 2002b; Stam et al., 1996, 2003; Feldmann & Bhattacharya, 2004). Various types of synchronization based on nonlinear dynamical theory have been demonstrated to be the more powerful mechanism than narrow-band frequency synchronization (e.g. coherence function). Two relevant concepts are: generalized synchronization (Rulkov et al., 1995), a state in which a functional dependence between the systems exist, and phase synchronization (Rosenblum et al., 1996), a state in which the phases of the systems are correlated whereas their amplitudes may not be. In brief, these measures quantify, for a short time, the grade of predicting the state-space evolution in one system by that in the other, simultaneous system.

By analyzing the reconstructed phase space, such invariant quantities are theoretically useful in neurophysiology due to their ability to detect nonlinear interactions hidden to standard linear approaches. Nevertheless, the application of these methods to neurophysiological signals is not a plain subject. On the one hand, these signals are often noisy, non-stationary and of finite length. On the other hand, theoretical studies indicated that these indexes are not able to reveal any causal relationship among signals (Quian Quiroga et al., 2000). In this work, we go through these questions by using the modified *similarity index*, a robust set of interdependence measures (Arnhold et al., 1999; Quian Quiroga et al., 2000, 2002), for the analysis of meditation EEG. Instead of estimating predictions, similarity index quantifies how neighborhoods (i.e., recurrences) in one

attractor map into the other. This method has the advantages of sensibility to nonlinear interdependence and potential of detecting asymmetric relationships (Arnhold et al., 1999; Le van Quyen, 1998). We thus investigated the capability of this multivariate method in characterizing the nonlinear interdependence behaviors of brain dynamics under Chan meditation. Details of the algorithm are illustrated in Chapter IV.

#### **I-4 Aims of This Work**

Meditation has been used as health-enhancing techniques for centuries. Numerous studies have focused on the physiological and psychological effects of meditation, with few addressing the underlying mechanisms. Consequently, how to characterize these states of consciousness based on a scientific approach becomes a matter of significance in understanding the meditation scenario. We thus conducted a series of studies on meditation EEGs to explore the brain dynamics in the process. The meditation EEG, although it has been investigated since the 1960s, is still an open question (Anand *et al.*, 1961; Kasamatsu and Hirai, 1966; Wallace, 1970; Banquet, 1973; Williams and West, 1975; Woolfolk, 1975).

A number of papers have reported the EEG findings of subjects practicing various meditation techniques. Up to the present, little has yet been disclosed regarding the electrophysiological characteristics of the CNS under a particular state of consciousness—orthodox Chan-Buddhist meditation. In the course of Chan meditation, meditators experience various states of consciousness. Characterization of the EEG activities in different Chan meditation states may help explore neuronal network and CNS properties involved in such “beyond-consciousness” states. One important goal of our research is to assess the nature of the system’s dynamics and its distinctive changes when brain waves make transitions between several states during the meditating process.

This dissertation was mainly focused on the Chan-meditation EEG signals, with the



reference of a CAM instrument, ARDK. The ARDK measure might provide a feasible index for the effects of Chan meditation on the health. The meditation EEG analysis, on the other hand, explored possible meditation scenarios and spatial-temporal characteristics of brain dynamics revealing as electrical potential changes that correlated with different Chan meditation states.

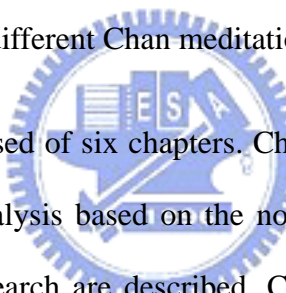
To reliably estimate the nonlinear dynamic characteristics, intensive work is normally required for obtaining appropriate implementing parameters. The dissertation reports an alternative way of efficiently determining the parameters. Based on the nonlinear dynamical modeling of brain function, this study has developed two analyzing schemes, the averaged complexity index ( $\bar{\delta}$ ) and the similarity index ( $S$ ), to investigate the effects and phenomena of meditation EEGs. In addition, the popular power spectral analysis and coherence evaluation were applied to meditation EEGs for comparison.

We started with the exploration of long-time meditating EEG records to obtain the meditation EEG schema. We use an efficient algorithm of averaged complexity index (Lo & Chung, 2000, 2001) that is feasible for long-term monitoring. Running  $\bar{\delta}$  measures may reflect how the brain dynamics switches between various states of consciousness. Consequently, this study brings forth the time evolution of the meditating EEG scenarios.

According to the preliminary findings of meditation scenarios, we speculated that the deep meditation state was accompanied by an increase of beta activity which correlated positively with complexity. Our study accordingly employed complexity measures as well as spectral analysis in the Chan-meditation EEG analysis of spatial-temporal characteristics. Here, we mainly investigated the experienced Chan-meditation practitioners because, compared with novices, advanced practitioners might experience different physiological, cognitive, and psychological states and traits.

Since the interaction between separate brain regions is neurophysiologically very

significant and appealing, measurement of the interdependence plays an important role in meditation EEGs. While the predominant EEG findings have indicated an increase of alpha–theta range coherence during meditation (e.g. Travis & Wallace, 1999; Dillbeck & Bronson, 1981; Orme-Johnson & Haynes, 1981), relative little is known about the nonlinear synchronization of EEG evolved with the meditation process. This dissertation further presents our study of the brain interactions varying with the meditation stages based on the nonlinear multivariate analysis. This method of “similarity index” allows the study of nonlinear interdependence among multi-recording sites and represents an alternative to the coherence function. Besides doing a 40-min Chan meditation, each practitioner was also asked to do an additional guarding Zen Chakra practice. This dissertation in the end presents our further study in characterizing the nonlinear interdependence behaviors of multichannel scalp EEG under different Chan meditation stages.



This dissertation is composed of six chapters. Chapter I introduces the background of meditation studies and data analysis based on the nonlinear dynamic theory. In addition, motivation and aim of this research are described. Chapter II reports the results and our findings from ARDK device. The statistical results of comparison between experimental subjects (meditation practitioners) and controls are presented at the end of the chapter. Chapter III is focused on the experimental setup. The beginning of this chapter discusses the experimental procedure of long-time EEG monitoring. Profiles of Chan-meditation EEG under different meditating stages are then introduced. One of the aims in this study was to explore the meditation effects on brain synchronization. Details of the signal processing methods for evaluating brain synchronization are illustrated in Chapter IV. Chapter V presents the profile of meditation EEG based on the analyses of complexity index and similarity index. The characteristic patterns of meditation EEGs will be presented with their corresponding trajectories and  $\delta$ 's. In addition, various scenarios will be explored using running  $\delta$  analysis. Degrees of interdependence varying with meditation stages are

conducted. Finally, the inter-session and inter-group differences are justified by statistical analysis. The last chapter summarizes the results of this research work and discusses possible mechanisms correlated with the findings.



## **Chapter II**

# **EVALUATION OF CHAN MEDITATION BASED ON TCM**

## **PRINCIPLE**

As complementary and alternative medicine (CAM) became more appealing to the general public, researchers began taking a more serious attitude toward such empirical approaches for health maintenance and promotion developed in different cultures. Due to the therapeutic effectiveness and its holistic theorem, a number of CAM-related instruments have been devised and employed not only for medicine research but also for clinical applications. They are easily implemented and have been declared to be able to provide indexes reflecting the emotional, mental and physical health. Consequently, CAM instruments may offer an alternative to study the underlying mechanisms and activities during meditation that have not been disclosed by conventional instruments.

Energy medicine is a domain in CAM that deals with two types of energy field, physical-energy and putative-energy fields. Energy-medicine researchers propose that energy fields (also called biofields) surround and flow throughout the living beings that have not been measured by conventional instruments (Russek & Schwartz, 1996; Oschman, 2000; Hintz et al, 2003). Illness then results from disturbances of the subtle energies and imbalances in the vital energy field of the body. This vital energy or life force is known under different names in different cultures, such as qi in Traditional Chinese Medicine (TCM). Therapies involving energy fields such as meditation, acupuncture and qi gong (Sancier & Holman, 2004) accordingly treat the diseases by restoring the yin-yang balance and the flow of qi.

In this chapter, we investigate, from the viewpoint of energy medicine, phenomena of the human life system under the orthodox Chan meditation practice. Besides those derived

from conventional medical instruments (EEG, ECG, GSR etc.), we aim to employ the CAM instruments- ARDK to study the biofield characteristics of Chan meditation practitioners to gain more insight into the underlying mechanism.

## **II-1 Introduction of Meridian Energy: ARDK Estimation**

### *Ryodoraku theory*

The Ryodoraku theory was developed by a research group lead by Dr. Yoshio Nakatani in Japan since 1949 to 1957. They fed a current into some specific acupoints and measured the electrical value reflected to investigate the meridian electrical properties corresponding to these acupoints. Meridian points are the key to all acupuncture practice. Meridian points can be deemed as the window to a body's inner activities because they reflect the system's current functionality. They found that the measured electrical value of these acupoints on the skin will reflect the health condition which matches the TCM theory saying “disease is reflected by the twelve source acupoints”.

### *Instrument–ARDK*

ARDK (Automatic Reflective Diagnosis System) is a meridian diagnosis system developed on the basis of integrating Ryodoraku theory, Chinese Meridian theory, Russian space research, western clinic symptoms data and statistical analysis. It was developed by the Russian Central Scientific Research Institute during the period of 1978 - 1992. This method has been tested on several thousand trials in clinical studies of which the ARDK data have been analyzed and validated. Based on the large pool of >100,000 clinical subjects in Russia and >5,000 clinical subjects in Taiwan, ARDK measurement attains an accuracy rate up to 90% now. ARDK as a fast, accurate and reliable diagnostic medium is proven to be helpful in detecting some factors that indicate the risk of disease before it

becomes symptomatic.

### *Recording and analyzing*

The ARDK sensor gets data through skin point electrical conduction (Fig. 2-1). By applying the probe to a single representative point of a meridian, the ARDK measures each meridian's activity level. After measuring all 24 points (12 left meridians + 12 right meridians (Fig. 2-2)), the computer program will categorize these values by using statistical methods. The subject's meridian energy data is collected safely because the maximum detecting current fed into subject's body by ARDK during measurement is  $200\mu\text{A}$ , which is much lower than a person can feel. The measurement of one diagnostic point takes less than 5 seconds and the entire measurement process will only take about 5 minutes to complete. Numerical values of the test vary depending on the physical fitness physiological status of the subject. The device then shows the results on the computer screen. The results we will use for further analysis are as follows:



Fig. 2-1 The measurement probe (left) and the measurement window (right) of ARDK

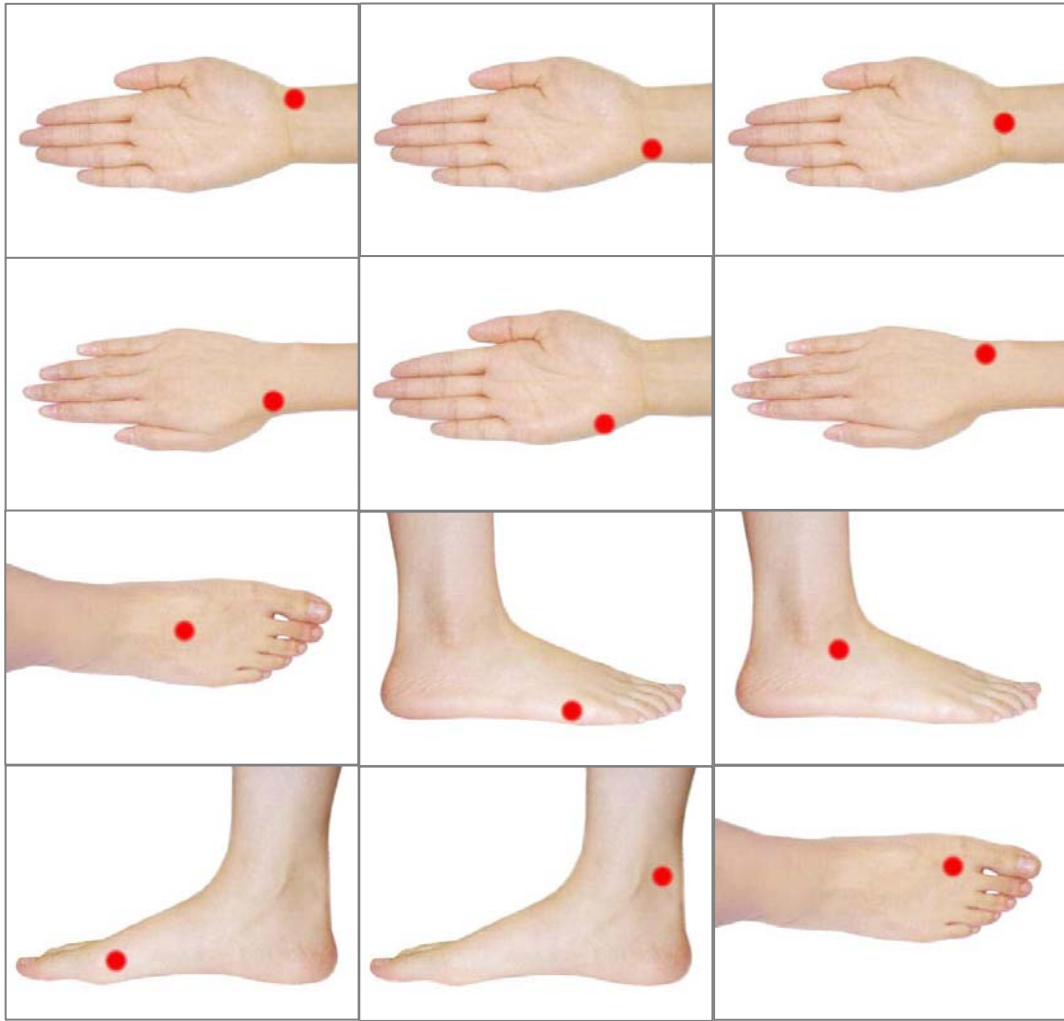


Fig. 2-2 The measurement points of ARDK. (The left side is analogous to the right side)

### (1) Meridian Chart

In the Meridian Chart (Fig. 2-3), the horizontal axis denotes the 24 different meridians and the vertical axis denotes the activity level of meridians. Each symbol “+” in this chart represents one meridian. There are three different colors of horizontal dash lines on this chart. The black dash line represents the mean value for total 24 meridians, the green dash lines represent the upper and lower bound for “Best” value and the red dash lines represent the upper and lower bound for “Good” value. The value outside the red dash lines denote “too High energy” or “too Low energy” condition.

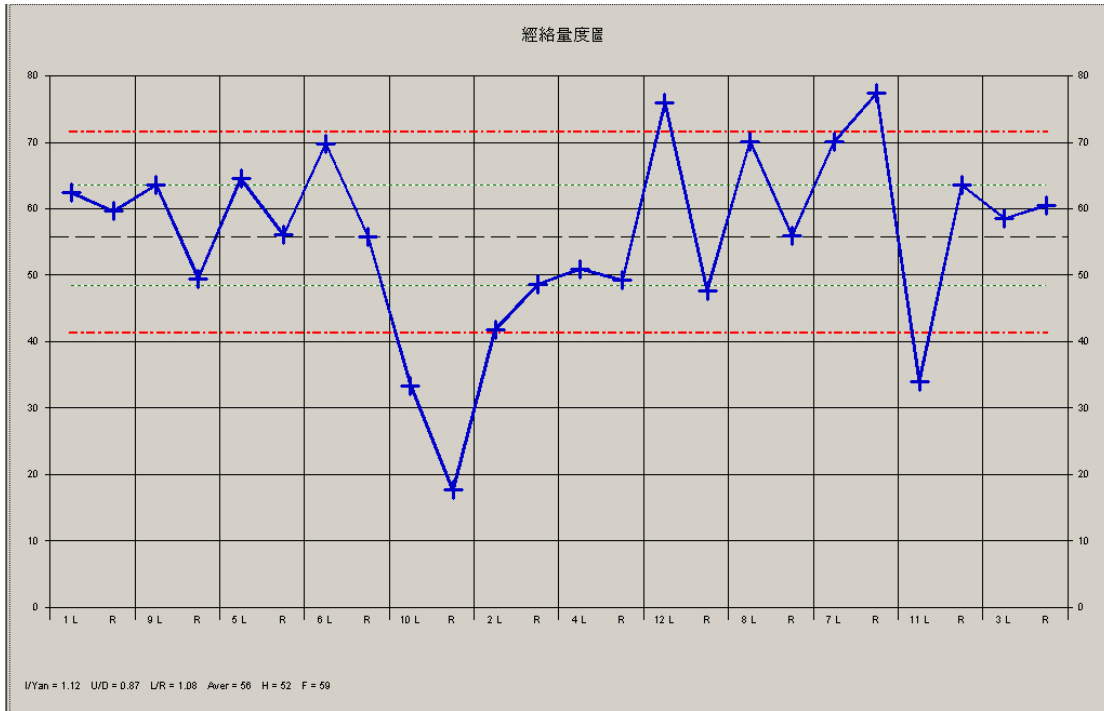


Fig. 2-3 The meridian chart shows the energy value of 24 acupoints

(2) Health Condition Ratio



It was discovered that there were certain relationships among the 24 acupoints. The ratio between acupoints correlates different health condition. When there is an illness, the ratio will be abnormal. Table 2-1 shows 5 health condition parameters and their range of normal values.

Table 2-1 The items of Health Condition Ratio

Item	Health Condition Ratio	Normal
Body Energy	The average of the 24 acupoints. A high average indicates excess Qi and Blood while a low average indicates a deficiency of Qi and Blood.	$25 \leq \text{Value} \leq 55$
Metabolism Function	The ratio of the total of all Yin meridians divided by the total of all Yang meridians. A high ratio shows that the metabolism of the body is slower than normal while a low ratio shows that the metabolism of the body is faster than normal.	$0.8 \leq \text{Ratio} \leq 1.2$



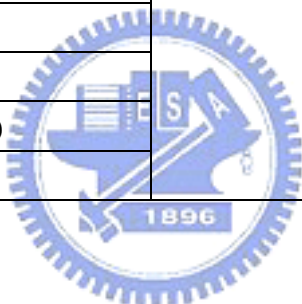
Mental State	The ratio of the total of all hands meridians divided by the total of all feet meridians. A high ratio indicates an increase in mental activities and the subject has higher mental stress with anxiety, anger and halitosis. A low ratio indicates a decrease in mental activities, the subject gets drowsy, their attention is not focused, their memory is poor, and their response time slows down, etc.	$0.8 \leq \text{Ratio} \leq 1.2$
Musculoskeletal System	The ratio of the total of all left meridians divided by the total of all right meridians. The degree of balance between the Qi and Blood in the right side and left side of body affects the function of the musculoskeletal system. When the musculoskeletal system is unbalanced, there will be obstacles. The subject will feel pain or soreness in his body.	$0.8 \leq \text{Ratio} \leq 1.2$
Autonomic Nervous System	The balance condition of the autonomic nervous system. The higher the ratio the more unbalance the autonomic nervous systems is. There are many factors that may result in an imbalance in the autonomic nervous system. Generally, this is divided into internal causes (e.g. diseases of the internal organs, endocrine disorders) and external factors (e.g. mental stresses, pressure from work, and fatigue). Based on TCM theory, this results from an imbalance of Qi and Blood in part or all of the body. An abnormality of the subject's autonomic nerves possibly results in difficulty sleeping or pain.	$\text{Ratio} \leq 2$

### (3) System Reports

System Reports shows the condition of overall human body systems. Table 2-2 shows the 16 items of System Reports and their standard range of values. The unit of each item is percentage, the higher the value the higher the probability to get problems in that system. The last item "System Reports (SR)" is the rough value representing the overall items.

Table 2-2 The items of System Reports

Item	Standard
Body energy (BE)	Value $\leq 25\%$ : Normal $\rightarrow$ Best Value $\leq 50\%$ : Normal $\rightarrow$ Good $50 < \text{Value} \leq 75\%$ : Abnormal $\rightarrow$ Not bad Value $> 75\%$ : Subhealth(not feel good but haven't been sick) $\rightarrow$ Caution
Mental state (MS)	
Autonomic Nervous System (ANS)	
Thyroid Gland Function (TGF)	
Musculoskeletal System (MS)	
Liver Function (LS)	
Digestive System (DS)	
Respiratory System (RS)	
Endocrine System (ES)	
Immune System (IS)	
Cardiovascular System(CS)	
Reproductive System(Rp)	
Kidney Function(KF)	
Urinary System(US)	
Metabolism Function(MF)	
System reports(SR)	



## II-2 Methods and Materials

### *Subjects and Procedure*

The experimental group included 18 Chan-meditation practitioners (13 males and 5 females; mean age  $27.3 \pm 3.56$  years) who had been regularly practicing Chan meditation for an average of 6.6 years (ranging from 3 to 12 years) in Taiwan Chan Buddhist Association. 17 control subjects (16 males and 1 females; mean age  $26.3 \pm 5.21$  years) had no experience of meditation. Experimental subjects took a 30-minute meditation, sitting in the full-lotus or half-lotus position with eyes closed. Control subjects were asked to relax their mind and body with eyes closed as possible as one can for 30 minutes. Before and after the 30-minute

meditation or rest, each subject's meridian energy data was collected by ARDK.

### *Statistical analysis*

Four sets of data were generated: (1) experimental subjects before meditation (M1) and (2) experimental subjects after 30 min of meditation (M2); also (3) Control group before eye-closed rest (C1) and (4) Control group after 30 min of rest (C2). Data M1 and C1 were baseline state to see if the passing of time under these conditions would create changes of the meridian energy.

In the first stage of statistical analysis we performed multiple paired Student's *t*-tests on the difference of Health Condition Ratios and System Reports between the two periods- before and after meditation practice in the experimental subjects and before and after rest in the control subjects. For comparison between groups (M1 vs C1, M2 vs C2), we used unpaired *t*-tests for pre and post recording. Only significant effects ( $P < 0.05$ ) involving factors are reported below.



## **II-3 Results**

### *Health Condition Ratio*

Table 2-3 shows the number of subjects whose 5 health condition parameters are within the range of normal values. More meditators exhibited a better performance in the overall Health Condition Ratio as compared with control subject for both pre and post recording, especially in Body Energy and Musculoskeletal System.

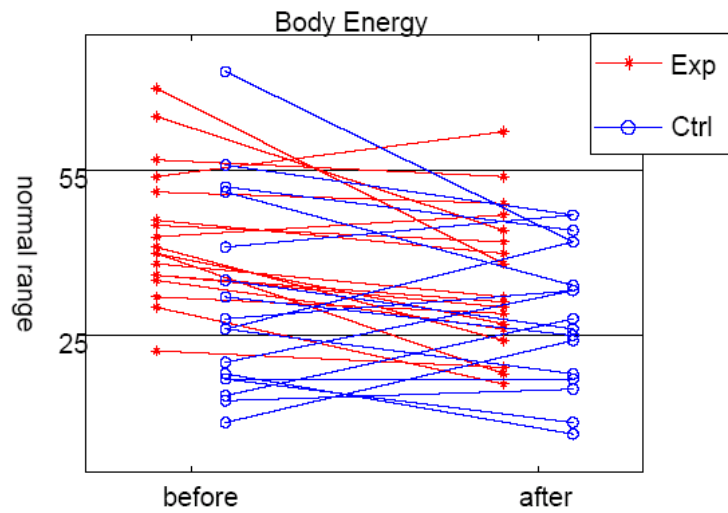
As showed in Fig. 2-4, the experimental subjects had a decreased value in the factors Body Energy ( $P < 0.01$ ) and Musculoskeletal System ( $P < 0.05$ ) after meditation while the control subjects have no such tendency. On the other hand, the ratio of Autonomic Nervous System increased progressively after meditation ( $P < 0.05$ ) while the effects of rest were not

consistent for the control subjects. The average of the items of health condition that showed significant between- and within-group change was displayed Fig. 2-5.

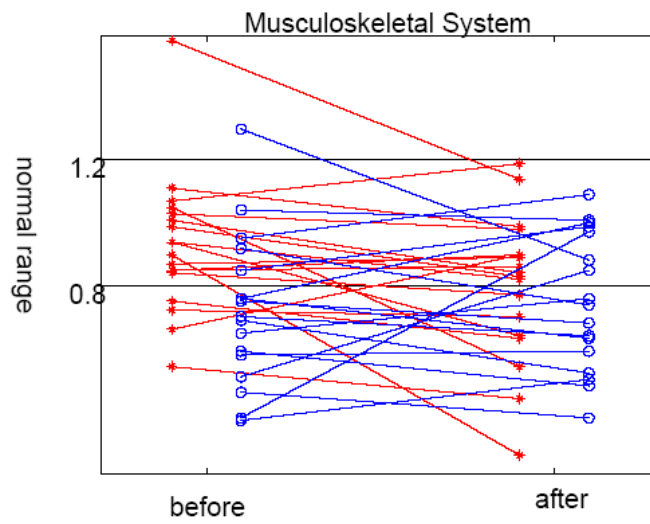
For comparison between groups in the baseline state, the value of Body Energy ( $P < 0.05$ ) and Musculoskeletal System ( $P < 0.01$ ) was higher in the experimental group compared with the control group, i.e.  $M1 > C1$  for these two factors (Fig. 2-5). Group comparison for Metabolism Function demonstrated a significant increase in the control group compared with the meditation group. ARDK estimates of 5 health conditions revealed no significant difference for the two groups after meditation as well as rest state

Table 2-3 Mean, standard deviation and the number of subjects whose 5 health condition parameters are within the range of normal values

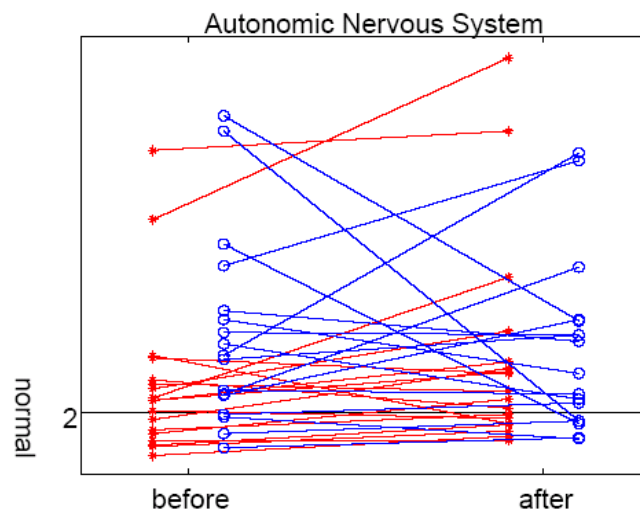
	Normal subjects	Body Energy	Metabolism Function	Mental State	Musculoskeletal System	Autonomic Nervous System
Exp Group (18)	before	14	14	8	13	7
	Mean± std	43.36 ± 12.23	1.07 ± 0.24	1.21 ± 0.31	0.93 ± 0.22	2.44 ± 1.26
	after	13	10	10	11	7
	Mean± std	34.11 ± 17.31	1.16 ± 0.33	1.13 ± 0.37	0.82 ± 0.30	2.89 ± 1.29
Ctrl Group (17)	before	8	9	6	4	4
	Mean± std	31.06 ± 18.00	1.25 ± 0.30	1.24 ± 0.47	0.72 ± 0.24	3.24 ± 1.55
	after	11	7	7	7	5
	Mean± std	28.88 ± 12.90	1.27 ± 0.30	1.22 ± 0.36	0.75 ± 0.22	2.99 ± 1.40



(a)



(b)



(c)

Fig. 2-4 The value of Body Energy (a), Musculoskeletal System (b) and Autonomic Nervous System (c) for every subject during the two states.

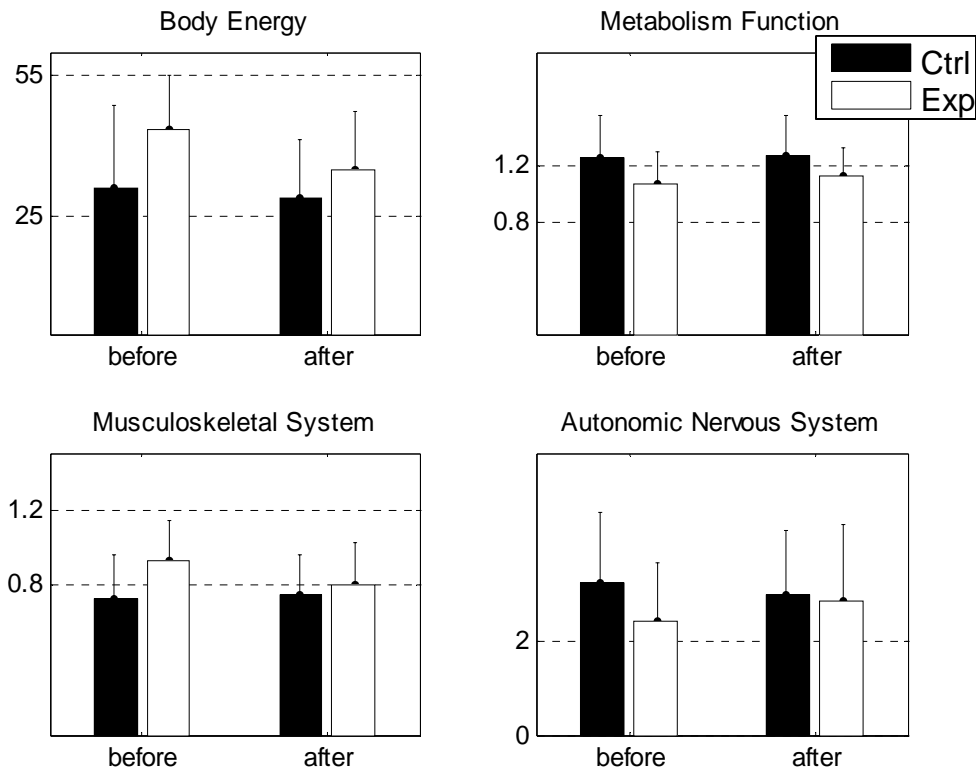


Fig. 2-5 Mean value of the items of health condition that showed between- and within-group changes.

### System Reports

Mean, standard deviation and the number of subjects whose parameters of system reports are within the range of normal values are showed in Table 2-4. Fig. 2-6 is the mean probabilities of system reports for 18 meditators and 17 control subjects during the both states. In the system reports, the items in which more than a half of the group subjects were in the range of the normal health are Body Energy, Mental State, Autonomic Nervous System, Thyroid Gland Function and Metabolism Function. In the baseline state, experimental group showed an average of overall better health condition than the control group, especially in BE, DS, RS, IS ( $p < 0.01$ ), ANS, TGF, LF, ES and SR ( $p < 0.05$ ). After 30-min of meditation or rest, experimental group presented better health condition than the

Control group in IS, US ( $p<0.01$ ), RS, SR, CS and ES ( $p<0.05$ ).

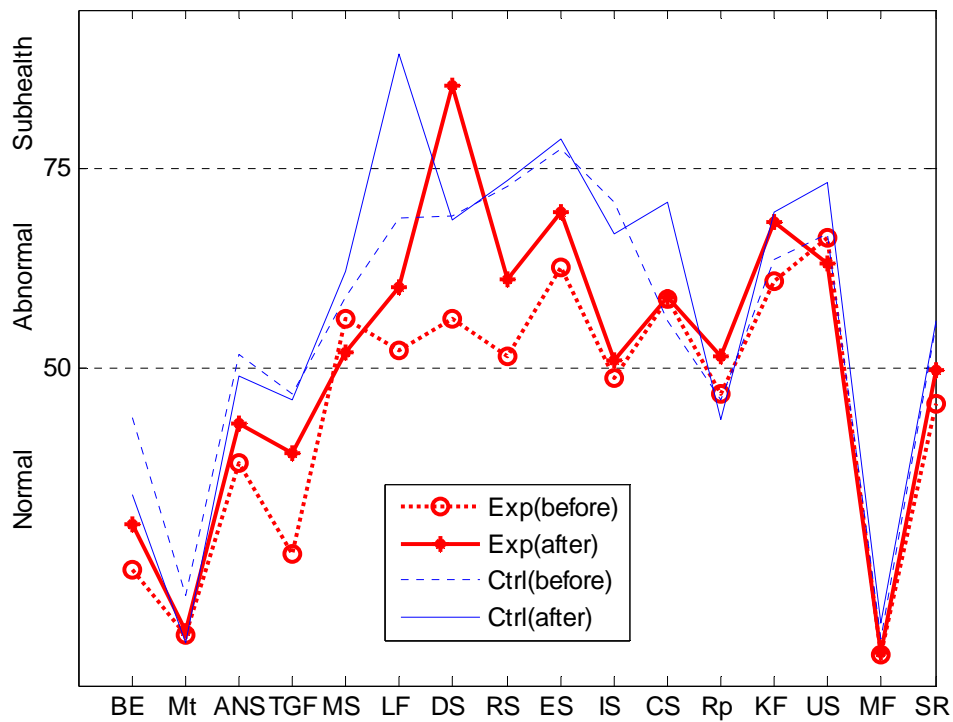
The effects of 30-min meditation resulted in a significant increase of probabilities in five items - ANS, TGF, LF, RS and SR for the experimental subjects while the effects of rest were not apparent for the control group except for an increase in CS. This tendency means to get problems in that system which is on the contrary of our supposition. The differences of other items did not reach significance in both groups because of highly individual variability.



Table 2-4 Mean (standard deviation) and the number of subjects whose parameters of system reports are within the range of normal values.

Mean(Std) and Normal subjects		<b>BE</b>	<b>Mt</b>	<b>ANS</b>	<b>TGF</b>	<b>MS</b>	<b>LF</b>	<b>DS</b>	<b>RS</b>
Exp Group (18)	before	16	18	16	14	9	8	4	9
	Mean (std)	24.54 (21.40)	16.47 (16.00)	37.89 (15.12)	26.50 (28.89)	56.21 (17.79)	52.08 (23.47)	56.26 (14.19)	51.50 (21.86)
	after	14	16	14	10	7	6	3	5
	Mean (std)	30.37 (18.67)	16.93 (23.37)	43.00 (19.64)	39.09 (31.03)	51.86 (19.83)	60.02 (14.62)	85.51 (90.79)	61.06 (18.32)
Ctrl Group (17)	before	9	15	10	7	8	4	3	3
	Mean (std)	43.71 (22.88)	21.24 (22.93)	51.59 (22.78)	46.76 (34.37)	58.88 (15.78)	68.71 (18.90)	69.06 (14.37)	72.82 (20.41)
	after	12	17	9	8	4	2	2	2
	Mean (std)	33.94 (24.74)	15.41 (15.54)	49.00 (22.86)	45.88 (37.81)	62.18 (15.56)	89.53 (94.06)	68.41 (15.20)	73.41 (16.01)
Mean(Std) and Normal subjects		<b>ES</b>	<b>IS</b>	<b>CS</b>	<b>Rp</b>	<b>KF</b>	<b>US</b>	<b>MF</b>	<b>SR</b>
Exp Group (18)	before	5	8	6	9	5	3	18	13
	Mean (std)	62.54 (20.51)	48.68 (28.49)	58.62 (19.85)	46.66 (27.51)	60.89 (16.57)	66.29 (14.95)	13.98 (13.18)	45.38 (12.16)
	after	1	8	6	8	2	4	18	10
	Mean (std)	69.47 (14.88)	50.81 (18.48)	58.93 (18.81)	51.34 (23.99)	68.19 (15.83)	63.06 (12.32)	14.25 (9.83)	49.57 (11.95)
Ctrl Group (17)	before	1	4	5	7	6	3	9	15
	Mean (std)	77.53 (16.42)	70.88 (21.14)	55.82 (18.70)	46.00 (36.49)	63.53 (22.51)	66.71 (18.39)	43.71 (22.88)	21.24 (22.93)
	after	2	4	5	7	4	0	12	17
	Mean (std)	78.82 (16.77)	66.76 (18.25)	70.65 (17.95)	43.41 (31.03)	69.59 (17.87)	73.24 (11.09)	33.94 (24.74)	15.41 (15.54)





	BE	Mt	ANS	TGF	MS	LF	DS	RS	ES	IS	CS	Rp	KF	US	MF	SR
C1>M1	**	-	*	*	-	*	**	**	*	**	-	-	-	-	-	*
C2>M2	-	-	-	-	-	-	-	*	*	**	*	-	-	**	-	*
M2>M1	-	-	*	*	-	*	-	*	-	-	-	-	-	-	-	*
C2>C1	-	-	-	-	-	-	-	-	-	-	**	-	-	-	-	-

Fig. 2-6 The mean of System reports for both groups before and after the meditation or rest. \* $P < 0.05$ , \*\* $P < 0.01$

## II-4 Discussion

More meditators exhibited a better performance in the overall Health Condition Ratio as compared with control subject for both pre and post recording, especially in Body Energy and Musculoskeletal System.

Body Energy is the average of the measurements from the 24 acupoints. A high average indicates excess Qi and Blood while a low average indicates a deficiency of Qi and Blood. It is evident that meditators exhibit a better performance of Body Energy than the control

subjects. This may be due to the regular practice of meditation that produces the long-term changes with greater body energy. A decline of Body Energy after meditation may be related to the deep relaxed and calm state with less energy consumed.

Metabolism Function is determined from the ratio of the total of all Yin meridians divided by the total of all Yang meridians. A high ratio for the C1 shows that the metabolism of the body for nonmeditators is slower than that for the meditators in the baseline state.

The result of Musculoskeletal System indicates the balance condition of all left meridians and all right meridians. Measurements showed that more meditators are bilateral than control subjects. In addition, meditation can cause the increased activity of the Qi and Blood in the right side of body, while the control subjects remain about unchanged before and after the rest. It is hypothesized that the imbalance of the Musculoskeletal System caused by meditation is associated with the posture (left or right lotus posture).

Finally, the ratio of Autonomic Nervous System after meditation increased after meditation. In general, meditators possess a more adaptive pattern of stress response than controls (Telles et al, 1995). Previous studies showed that autonomic activities during meditation are characterized by decreased sympathetic activity (Delmonte, 1985; Walton et al., 1995; Young & Taylor, 1998) and increased parasympathetic activity (Kubota et al., 2001; Young & Taylor, 1998). Although there are no definite connections between autonomic nervous system based on Traditional Chinese Medicine theory and on modern medicine, meditation strengthens and enhances the ability to cope with stress. Ultimately, the ratio of Mental State remains almost unchanged for both groups in the current study.

The ARDK parameters of System Reports as well as Health Condition Ratio are a general idea of the overall body system and show large individual differences. Even so, our results imply that (1) extended practice of meditation may cause a long-term effect on the

participants to have better health condition and (2) meditation exhibits greater influence on the short-term state of body system than a rest does since nonmeditators keep themselves in a state of physical stability after taking a rest.



## Chapter III

### MATERIALS and SUBJECTS

In this chapter, two experimental setups were introduced. The first experiment was designed to study the spatiotemporal characteristics of Chan meditation EEG. Data was collected to give a meditation EEG overview of nonlinear dynamics. Another topic of interest in the meditation study is the synchronization between separate brain regions. In section III-3, the second experiment was introduced to investigate the synchronization under different meditating phases.

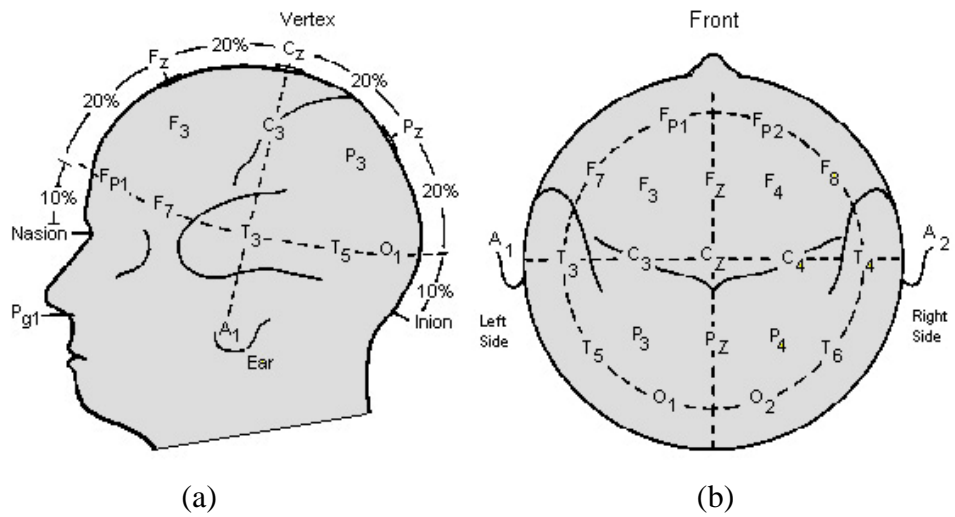
#### III -1 Introduction of EEG

For decades, the electrical activity of the human brain (electroencephalogram, EEG) has been extensively studied in order to help clinicians diagnose and treat brain disfunctions. The German psychiatrist Hans Berger firstly recorded human brain wave (voltage fluctuations) using an amplifying machine in 1924, (Berger, 1929). The human EEG signals represent the cortical electrical activity recorded at different sites on the scalp (non-invasive recording) or on the cortex (invasive recording). The cortical potentials are the integrated excitatory (EPSP) and inhibitory postsynaptic (IPSP) potentials developed by the cell body and large dendrites of pyramidal neurons. Scalp EEG measures thus represent the accumulated activity of hundreds or thousands of neural cells near the recording electrodes (Cooper et al., 1980; Oohashi et al., 2000; Niedermeyer & Lopes Da Silva, 1999). During the past decades, advanced technologies have been continually brought forth for brain function analysis, for example, functional magnetic resonance imaging (fMRI) (Logothetis, 2001), magnetoencephalography (Cohen, 1972), position emission tomography (PET) imaging (Young *et al.*, 1999), infrared-imaging system (Holst, 1998), etc.

Nevertheless, EEG has still been the most suitable parameter for long-term monitoring of brain functions exhibited as the lump variations of electrical activities. For instance, the effort to quantify sleep stages by EEG activities in the mid twentieth century has nourished the field of sleep study and further helped understand sleep problems, like insomnia (De Carli et al., 2004).

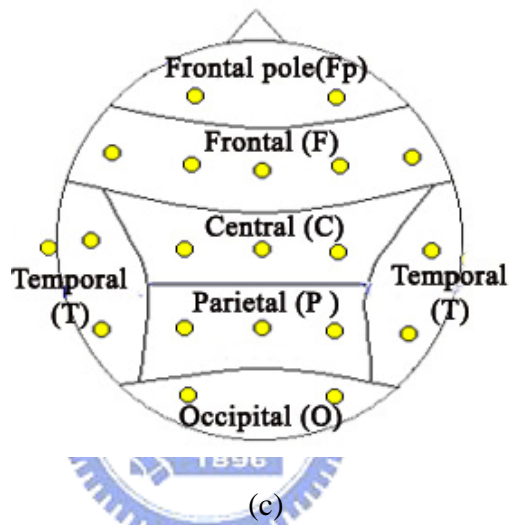
As normally characterized by frequency, the EEG patterns are conveniently classified into four frequency ranges: the delta ( $\Delta$ ,  $f < 4\text{Hz}$ ), theta ( $\theta$ ,  $4\text{Hz} \leq f < 8\text{Hz}$ ), alpha ( $\alpha$ ,  $8\text{Hz} \leq f < 13\text{Hz}$ ), beta ( $\beta$ ,  $13\text{Hz} \leq f \leq 35\text{Hz}$ ) and gamma ( $\gamma$ ,  $f > 35\text{Hz}$ ). The role of the EEG in monitoring the nervous system has been explored with regard to normal and pathological conditions. Spatiotemporal features provide an access to the detection of focal EEG phenomena and to the exploration of regional function mapping (Kalayci and Özdamar, 1995). Beside the common time-domain and frequency-domain analysis methods, we employed the nonlinear dynamic approach to quantify the time-varying EEG spectral properties.

In this work, EEG data were recorded from the scalp according to the definition of 10-20 system (see Fig. 3-1). The EEG signals were recorded by a 30-channel electrode array with a common linked-mastoid (MS1-MS2) reference. Fig. 3-2 displays the recording montage. The impedance was less than  $5\text{k}\Omega$  For each electrode.



(a)

(b)



(c)

Fig. 3-1 Illustration of 10-20 system: profile view (a) and top view (b). Each region has a letter to identify the lobe location (c). Note that there exists no central lobe and the "C" letter is only used for identification purposes only.

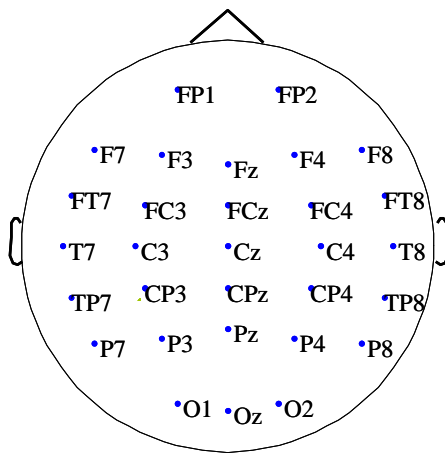


Fig. 3-2 The 30-channel electrode placement.

### III -2 Spatiotemporal Characteristics of Chan Meditation EEG

The preliminary study is devoted to the investigation of meditation EEG features and schema. Following experiment reports the further investigation of deep meditation state by means of selecting the practitioners with long-term practicing experiences.

#### III -2-1 Subjects

The EEG signals were collected from 17 Chan-Buddhist practitioners and 16 matched control subjects. Seventeen meditators (11 males and 6 females), average age 29.5 years, had been practicing Chan-Buddhist meditation for an average of 6.7 years (range 2 to 12 years) in Taiwan Chan Buddhist Association. Sixteen control subjects (11 males and 5 females), average age 27.3 years, had no experience of any forms of meditation at all.

After the preliminary study, we speculated that the deep meditation state was accompanied by an increase of beta activity which correlated positively with dimensional complexity. However, comparatively fewer studies reported the findings of beta wave and its correlation with different consciousness states. Das & Gastaut (1955) first proposed *samadhi* of Kriya yogi correlating with increased amount of fast beta activity. Thereafter yet very rarely, high-frequency beta wave or even higher frequency of gamma wave was recorded for advanced meditators capable of achieving deep meditation states or *samadhi* (Banquet, 1973; West, 1980; Benson et al, 1990; Benson et al., 1990; Istratov et al., 1996; Lo et al, 2003; Lehmann et al, 2001; Lutz et al, 2004). More new findings showed that EEG of well experienced Tibetan Buddhist practitioners exhibited an increase of even higher frequency of 35-44Hz gamma wave (Lehmann et al., 2001; Lutz et al., 2004). Thus, it was suggested that 1) generalized high-frequency beta rhythm characterized the deep meditation stage or 2) more advanced practitioners demonstrated an increase of fast beta activity, while unexperienced meditators demonstrated autonomic relaxation. Consequently, some modifications were performed in our further study of the Chan-meditation brain dynamics

varying with the meditation process. Since consistently substantial effects of meditation on EEGs were observed mainly in experienced meditators, we mainly investigated the practitioners with long-term practicing experiences. Additional six experienced meditators and matched controls were included for the analyses.

The experimental group now included 23 Chan-meditation practitioners (16 males and 7 females; mean age  $31.5 \pm 5.7$  years) who had been regularly practicing Chan meditation for an average of 8.4 years (ranging from 2 to 12 years). Normally, meditators have participated in meditation session lasted 90 min at least once a week and practiced for an average of 30-minute meditation on a daily basis. Twenty-three control subjects (15 males and 8 females; mean age  $29.5 \pm 3.9$  years) had no experience of meditation. Subjects in both groups were all healthy, without any reported accident or illness that might affect their EEG patterns.

### **III -2-2 Procedures and materials**

Experimental subjects took a 40-minute meditation, sitting in the full-lotus or half-lotus position with eyes closed. Each hand formed a special mudra (called the Grand Harmony Mudra), laid on the lap of the same side. Control subjects were asked to sit and relax their mind and body with eyes closed, without falling asleep for the same period. They were asked to “not practice any mental technique but merely to sit comfortably, keep the eyes closed and think about nothing in particular, just ordinary resting”. Informed consent was obtained from all of them in written form after the experimental procedures had been fully explained. After the EEG recording, the participant completed a questionnaire with respect to relaxation, awareness and the meditation condition, i.e. the feeling, quality and depth of the meditation.

In the meditation research study, it is difficult to access changes of the consciousness state during meditation. Meditators once transcending the physiological and mental state



cannot signal the operator. One reason is that the experimental subjects frequently forget. In other words, meditators cannot attain the optimal meditation if they are obligated to follow the experimental protocol. As a consequence, quantitative results together with the post-experiment interview may provide us with a glimpse of the meditation scenario.

The EEG signals were sampled at 200 Hz after the band-pass filtering with 0.3-40Hz passband. The artifacts such as eye blinking, eyeball movement and muscle activities were manually removed by naked-eye diagnosis. The 40-min recording period of meditation/relaxation was divided into three intervals of the first 20-min, the mid 10-min and the last 10-min session. Three 5-min, artifact-free EEG epochs were extracted from each interval for further analyses. After a preliminary bandpass filtering (1.56–30 Hz), each EEG epoch was analyzed by running measurement of complexity index and power spectra with a 5-second running window and a moving step of 2.5 seconds.



### **III -3 Synchronization in Different Meditating Phases**

One important goal is to assess the nature of the interaction between separate brain regions. Measurement of brain interdependence becomes a matter of significance in understanding the meditation EEG. This section reports the experimental setup of the investigation of meditation EEG synchronization.

#### **III -3-1 Subjects**

In this study, twelve Chan-meditation practitioners (mean age: 32.5 year; range: 28 – 41 years; four females; all right-handed) were investigated. Since reliable effects of meditation on the EEG activity were obtained mainly in experienced meditators, all were long-term practitioners with an average experience of 8.8 years (range 5 to 13 years) in Chan-Buddhist meditation practice. In Chan-meditation practice, one major technique of

attaining good-quality meditation is to guard and focus on the particular site (called Chakra), for example, Zen Chakra locating inside the third ventricle (Fig. 1-1). By means of Chakra focusing, experienced practitioners reported that they often could enter into a tranquil state of consciousness transcending beyond the physiological (the fifth), mental (the sixth), subconscious (the seventh), and Alaya (the eighth) conscious state.

### **III -3-2 Procedures and materials**

Previous studies on hundreds of practitioners revealed large between-group variations in EEG pattern. We thus aimed to investigate the within-subject behaviors during the entire meditation course. In the beginning 3 minutes, we collected the baseline data for each meditator under normal, eye-closed rest (R), without entering into meditation. Then they were instructed to begin a 40-min meditation (Lo *et al.*, 2003; Chang & Lo, 2005). After the meditation, the subjects were asked to keep their eyes closed for an additional 3-min transition period. Then they were asked to practice a 5-min Zen-Chakra focusing. During the recording period, the subjects sat in the full-lotus position with eyes closed. After the recording, the subjects were asked for an interview. M session indicates a 3-min artifact-free epoch extracted from the beginning after 30-min of meditation. Z session refers to the first 3-min artifact-free data segments under Zen-Chakra focusing.

The EEG signals were recorded by the 30-channel, common-reference (linked-mastoid MS1-MS2) electrode montage based on the international 10-20 system. As the number of interdependence measure increases with the square of channel number, a data reduction was required. We thus selected the following 19 locations for analysis: Fp1, F7, F3, T7, C3, P7, P3, P1, Fz, Cz, Pz, Fp2, F8, F4, T8, C4, P8, P4, O2. EEG signals were sampled at 200 Hz after 0.3-45 Hz band-pass filtering. Each EEG epoch (R, M and Z) was analyzed by running measurement of nonlinear interdependence using a 5-second window without overlap.

## Chapter IV

### METHODS

This chapter presents the quantitative approaches to characterize the EEG activities under Chan meditation. Fig. 4-1 illustrate the entire scheme employed in this study. We first introduce the method for characterizing the EEG nonlinear dynamical behaviors based on complexity-index analysis. Reconstruction of dynamics from observations is briefly explained in section IV-2. In section IV-3, we introduce the signal processing algorithms for single EEG channel. Average complexity index ( $\bar{\delta}$ ), reflecting the dimensionality of a time series, is then derived in detail in this section. Interdependence measure, described in Section IV-4, was used to investigate the interaction between different cortical regions. Section IV-5 illustrates the conventional linear analyses, mainly the spectral and coherence analyses, applied in this study for comparison. Finally, methods for statistical test are presented in section IV-6.

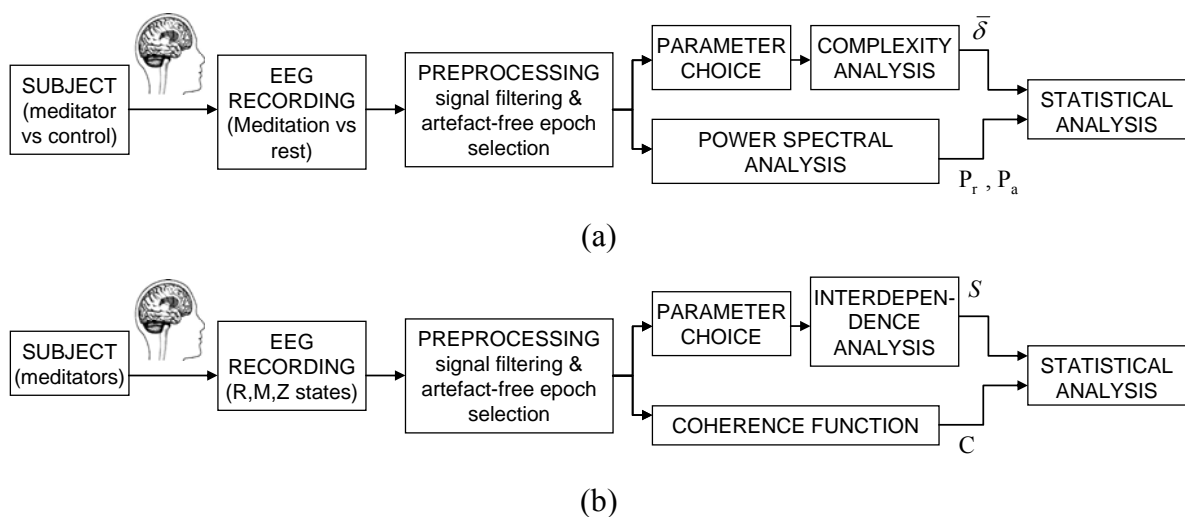


Fig. 4-1 Block diagram illustrating the entire scheme employed in this study (a) analysis spatiotemporal characteristics (b) synchronization of different meditating phases.

## IV-1 EEG Investigation Based on Nonlinear Time Series Analyses

During the past decades, methods for exploring nonlinear dynamical behavior based on time series analysis have been extensively used to decipher the underlying brain dynamics (Pereda et al., 2005). A dynamical system is a model that determines the evolution of a system given only the initial state, that is, the current state is a particular function of the previous state (Stam, 2005). Thus a dynamical system is described by two factors: state and dynamical model. The state of a dynamical system is determined by the values of all the variables that describe the system at a particular time instant (Stam, 2005). The phase space (or state space) defines all the possible states of the system variables under study. Consequently, the state of a system described by  $n$  variables can be represented by a point in an  $n$ -dimensional space. The transition of the system's state over time is governed by a set of rules or equations. The time evolution of the system is then given by a series of consecutive states (points) in the phase space; the trace connecting these points in time leading to an orbit is called the trajectory of the system.

Dynamical systems may behave in two different manners: linear and nonlinear. A dynamical system is linear if all the equations include only linear arithmetic operations; otherwise it is nonlinear. In a linear system, there is a linear relation between causes and effects satisfying superposition principle (homogeneity and scaling). On the other hand, a nonlinear system without following superposition may result in a large effect by a small cause (Stam, 2005). A dynamical system is deterministic if the equations of motion neither contain any noise term nor perform in the stochastic way. These are rather technical definitions for realistic biological systems. However, what should concern us in this work is that the neural network of the brain is likely to be a nonlinear deterministic system. This is based on the assumption that the investigated time series is derived from synergetic, self-organized neural systems showing a deterministic, nonlinear behavior (Tirsch et al., 2004).

The attractor of a system is a set of trajectories that contain long-term solutions  $s$  of all possible initial states after the initial transients have died out (Milnor, 1985). In the case of the nonlinear systems, attractors may be periodic, quasi-periodic, or more complicated behavior such as a chaotic state (Milnor, 1985; Stam et al., 2005). Attractors of period dynamics correspond to closed loops of limit cycle in the state space. Quasi periodic dynamics is a superposition of different periodic dynamics with unlike frequencies. Consequently, attractors exhibit a more complicated torus-like or donut-like shape. The chaotic or strange attractor is a very complex object with so-called fractal geometry which corresponds to deterministic chaos. There is some evidence for chaotic-like phenomena in EEG dynamics (Pritchard & Duke, 1992; Elbert et al., 1994).

Various phenomena can be considered as the dynamical system governed by a consistent set of laws. These laws determine the evolution of the system state over time. If we know the set of equations governing the basic systems variables, we can observe the outputs, attractors and the system properties. However, realistic investigation in clinical neurophysiology normally comes up with a set of observations, for example, multi-channel EEGs, rather than a set of differential equations or the system state (phase-space point). We do not know the nature of the dynamics underlying the system. Attractors are very important objects since they give us an image of the system dynamics. A more complex attractor normally results in a more complex dynamics. To correctly characterize the concluding behavior of a nonlinear dynamical system, the geometry of the attractors must be delineated. Owing to Taken's embedding theory (1981) we were able to quantify the nonlinear dynamics directly from the univariate time series recorded. We will review the concept of reconstructing the phase space in the next section. One of the most important mathematical quantities for characterizing an attractor is its dimension for a rough measurement of the irregularity or complexity of a signal (Abarbanel, 1996, Diks, 1999, Galka, 2000, Kantz and Schreiber, 2003). The larger the dimension of the attractor, the

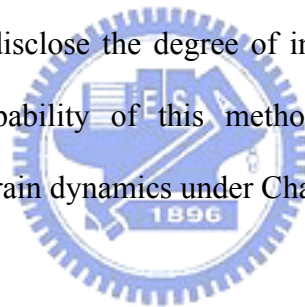
more complicated the behavior of the nonlinear system.

To reliably estimate the CNS dynamic parameters, we attempt to obtain appropriate implementing parameters to give a quantitative description of what is involved in the EEGs during meditation. Conventional tool such as correlation dimension is not feasible for long-term monitoring. Alternatively, we evaluate the averaged complexity index ( $\bar{\delta}$ ) that may reflect how the brain dynamics switches between various states of consciousness provided that the major aim is not to obtain exact values for dynamic parameters. Averaged complexity index, the main algorithm throughout this work, has been proved to be a useful tool in long-term biomedical signal processing.

Next, we illustrate the idea of interdependence between time series, which assess the existence of nonlinear interdependence between the EEG signals. This type of “nonlinear coupling” allows the study of nonlinear interdependence among multi-recording sites and represents an alternative to the coherence function. Nonlinear interdependence measure has been demonstrated to be capable of exploring brain dynamics under various physiological, pathological or mental states. Noticeable results include the analysis of, normal resting adults subjects (Breakspear and Terry, 2002a, 2002b), human subjects with epilepsy (Stam and van Dijk, 2002; Arnhold et al., 1999; Le van Quyen et al., 1999), distinctive auditory processing of music by musicians and non-musicians (Bhattacharya et al., 2001, 2003), and healthy term neonates during awake as well as during sleep (Pereda et al., 2003). This study focused on the nonlinear dynamical behaviors of the brain under Chan meditation.

By analyzing the reconstructed phase space, such invariant quantities like the phase synchronization (Rosenblum et al., 1996), generalized synchronization (Rulkov et al., 1995) or synchronization likelihood (Stam and van Dijk, 2002) may reveal nonlinear structures hidden to standard linear approaches (Pereda et al., 2005; Stam, 2005). In brief, these measures quantify, for a short time, the grade of predicting the state-space evolution in one system by that in the other, simultaneous system (Schiff et al., 1996). Theoretical studies

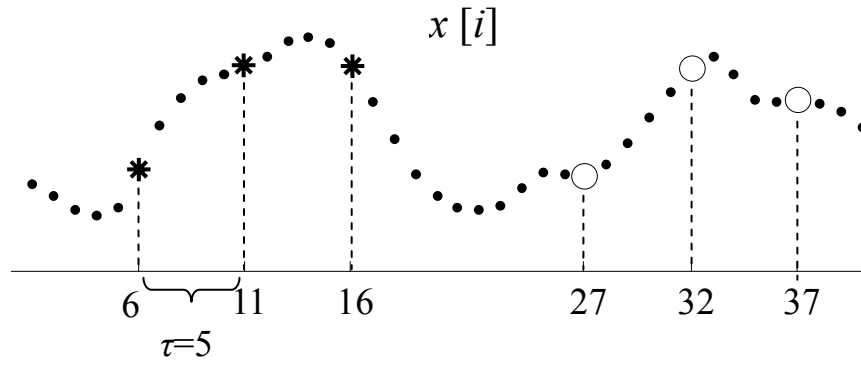
indicated that these indexes were not able to reveal any causal relationship among signals (Quian Quiroga et al., 2000). Besides, it has been reported (Pereda et al., 2001) that in order to determine both the significance and the nonlinearity of the interdependence it is necessary to make use of additional statistical tests. In spite of these limitations, several authors have proposed a robust set of measures (Arnhold et al., 1999; Quian Quiroga et al., 2000, 2002) One method called *similarity index*, instead of estimating predictions, quantifies how neighborhoods (i.e., recurrences) in one attractor map into the other. This method has the advantages of sensibility to nonlinear interdependence and potential of detecting asymmetric relationships, in which the dependence of one signal on another signal is different than vice versa (Arnhold et al., 1999; Le van Quyen et al., 1998). Based on the concept, the modified similarity index allows us to better choose the implementation parameters and to effectively disclose the degree of interactions even in noisy condition. We thus investigated the capability of this method in characterizing the nonlinear interdependence behaviors of brain dynamics under Chan meditation.



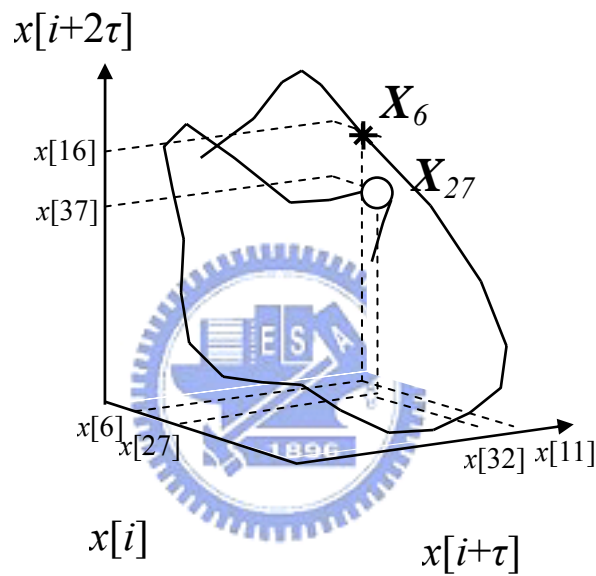
## IV-2 Embedding: Reconstruction of System Dynamics from Observations

The approach of nonlinear modeling described here is based upon the interpretation of the projection from a time series (output of a system) recorded from a scalp electrode to a multidimensional phase space trajectory of the corresponding system. Let  $\mathbf{X} = \{\mathbf{X}_i\}_{i=1}^N$  be the set of  $N$  points on the EEG trajectory, where  $\mathbf{X}_i$  is an  $n$ -dimensional point constructed from (1) the single-channel EEG, or (2) the  $n$ -channel EEG signals (Lo & Chung, 2000). In the single-channel case, the  $n$ -dimensional phase-space point  $\mathbf{X}_i$  is constructed according to the Takens (1981) embedding theory: a smooth map from the time series (e.g., EEG)  $\{x[i], i=1, \dots, N+(n-1)\tau\}$  to the phase-space trajectory  $\mathbf{X} = \{\mathbf{X}_i = (x[i], x[i+\tau], \dots, x[i+(n-1)\tau])\}_{i=1}^N$  preserves some of topological invariants of the original system. The EEG trajectory forms a strange attractor. Here  $\tau$  represents the time delay in number of samples. A time series and its corresponding phase space trajectory are shown in Fig. 4-2(a) and (b), respectively. Fig. 4-2 (a) displays a short segment of a time series. To embed this time series in a 3-dimensional phase space, three coordinates are needed to describe each point in the space. These coordinates are obtained by taking the amplitude values from the original and delayed time series  $x[i]$ ,  $x[i+\tau]$  and  $x[i+2\tau]$ . Here, the time lag is  $\tau = 5$ . For instance, the values at  $x[6]$ ,  $x[6+5]$ ,  $x[6+10]$  (indicated by ‘\*’ in (a) ) are plotted in the three dimensional space (Fig. 4-2(b)), resulting in the state-space point,  $\mathbf{X}_6$  (represented by ‘\*’). Another example  $\mathbf{X}_{27}$  is represented by ‘o’ in Fig. 4-2(b). Next, by moving  $x[i]$ ,  $x[i+\tau]$  and  $x[i+2\tau]$  one-sample forwards, we obtain  $x[i+1]$ ,  $x[i+1+\tau]$  and  $x[i+1+2\tau]$  that are used to reconstruct the next point in state space. By repeating this procedure for the whole time series, an equivalent attractor can be reconstructed.





(a)



(b)

Fig. 4-2 Schematic illustration of time delay embedding. A short segment of a time series is shown in (a), and its corresponding phase space trajectory shown in (b)

The embedding dimension is a very rough description of the “amount of space” an attractor occupies. It is necessary to condense the information and find a parameter that contains the features most relevant to the underlying mechanism. Dimensional analysis was thus developed from this purpose. The dimension of an attractor is a measure of its spatial extensiveness and the irregular geometry in phase space. Many researchers dropped the chaos hypothesis and referred their dimension estimate to a measure of relative complexity instead of an estimate of the intrinsic fractal dimension of a strange attractor (e.g. Pritchard

& Duke, 1992; Rey & Guillemand, 1997). Dimension of an attractor can be considered as a measure of the degrees of freedom or the ‘complexity’ of the dynamics. Several kinds of dimensions have been introduced in order to give more precise description of the “complexity” of a system. Moreover, dimensionality suggests a lower bound of the number of variables required to model the system. Among them, the correlation dimension has become the most widely used measure. Correlation dimension as a means of quantifying the “strangeness” of an attractor was introduced by Grassberger and Procaccia (1983a).

### **IV-3 Univariate Analysis: Complexity Index**

Although dimensional computation furnishes important information about the CNS characteristics, tools from nonlinear dynamical theory used for EEG analysis, such as correlation dimension, mostly suffer from the problems of indirect estimation, computational inefficiency and bias from implementing parameters (Lo and Principe, 1989; Yaylali, 1996; Lo and Chung, 2000). Thus they are not feasible for long-term schematic illustration of the meditation EEG. To deal with the problems, we introduced the method of estimating intrinsic dimensionality into multi-channel EEG analysis (Lo and Chung, 2000). Since dimensionality in a sense characterizes the global waveform complexity, we name it the “complexity index ( $\delta$ )”. Evaluation of complexity index is conceptually comprehensible and easily implemented based on local approaches (Fukunaga and Olsen, 1971; Pettis *et al.*, 1979; Verveer and Duin, 1995; Bruske and Sommer, 1998). Among the local approaches, the  $K$ 's nearest neighborhood ( $KNN$ ) analysis (Fukunaga and Flick, 1984; Passamante and Farrell, 1991; Michel and Flandrin, 1993; Trunk, 1976) provides an approach for directly estimating the  $\delta$ . The algorithm is illustrated in the following.

### IV-3-1 Definition and estimation

For each point in the set  $\mathbf{X}$  (e.g.,  $\mathbf{X}_i$ ), a  $K$ NN hypersphere is determined and formed by the  $K$ 's nearest neighboring (NN) points  $\{\mathbf{V}_{ij}\}_{j=1}^K$ ,  $\mathbf{V}_{ij} \in \mathbf{X}$  and  $\mathbf{V}_{i1} = \mathbf{X}_i$ . The  $\mathbf{X}_i$  is called the seed point of the  $i$ th hypersphere. Inside the  $i$ th hypersphere, the largest distance to the seed point  $\mathbf{X}_i$  is:

$$d_{i,KNN} = \|\mathbf{V}_{iK} - \mathbf{X}_i\| \quad (4-1)$$

where the operator  $\|\cdot\|$  evaluates the Euclidean distance. It was reported (Fukunaga & Flick, 1984; Lo & Chung, 2000) that

$$\frac{E\{d_{(K+1)NN}\}}{E\{d_{KNN}\}} = 1 + \frac{1}{Kn} \quad (4-2)$$

where  $E\{d_{KNN}\}$  is the first order moment of  $d_{KNN}$ , the  $K$ th NN distance of any hypersphere in  $\mathbf{X}$ . The equation points out the effect of  $K$  on classification error for a given number of space dimension  $n$ . Derivation of eq. (4-2) was in Appendix B. Thus, we proposed quantifying the global waveform complexity of EEG signals by estimating the dimensional complexity as follows (Lo & Chung, 2000):

$$\delta = \frac{1}{K} \left( \frac{E\{d_{(K+1)KNN}\}}{E\{d_{KNN}\}} - 1 \right)^{-1} \quad (4-3)$$

which provides the way to evaluate the complexity index. Here,  $E\{d_{(K+1)NN}\}$  and  $E\{d_{KNN}\}$  are the average of  $d_{i,(K+1)NN}$  and  $d_{i,KNN}$ , respectively, for all points on the EEG trajectory, i.e.,  $i=1, \dots, N$ . To obtain a reliable estimate of  $\delta$ , we normally average the  $\delta$ 's over a moderate range of  $K$ 's to obtain the final estimate. The average  $\delta$  is denoted by  $\bar{\delta}$ .

### IV-3-2 Efficient method for estimation

Although directly estimating the  $\delta$  using eq.(4-3) can be easily implemented, a large portion of computer time is spent on searching for the  $K$ NN and  $(K+1)$ NN distances.

Undoubtedly, computer time required by the algorithm implemented in this manner is highly dependent on the values of  $K$  and  $N$ . A large  $K$  costs more effort in the competition process. A large  $N$  indicates a large number of distances to be computed.

The authors proposed an approach that does not require computing all the inter-point distances and reduces the exhaustedly sorting process (Lo & Chung, 2001). The approach mainly adopted the eigenfunction and principal-axis analysis. Let  $[\mathbf{X}]$  be an  $N \times n$  matrix with its  $i$ th row vector representing the  $i$ th  $n$ -dimensional point  $\mathbf{X}_i$  on the EEG trajectory. The eigenvector associated with the largest eigenvalue of the covariance matrix of  $[\mathbf{X}]$  is denoted by  $[\Phi]$ , a  $1 \times n$  row matrix. And  $\|\Phi\|=1$ . Then the transformation  $[\mathbf{Y}]=[\mathbf{X}][\Phi]^T$  results in an  $N \times 1$  column matrix containing  $N$  scalars  $y_i, i=1, \dots, N$  on the principal axis (the largest eigenvector). As a result, the inter-point distances of  $\mathbf{X}_i: d_{ij}, j=1, \dots, N$  are mapped to

$$\rho_{ij} = \|y_j - y_i\| = \|(\mathbf{X}_j - \mathbf{X}_i)\Phi^T\|. \quad (4-4)$$

Using  $\rho_{ij}$  as reference, the sorting process for determining the  $d_{i,KNN}$  and  $d_{i,(K+1)NN}$  becomes less laborious. Details of implementation were given in (Lo & Chung, 2001).

### IV-3-3 Applications to meditation EEG

Dimensional complexity is always biased by the choice of parameters. Here the time delay  $\tau$  was determined by the first zero-crossing of the corresponding autocorrelation function. Embedding dimension  $n$  was selected from the saturated value of complexity index with embedding dimension  $n$  increasing. The value of  $n$  resulting in  $\delta$  saturation is  $n=15$ . Accordingly, minimum  $n$  of 15 is appropriate. As  $\delta$  evaluation is rather insensitive to these parameters in our study, we took for all the EEG segments the maximal values  $n=15$  and  $\tau=5$  samples (0.025 second). According to our experiences in meditation EEG, a moderate choice of implementing parameters for the running  $\bar{\delta}$  measurement was as follows, window length:  $N=1,000$  samples (5 seconds), moving step: 500 samples (2.5

second). The final estimate,  $\bar{\delta}$ , was obtained by averaging the  $\delta$ 's computed with  $K$  ranging from 20 to 35.

#### IV-4 Multivariate Analysis: Nonlinear Interdependence Measure

Methods discussed so far are involved with one signal only. Since the interaction between separate brain regions is neurophysiologically very significant and appealing, the application of multivariate time series analysis also plays an important role in the EEG study (Bhattacharya et al. 2001; Stam, 2005). Intensive study on synchronous oscillations has been conducted to investigate the important mechanism by which specialized cortical and subcortical regions integrate their activity into different functions and different spatial scales (Singer, 2001). A number of studies have proposed the viewpoint of considering brain dynamics as a large ensemble of coupled nonlinear dynamical subsystems. Accordingly, significant nonlinear synchronization has been detected on the macroscopic scales of EEG channels in healthy subjects (Breakspear and Terry, 2002a, 2002b; Stam et al., 1996, 2003; Feldmann & Bhattacharya, 2004). Among various types of synchronization based on nonlinear dynamical theory, we used method of modified *similarity index*.

##### IV-4-1 Definition and estimation

The algorithm for calculating nonlinear interdependence is described below. From time series simultaneously measured in two systems  $\mathbf{X}$  and  $\mathbf{Y}$ , we can reconstruct delay vectors  $\mathbf{X}_i = (x[i], x[i + \tau], \dots, x[i + (n-1)\tau])$  and  $\mathbf{Y}_i = (y[i], y[i + \tau], \dots, y[i + (n-1)\tau])$ ,  $i=1, \dots, N$ , where  $N$  is the total number of state points,  $m$  is the embedding dimension and  $\tau$  denotes the delay in sample. A  $K$ NN hypersphere, formed by the  $K$ 's nearest neighboring (NN) points, is a cloud of  $K$   $m$ -dimensional neighboring points around each  $\mathbf{X}_i$ . Let  $r_{ij}$  and  $s_{ij}$ ,  $j=1, \dots, K$ , denote the time indices of the  $K$ NN points of  $\mathbf{X}_i$  and  $\mathbf{Y}_i$ , respectively. Then,  $K$

nearest neighbors of  $\mathbf{X}_i$  are  $X_{r_{i,j}}, j=1, \dots, K$ . For a given state point  $\mathbf{X}_i$ , the mean-square Euclidean distance (or the average radius of the *cloud* centered at this state point) to its  $K$ NN is defined as:

$$R_i^{(K)}(\mathbf{X}) = \frac{1}{K} \sum_{j=1}^K \|X_i - X_{r_{i,j}}\|^2 \quad (4-5)$$

Another point cloud around  $\mathbf{X}_i$  is formed with respect to its *mutual* neighbors  $X_{s_{i,j}}$ , which share the same temporal indexes of the  $K$ NN of  $\mathbf{Y}_i$ . In this sense, the  $\mathbf{Y}$ -conditioned mean-square Euclidean distance is defined by replacing the true nearest neighbors of  $\mathbf{X}_i$  by the *mutual* neighbors (Quian Quiroga et al., 2000):

$$R_i^{(K)}(\mathbf{X}|\mathbf{Y}) = \frac{1}{K} \sum_{j=1}^K \|X_i - X_{s_{i,j}}\|^2 \quad (4-6)$$

The average square radius of  $\mathbf{X}_i$  to all the remaining points in the phase space is given by

$$R_i(\mathbf{X}) = \frac{1}{N-1} \sum_{j=1, j \neq i}^N \|X_i - X_j\|^2 \quad (4-7)$$

Then, for two strongly synchronized systems, both sets of neighbors, self and mutual, mostly coincide and  $R_i^{(K)}(\mathbf{X}) \approx R_i^{(K)}(\mathbf{X}|\mathbf{Y}) \ll R_i(\mathbf{X})$ ; whereas for independent systems, mutual neighbors are more scattered, which leads to  $R_i^{(K)}(\mathbf{X}) \ll R_i^{(K)}(\mathbf{X}|\mathbf{Y}) \approx R_i(\mathbf{X})$ . Thus, the degree of interdependence of these two systems is reflected by the similarities (or dissimilarities) between these two cloud types formed by self and mutual neighbors, respectively. Accordingly, the strength of similarity between these two point clouds is termed as similarity index  $S$  (Arnhold et al., 1999; Quian Quiroga et al., 2000) and is defined below:

$$S^{(K)}(\mathbf{X}|\mathbf{Y}) = \frac{1}{N} \sum_{i=1}^N \frac{R_i^{(K)}(\mathbf{X})}{R_i^{(K)}(\mathbf{X}|\mathbf{Y})} \quad (4-8)$$

In order to maximize the sensitivity to the underlying synchronizations and gain the robustness against noise, we proposed a modified version of  $S$  measure with adjusted range of  $K$ NN. Following our previous study of dimensional complexity index (Lo & Huang,

2007; Travis et al., 2002), a reliable estimate of dimensional complexity of a system was obtained by averaging the complexity indexes over a moderate range of  $K$ 's. A small  $K$  causes superimposed noise, while a large  $K$  results in a measurement involving multi-modal effects (Lo & Huang, 2007). To determine a robust measure against noise, it follows that the final estimate of nonlinear interdependence is the averaged  $S^{(K)}(X|Y)$  over an appropriate range of  $K$ 's and is denoted by  $S(X|Y)$ .

#### IV-4-2 Asymmetric property of interdependence measure

$S(X|Y)$  works by directly assessing the statistical dependence of the state-space structure of  $\mathbf{X}$  on that of  $\mathbf{Y}$  in order to test whether closeness in  $\mathbf{X}$  implies closeness in  $\mathbf{Y}$  and *vice versa*. For identical systems (where the set of self nearest and mutual neighbors are identical) both these indexes equal to the maximum value (=1), whereas for completely independent systems, the indexes are close to zero. The opposite interdependence ( $S(\mathbf{Y}|\mathbf{X})$ ) can be computed analogically and they are in general asymmetric (i.e.,  $S(\mathbf{Y}|\mathbf{X}) \neq S(\mathbf{X}|\mathbf{Y})$ ). Therefore,  $\mathbf{X}$  can depend on  $\mathbf{Y}$ , and at the same time,  $\mathbf{Y}$  can depend on  $\mathbf{X}$ . The asymmetry of  $S$  is one of the main advantages over other nonlinear measures such as the mutual information and the phase synchronizations. The fact that  $S$  is asymmetric allows us to study not only topographic patterns but also functional properties.  $S(\mathbf{X}|\mathbf{Y})$  assesses the influence of signal  $\mathbf{Y}$  on signal  $\mathbf{X}$ . Alternatively speaking, signal  $\mathbf{Y}$  is regarded as the source or the active role of activity. On the contrary,  $S(\mathbf{Y}|\mathbf{X})$  quantifies the influence of signal  $\mathbf{X}$  (source) on signal  $\mathbf{Y}$  (sink) (Arnhold et al., 1999; Quiroga et al., 2000). If  $S(\mathbf{Y}|\mathbf{X}) > S(\mathbf{X}|\mathbf{Y})$ , degree of dependence (DOD) of  $\mathbf{Y}$  on  $\mathbf{X}$  is higher than DOD of  $\mathbf{X}$  on  $\mathbf{Y}$ . In other words,  $\mathbf{X}$  has greater influence on  $\mathbf{Y}$  than vice versa,  $\mathbf{X}$  is said to be more 'active' and  $\mathbf{Y}$  is more 'passive'. It is, in principle, easier to predict the state of the response from the state of the driver than vice versa. In this way, the directional influence can be detected. One must notice, however, that we do not imply existence of any causal relation, a priori. By

considering each electrode either as a sink or as a source of activity, we may thereby get further information about the direction of the interaction (Quian Quiroga et al., 2002).

Another interpretation of measured asymmetry is that it also can reflect the different dynamical properties of each signal, in particular their dimensional complexity (Schiff et al., 1996; Arnhold et al., 1999). Some later numerical studies confirmed the conjecture that the active role was more complex, exhibiting a higher intrinsic dimension; while the passive role (sink) had lower dimension (Arnhold et al., 1999; Quian Quiroga et al., 2000). Arnhold et al. (1999) used a simple case as an example to explain the origin of active/passive relationships. For two identical time sequences,  $\mathbf{X} = \mathbf{Y}$ , we use different embedding dimensions  $n_X$  and  $n_Y$  in the delay vector construction. We take  $n_Y < n_X$  and  $n_Y < n_{opt}$ , where  $n_{opt}$  is an optimal embedding dimension in the sense that for  $n < n_{opt}$  the point cloud  $\{\mathbf{Y}_i\}$  is not completely unfolded, while it is unfolded for  $n \geq n_{opt}$ . Thus each  $\mathbf{Y}_i$  can be considered as a singular projection of  $\mathbf{X}_i$  with non-unique inverse of  $\mathbf{Y}$ . Assume now that  $\mathbf{X}_s$  is a close neighbor of  $\mathbf{X}_i$ . Then also  $\mathbf{Y}_s$  must be a close neighbor of  $\mathbf{Y}_i$ . But the opposite is not true: closeness in  $\mathbf{Y}$  does not necessarily imply closeness in  $\mathbf{X}$ . As a consequence,  $S(\mathbf{Y}|\mathbf{X}) > S(\mathbf{X}|\mathbf{Y})$ . From the above conceptual argument, active/passive relationship mainly reflects the relative information of degrees of freedom, yet, infeasible for revealing a causality relationship. Systems with higher dimensional complexity are more active than those with lower.

Although this theoretical argument can become irrelevant for practical applications due to such inevitable issues like noise, nonstationarity or shortness, asymmetry of measured interdependence has been proposed to be very useful in understanding coupled neurophysiology systems even if no causal relationships can be deduced from such asymmetries (e.g. Feldmann & Bhattacharya, 2004; Arnhold et al., 1999).



### **IV-4-3 Applications to meditation EEG**

There is no unique way to choose the implementing parameters. However, our previous study of complexity-index estimation for meditation EEG has established a moderate choice of parameters as:  $\tau = 5$ ,  $n = 15$  and window length  $N = 1000$ . The units of  $\tau$  and  $N$  are samples. The time delay  $\tau$  was determined by the first zero-crossing of the corresponding autocorrelation function. Embedding dimension  $n$  was determined by the convergent estimate. The final estimate,  $S(X|Y)$ , was obtained by averaging the  $S^{(K)}(X|Y)$  computed with  $K$  ranging from 20 to 35.

### **IV-5 EEG Investigation Based on Spectral Power Analysis and Coherence Function Analysis**

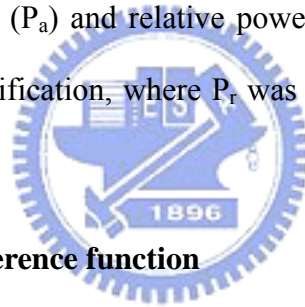
The nonlinear approaches allow a more comprehensive picture of the empirical data. Therefore, complementing the conventional, popular linear methods, we also employed the methodologies developed on the nonlinear-model basis in order to explore the multi-facet properties of brain dynamics based on EEG signals. For comparison and reference, we firstly conducted linear analysis on meditation EEG data. It is because, over the past forty years, EEG studies of meditation states have been mostly based on traditional linear approach of frequency and coherence analysis.

The primary findings have implicated increases in theta and alpha band power and decreases in overall frequency (for reviews, see Cahn & Polich, 2006; Andresen, 2000; West, 1980; Woolfolk, 1975). Increased alpha–theta range coherence among recording sites has been observed intra- and interhemispherically for state effects during meditation (Aftanas & Golocheikine, 2001; Dillbeck & Bronson, 1981; Gaylord et al, 1989; Travis, 2001; Travis & Pearson, 1999; Travis & Wallace, 1999; for reviews, see Cahn & Polich, 2006). In order to gain more insight into CNS dynamics varying with the states of Chan

meditation, our study accordingly employed spectral analysis and coherence function for further comparison with the results from nonlinear methods. In this section, we illustrate the traditional linear approach employed in the study

#### **IV-5-1 Estimation of spectral power**

EEG power spectra were estimated by conventional Fourier transformation of consecutive 5-second segments (overlapping 2.5 seconds) windowed by Hanning function. We evaluated spectral powers of various bands, including delta ( $\Delta$ , 0.2±3.8 Hz), theta ( $\theta$ , 4.0±7.8 Hz), alpha-1 ( $\alpha$ -1, 8.0±10.0 Hz), alpha-2 ( $\alpha$ -2, 10.2±12.8 Hz) and beta ( $\beta$ , 13.0±30.0 Hz), using a total of 360 data points (number of selected 5-sec epochs under meditation or rest) that can be common representative of the entire session of interest. In this article, the absolute power ( $P_a$ ) and relative power ( $P_r$ ) of each frequency band were employed in EEG pattern classification, where  $P_r$  was the ratio of each band power to the total power.



#### **IV-5-2 Estimation of coherence function**

Cross-correlation function is one of the most classical measures of interdependence between two time series. It measures the linear correlation, as a function of time shift ( $\tau$ ), between two variables  $X$  and  $Y$ . If  $x(t)$  and  $y(t)$  are signals normalized to have zero mean and unit variance, their cross-correlation function is:

$$r_{xy}(\tau) = \frac{1}{N - \tau} \sum_{k=1}^{N-\tau} x(k + \tau)y(k) \quad (4-9)$$

where  $N$  is the total number of samples and  $\tau$  is the time difference between two signals.

Coherence function, a generalization of correlation in the frequency domain, provides a straightforward medium for the assessment of ‘interaction’ at a specific frequency (Nunez et al., 1997; 1999). Coherence between two signals is the ratio between their cross-spectral density– which is also the Fourier transform of eq. (4-9) – and their individual auto-spectral

density. However, due to the limitation of the length of wide-sense, stationary EEG, one can only obtain an estimate of the true spectrum. Smoothing techniques are often used to improve the performance of the spectral estimators. Thus, we estimate the coherence function using Welch's method that mainly averages the modified periodogram (Welch, 1967). EEG signals are usually subdivided into  $M$  overlapping, equal sections. Then the spectra are estimated by averaging the periodograms of these sections. Finally, the coherence is calculated as:

$$C_{xy}^2 = \frac{\left| \langle S_{xy}(f) \rangle \right|^2}{\left| \langle S_{xx}(f) \rangle \right| \left| \langle S_{yy}(f) \rangle \right|} \quad (4-10)$$

where  $\langle \cdot \rangle$  indicates the arithmetic operation of averaging over the  $M$  segments.

EEG coherence is a measure of the synchronization between two recording sites and may be interpreted as an expression of their functional interaction. We studied EEG coherence in the phases of meditation (M and Z) in comparison with the rest (R). The aims of this study are to investigate the changes of EEG coherence between left and right hemispheres and frontal versus occipital cortex during meditation. In order to test the spatial homogeneity of EEG coherence, Thatcher et al. (1986) proposed a two-compartmental model of EEG coherence in which different features of coherence were produced by different length fiber systems. Based on this model, EEG coherence was produced by at least two separate sources (1) the action of short length axonal connection, and (2) the action of long distance connections. Excluding the contribution of volume conductor, coherence between near electrodes is mainly influenced by short connections since the axonal density per unit volume of cortex in the short-axoned stellate and Martinotti cells is approximately 10–100 times higher than the density in the long-axoned pyramidal cells (Braitenberg, 1978; Locatelli, et al., 1998). On the contrary, the coherence between distant electrodes is mainly due to long axon connections.

As the number of parameters was very high ( $\frac{1}{2}n \times (n - 1)$  for each frequency band for  $n$ -channel EEG data), we decided to reduce the number of coherence parameter to be put under calculation. For simplification, EEG coherence was computed for 19 scalp locations from 30 channel EEG recordings as showed in Fig. 4-2. Coherences for delta ( $1.5 \leq \delta < 4$  Hz), theta ( $4 \leq \theta < 8$  Hz), alpha-1 ( $8 \leq \alpha-1 < 10$  Hz), alpha-2 ( $10 \leq \alpha-2 < 13$  Hz), beta-1 ( $13 \leq \beta-1 < 15$  Hz), beta-2 bands ( $15 \leq \beta-2 < 25$  Hz) and beta-3(gamma-1) bands ( $25 \leq \beta-3 < 35$  Hz) were calculated as the mean coherence values of the three 3-min epochs selected (R, M and Z).

In order to evaluate whether the changes were mostly related to the short axonal fibers or to the long ones, coherences were calculated according to Thatcher et al. (1986) by averaged coherence among ‘local’ and ‘far’ recording sites overlying the distribution of different cortico-cortical fibers in order to have information about transmission of the underlying fibers. The average of the coherences between electrodes located in frontal and antero-temporal regions were used for calculating the local anterior coherence (A, as showed in Fig. 4-2(a) Fp1–F7, Fp2–F8, Fp1–F3, Fp2–F4, Fp1–C3 Fp2–C4, F7–C3, F8–C4, F3–C3 F4–C4, F3–F7 and F4–F8). For the posterior brain region, the local posterior coherence was calculated as the average of coherence values between temporo-parieto-occipital electrode pairs (P, as showed in Fig. 4-2(a) O1–P3, O2–P4, O1–P7, O2–P8, O1–C3, O2–C4, P3–C3, P4–C4, P7–C3, P8–C4, P3–P7, P4–P8 and). For posterior to anterior coherence (P-A), we averaged coherences between pairs of electrodes O1–Fp1, O2–Fp2, O1–F3, O2–F4, O1–C3, O2–C4, O1–P3 and O2–P4 and for anterior to posterior coherence(A-P) Fp1–O1, Fp2–O2, Fp1–P3, Fp2–P4, Fp1–C3, Fp2–C4, Fp1–F3 and Fp2–F4, respectively(see Fig. 4-2(b)). This far coherence is assumed to be the mean coherence transmitted by the superior longitudinal fasciculus in both postero-anterior and antero-posterior directions (Locatelli, et al., 1998). In order to evaluate interhemispheric change with meditation, data from eight homologous right-left (R-L) electrode pairs were also examined. The R-L electrode pairs are as follows: Fp2-Fp1, F8-F7, F4-F3, T8-T7,

C4-C3, P8-P7, P4-P3, O2-O1.

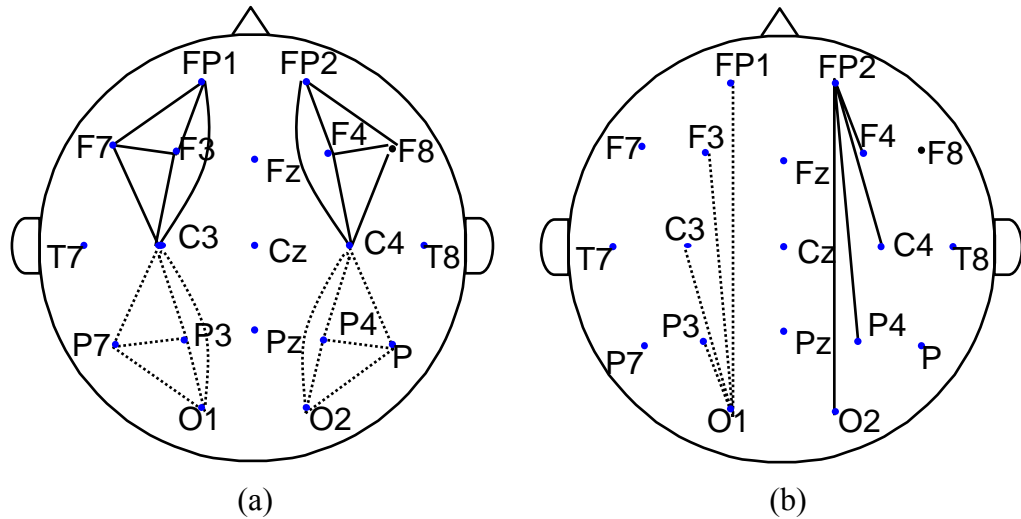


Fig. 4-3 Recording sites for ‘local’ and ‘far’ coherences (a) local anterior and posterior coherences (dotted line) (b) antero-to-posterior and postero-to-anterior directions (dotted line)

## IV-6 Statistical Analysis

### IV-6-1 Spatiotemporal characteristics of Chan meditation EEG

Statistical analyses were carried out using the software package MATLAB (The Math Work, Inc., U.S.A.) to test possible differences between (1) meditation and control groups, (2) 30 recording sites and (3) three sessions during meditation or rest in EEG power and  $\bar{\delta}$ . We used the repeated-measures ANOVAs (with post hoc paired *t*-test for characterizing significant interactions), with the group as between-subject factor and the session and the electrode as within-subject factors. The Greenhouse–Geisser correction of *P*-values was applied to the degrees of freedom when appropriate. Due to the skewed distribution of EEG band power, logarithmic transformation of each  $P_a$  was applied to obtain a better

approximation of a normal distribution. Only significant effects ( $P<0.05$ ) involving factors are reported below.

#### IV-6-2 Synchronization in different meditating phases

Each EEG data set was divided into 36 non-overlapping, consecutive 5-sec segments. In each session,  $S$  indexes were calculated for 342 (=18×19) pairs composed by 19 electrodes. Meanwhile, coherence for each frequency band and for A, P, P-A and A-P connections were calculated from 171 (=18×19/2) pairs composed by 19 electrodes. For each subjects, data was averaged over 36 segments for each session. Means and standard deviations of each state were then calculated. To justify the Normal distribution of the results, we adapted the Kolmogorov-Smirnov Goodness of Fit Test. Statistical differences of  $S$  indexes and coherence were determined using paired Student's  $t$ -test for the comparison between baseline state R versus the meditation states M and Z. Then, results with significant difference (error probability of  $P<0.05$ ) are reported below. For each pair of channels, variations between sessions were evaluated by calculating differences ( $d$ -values) between mean  $S$ 's of two sessions, and then normalized by their standard deviation:

$$d = \frac{\bar{D}}{\sqrt{\frac{\sigma_D^2}{n}}}, \quad D = S_Z - S_R \text{ or } S_M - S_R \quad (4-11)$$

Also, Coherence modifications between sessions were performed by calculation of differences ( $d$ -values) between mean coherence values of the two sessions, normalized to their standard deviation:

$$d = \frac{\bar{D}}{\sqrt{\frac{\sigma_D^2}{n}}}, \quad D = C_Z - C_R \text{ or } C_M - C_R \quad (4-12)$$


## Chapter V

### RESULTS

This is the first attempt to investigate the EEG phenomena, for this particular group, in the course of Chan-Buddhist meditation based on nonlinear dynamics. As the complexity index reflects the fractional dimension of CNS, it provides certain nonlinear measures that can be used to monitor the meditation process. Section V-1 shows the results of spatiotemporal characteristics of Chan Meditation EEG using complexity measure. Section V-2 shows the results of coherence function and  $S$  measure to investigate the EEG synchronization in different meditating phases.

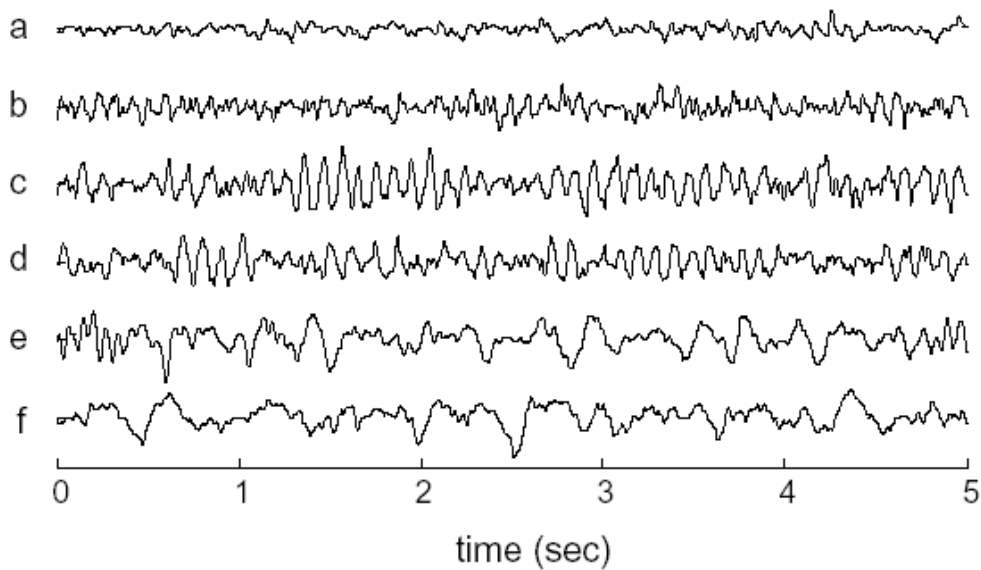
#### V-1 Spatiotemporal Characteristics of Chan Meditation EEG

##### V-1-1 Meditation EEG features



The meditation EEG records collected from Chan-Buddhist disciples exhibit some characteristic features that have been constantly observed. Six typical EEG rhythms shown in Fig. 5-1 demonstrate the time, frequency properties as well as their complexity indexes. In Fig. 5-1(a), the top tracing characterizes the deep meditation (also called ‘*samadhi*’ or ‘*transcendence*’) EEG that may be correlated with the Alaya (eighth) conscious state and is often observed in experienced meditators. The EEG at this stage was found to be characterized by the “silent” beta rhythm with small amplitude (to be symbolized by  $\Phi$  in this paper). The second tracing ‘b’ represents normal high frequency  $\beta$  rhythm which was observed mostly when the meditator entered into a peaceful, body-mind unified, and somehow beyond normal consciousness state. The tracings ‘c’ and ‘d’ are mainly  $\alpha$  rhythms with  $\alpha$ -1 component appearing in the 4<sup>th</sup> tracing. Slower  $\alpha$  (8~10Hz) with larger amplitude was frequently reported in the beginning of meditation (West, 1980) and was related to the

mindful-concentration state. In Chan-Buddhist practice, meditators normally concentrate their mind on particular Chakra(s) in the beginning to release themselves from the flight of the imagination. We found that the EEGs of a few subjects at this meditating stage exhibited a large portion of slow  $\alpha$  rhythm. As the Chan meditation proceeds, much slower  $\theta$  and  $\Delta$  rhythms may appear in some subjects. According to subjective narration by meditators, they may feel drowsy or enter the seventh consciousness (sub-consciousness). Patterns 'e' and 'f' at the bottom demonstrate generalized slow activities dominated respectively by  $\theta$  and  $\Delta$  rhythm. Fig. 5-1(b) plots the corresponding Fourier spectra. All the six segments in Fig. 5-1(a) have been baseline corrected by a wavelet high-pass filter.



(a)

Fig. 5-1 Meditation EEG characteristics. (a) The 5-sec EEG segments demonstrate six major prototypes observed during meditation (from top downwards): flat beta, high-frequency beta, alpha, alpha-1, theta and delta activities. (b) Fourier magnitude spectra of meditation EEG prototypes in (a), with baseline and low frequency components removed. (c) The 2D phase trajectories and (d) complexity indexes ( $\delta$ ) varying with  $k$  (number of nearest neighbors) for meditation EEG prototypes in (a). Range of  $k$  (20~35) used to estimate  $\bar{\delta}$  is shown by two dashed lines.



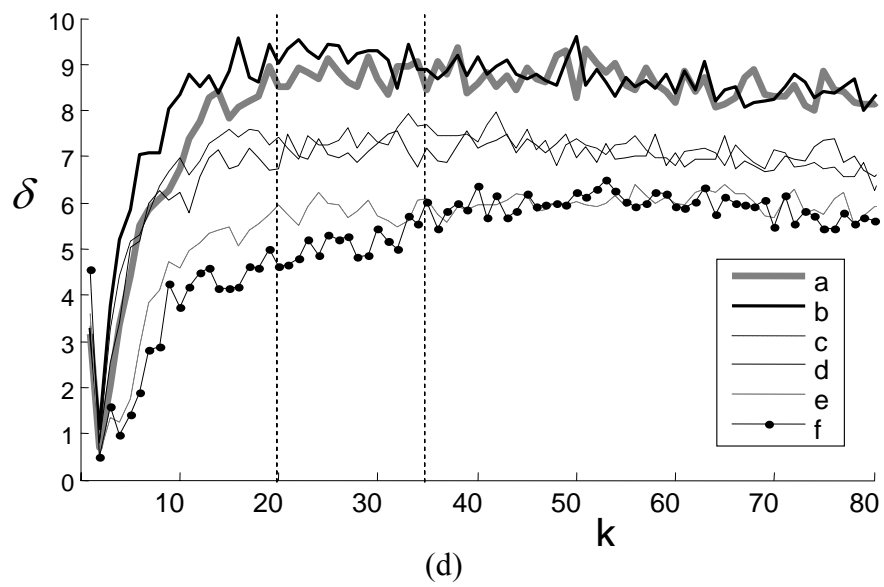
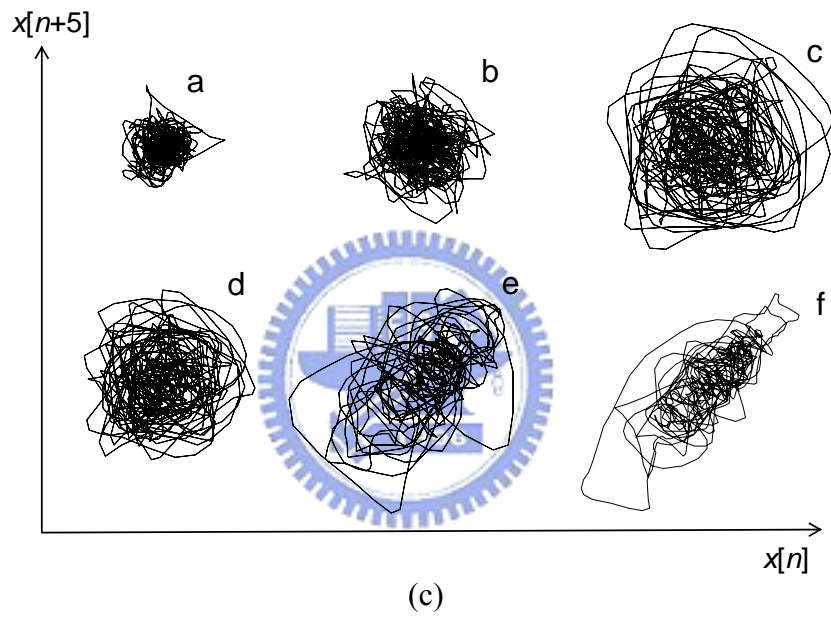
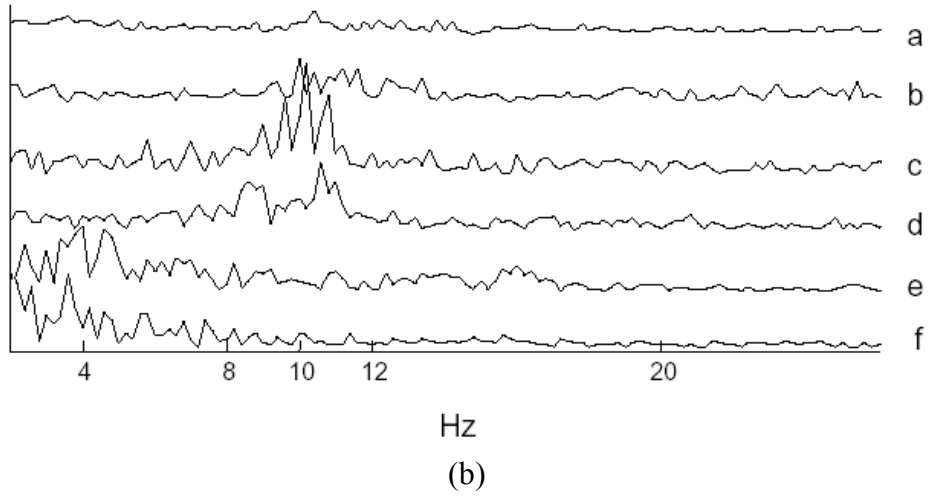


Fig. 5-1 (continue)

In Fig. 5-1(c), the 2D (two-dimensional) phase trajectories are constructed from the EEG epochs in Fig. 5-1(a) using a delay of 5 samples (0.025 second). Apparently, the silent and  $\beta$  patterns have phase trajectories of shrinking dynamic extent, yet with higher degrees of irregularity. The  $\alpha$  trajectory exhibits harmonious orbital patterns with high coherence. Both the  $\theta$  and  $\Delta$  trajectories involve dynamics of multi-modes, that is, the system dynamics are governed by two or more nonlinear mechanisms with different degrees of freedom. In Fig. 5-1(c), the  $\theta$  and  $\Delta$  trajectories apparently travel different spans in the phase space. This phenomenon is mostly caused by the simultaneous emergence of multiple EEG rhythms, for instance, the  $\Delta$  accompanied by  $\beta$  rhythm. In the case, outer orbits track the  $\Delta$  activity, while the inner orbits follow the  $\beta$  rhythm. This phenomenon results in two distinct estimates for the complexity index  $\delta$ . First, small  $K$  indicates that the  $d_{i,KNN}$  ( $KNN$  distance), obtained after searching all the orbital points, most likely characterizes orbits of the same attribute. As  $K$  becomes large, the  $d_{i,KNN}$ , on the other hand, may represent the inter-distance between two orbital points that track different EEG rhythms. Fig. 5-2 illustrates the dependence of complexity index  $\delta$  on  $K$  for three  $\Delta$  trajectories. Two distinct platforms appear on each curve, reflecting the multi-modal nonlinear mechanism. The lower platforms ( $K$  below 40) tend to characterize the  $\Delta$  trajectories; while the higher platforms ( $K > 60$ ) characterize the mix-modal nonlinear dynamics since computing the  $KNN$  distances often involves pairs of orbits corresponding to different EEG rhythms. As a consequence, the  $\delta$  estimated is much higher. To determine the appropriate range of  $K$ 's, it follows that a small  $K$  actually emphasizes the effects of superimposed noise while a large  $K$  causes the measurement involving multi-modal effects. Since the phenomenon of multi-modal effect is not evident for normal  $\alpha$ ,  $\beta$  and  $\Phi$  rhythms,  $\bar{\delta}$  computation is rather insensitive to a wide range of  $K$ . Accordingly, reliable estimates of  $\bar{\delta}$  can be obtained with  $K$  ranging from 20 to 35 that are feasible for characterizing different EEG patterns.

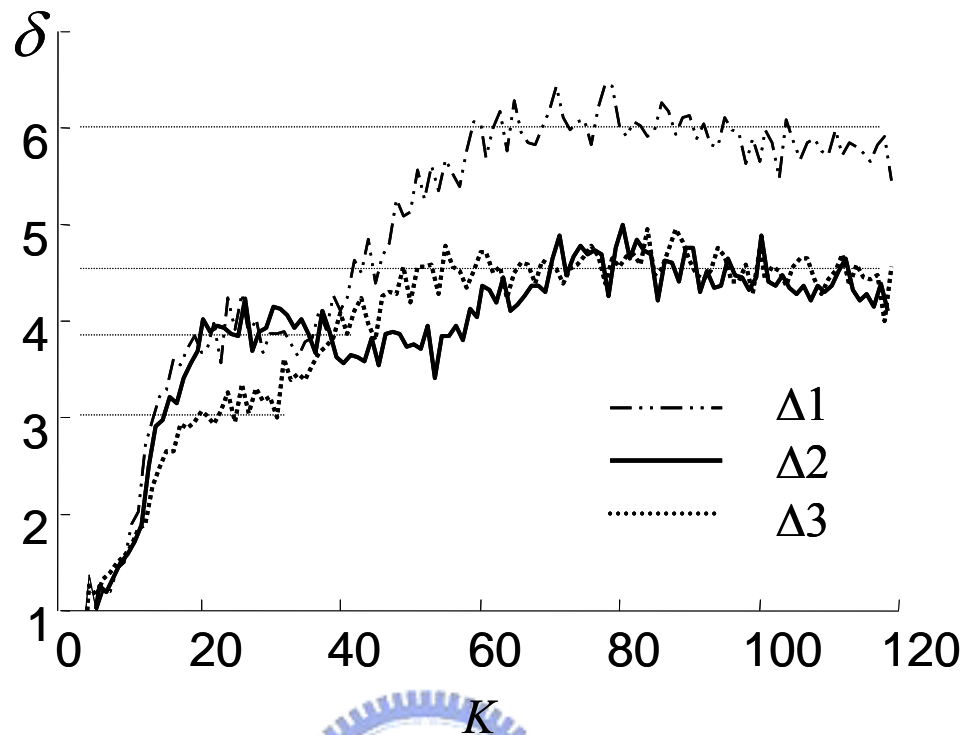


Fig. 5-2 The dependence of  $\delta$  on values of  $K$  when analyzing the complexity index of the  $\Delta$  rhythmic activity (for  $n=6$ ,  $\tau=5$  and  $N=1000$ ).

At the current stage, the profiled meditation EEG patterns can be effectively differentiated into different groups based on the complexity-index analysis. The first issue encountered is the selection of implementing parameters. There is no analytical way to determine optimal parameters. Empirically based selection of time delay  $\tau$  and embedding dimension  $n$  provides satisfactory results for interpreting meditation stages. In order to track potentially rapid changes in complexity, the analysis is performed over a short window length of 5 sec ( $N=1000$ ). Embedding dimension is chosen to be 15 since, for  $n$  above 15, the tendency of complexity index remains unchanged and the results of EEG analysis do not present significant changes. Time delay  $\tau$  is determined by the first minimum of the autocorrelation function of EEG (Elbert *et al.*, 1994). The parameters applied in this study are: dimension  $n=15$ , time delay  $\tau=5$  samples (0.025 second), and

length  $N=1000$  samples (5 seconds). The final estimate,  $\bar{\delta}$ , is obtained by averaging the  $\delta$ 's derived with  $K$  ranging from 20 to 35. Fig. 5-1(d) displays the relationship between complexity index and the  $K$ 's nearest neighboring for the EEG's in Fig. 5-1(a). Vertical, dashed lines indicate the averaged range of  $K$  (20~35) for estimating  $\bar{\delta}$ . As shown in Fig. 5-1(d), fast  $\beta$  tracings 'a' and 'b' exhibit higher values of  $\bar{\delta}$  while slow activities consisting of predominant  $\alpha$  and  $\theta$  result in lower dimension. Based on nonlinear computation, the profiled meditation EEG patterns can be effectively differentiated into three groups. As shown in Table 5-1, Group I contains the patterns of great interest in our meditation EEG study. Complexity-index analysis fails to discriminate between the  $\beta$  and the "silent" ( $\Phi$ ) patterns. Group II is accordingly denoted by ' $\Phi/\beta$ '. Both are highly correlated with the serene, "beyond-consciousness" brain dynamics according to our investigation. Average complexity index of this group is  $8.83 \pm 0.49$ , estimated from 59 sampled epochs comprising the small-amplitude, high-frequency rhythmic patterns during the meditation condition. Average  $\bar{\delta}$  for Group II is  $7.23 \pm 0.48$ , estimated from 69  $\alpha$ -rhythm epochs. Complexity-index analysis fails to discriminate between  $\alpha$ -1 and  $\alpha$ -2 patterns. Group III apparently has the lowest  $\bar{\delta}$  ( $6.55 \pm 0.59$ ) and contains  $\theta$  and  $\Delta$  patterns which occurred intermittently in the midst of meditation. EEG patterns of this group are thus denoted by ' $\theta+\Delta$ '. Furthermore, group III has a broader range of dynamical complexity mainly caused by multi-rhythmic patterns in this group. It should be noted that each meditator has his/her particular symphony of meditation EEG patterns. Not every pattern appears in the meditation course. We thus explore the meditation EEG schema in the next section based on the variation of running  $\bar{\delta}$ . Table 5-1 also lists the relative power of each group.

Table 5-1 The statistical results of complexity index ( $\bar{\delta}$ ) and relative powers in different frequency bands of characteristic EEG features collected from 23 meditators (mean  $\pm$  std for each group); implementing parameters applied:  $n=15$ ,  $\tau=5$  samples, epoch length: 5 seconds (1000 samples),  $20 \leq K \leq 35$ .

Group	$\bar{\delta}$ (Mean $\pm$ std)	Number of epochs analyzed	$P_r(\theta+\Delta)$	$P_r(\alpha)$	$P_r(\beta)$
I: $\Phi/\beta$	$8.83 \pm 0.49$	59	$0.28 \pm 0.14$	$0.50 \pm 0.14$	$0.21 \pm 0.08$
II: $\alpha$	$7.23 \pm 0.48$	69	$0.17 \pm 0.10$	$0.74 \pm 0.11$	$0.09 \pm 0.03$
III: $\theta+\Delta$	$6.55 \pm 0.59$	56	$0.77 \pm 0.15$	$0.16 \pm 0.15$	$0.06 \pm 0.03$

### V-1-2 Chan Meditation EEG scenarios

This section discusses long-term evolution of CNS dynamics, based on running  $\bar{\delta}$ 's, under various states of consciousness during meditation. Increased insight into correlation between the “consciousness” states and the nonlinear quantitative indexes may provide access to both the meditation depth and the meditation scenario. Fluctuation of  $\bar{\delta}$  reflects time evolution of the CNS nonlinear mechanisms generating the meditation EEG activities profiled in the previous section. Three distinct groups of EEG phase trajectories are discernible in consideration of characterizing the meditating EEG patterns based on the estimated  $\bar{\delta}$ . In consideration of providing an overview of meditation EEG records, the running  $\bar{\delta}$  is directly displayed as a gray-scale chart by mapping the resulting range of  $\bar{\delta}$ , ( $\bar{\delta}_{\min}, \bar{\delta}_{\max}$ ), into the gray-scale range, (0, 255). The running measurement uses a window length of  $N=1000$  (5 seconds) and a moving size of 100 points (0.5 second).

We have reported previously (Lo, Huang, and Chang, 2003) our observation of a significant correlation between perception of the inner light (spiritual energy inside the

third ventricle, the Zen Chakra shown in Fig. 1-1) and the alpha blocking in the occipital cortical region, after performing a few studies on different subjects. On the other hand, there are more noisy recordings appearing on the O1 channel according to our experience. We thus focus our investigation on channel-O2 EEG that reflects a meditating stage of particular interest in Chan-Buddhist meditation. According to the results of analyzing the meditation EEG's of 17 experimental subjects, we identified three different groups (M1, M2, and M3) of meditation EEG scenarios. Each group reflects a typical temporal evolution of brain electrical activities and states of consciousness. Details are illustrated below. Table 5-2 illustrates the characteristics of three experimental groups and one control group. Fig. 5-3 displays the 25-minute running  $\bar{\delta}$  measures for the representatives in the control group (C1) and three experimental groups. Each long strip of gray-scale image traces the running  $\bar{\delta}$ 's for five minutes (approximately 600  $\bar{\delta}$ 's). Brighter gray (larger  $\bar{\delta}$ ) highly correlates with the occurrence of  $\beta$  rhythm or low-voltage activity ( $\Phi/\beta$ ). The  $\alpha$  rhythm mostly results in mid-tone grays. As the EEG oscillates at a slower rate, often accompanied by increasing amplitude ( $\theta+\Delta$ ), the gray becomes darkened. In the control group, a typical gray-scale chart of running  $\bar{\delta}$  mostly contains a large portion of mid-tone grays (C1 section in Fig. 5-3). On the other hand, the meditation EEGs of experimental subjects reveal quite different characteristics. In our study of seventeen experienced Chan-Buddhist meditators, the meditation scenarios, based on the running  $\bar{\delta}$  measures, can be categorized into three distinct groups: bright-to-mid/dark grays (M1), mid-to-bright grays (M2), and all-bright grays (M3). Meditators of group M1 reveal a meditation process beginning with  $\Phi/\beta$  activities, transiting through irregular  $\alpha$  or slow-rhythm ( $\theta+\Delta$ ) intermittent stage, and settling at the rhythmic  $\theta$  trains or  $\alpha$  dominated activities after a twenty-minute meditation. Most subjects in group M1 did not achieve good-quality meditation due to drowsiness (which normally occurred at the sub-consciousness state) or mental alertness. The meditation EEG of group M2 exhibits characteristics totally different

from that of group M1. In the beginning meditation,  $\alpha$  dominates the EEG, reflecting the brain state in relaxed, normal consciousness. As a meditating session continued, however,  $\beta$ -rhythm occurred or, alternatively, EEG power was significantly suppressed occasionally. A group-M2 meditator with seven-year meditation experience portrayed his meditation scenario as follows: "... as I felt the energy vibrating inside my body, I also perceived magnificent light, green, red, and purple light, that was beyond imagination, without doubt." Another one described the experience of entering a realm of totally peaceful and uniform mind after transcendence "... at which state I felt myself surrounded by sacred light." "Moreover, some kind of energy, or supernatural power drilled through my skull and rejuvenated my brain and body," added by the same person. And we find that most Chan-Buddhist disciples experience this kind of *supernaturalism*. Meditators in the third group (M3) reveal a common feature,  $\Phi/\beta$ , throughout the meditation course. The low-amplitude EEG sometimes has its amplitude suppressed down to almost null. Or, large amounts of  $\beta$ -rhythms may emerge. They mostly experienced the transcendental, sacred aura with mind-body uniformity during the entire meditation course. A typical example was recorded from one meditator with ten-year meditation experience, who is also an artist specializing in Buddhist-stature art painting. He is one of a few disciples in this Chan-Buddhist group who often perceive the sacred Buddhist statue with their Dharma eye. This observation coincides with our previous report (Lo, Huang, and Chang, 2003).

Table 5-2 Characteristics of EEGs and the range of more than 70% of  $\bar{\delta}$  for the control group and three experimental groups.

	O2 EEG characteristics	$\bar{\delta}$ range (1 <sup>st</sup> 5 min)	$\bar{\delta}$ range (last 5 min)
C1	$\alpha$ dominates, ( $\theta+\Delta$ ) emerges intermittently	7.0-8.3	7.0-8.3
M1	Transit from $\Phi/\beta$ to irregular, intermittent $\alpha$ or ( $\theta+\Delta$ )	>8.3	7.35-8.3
M2	Transit from $\alpha$ dominating to $\Phi/\beta$	7.0-8.3	>8.3
M3	$\Phi/\beta$ dominates throughout the meditation course	>8.3	>8.3

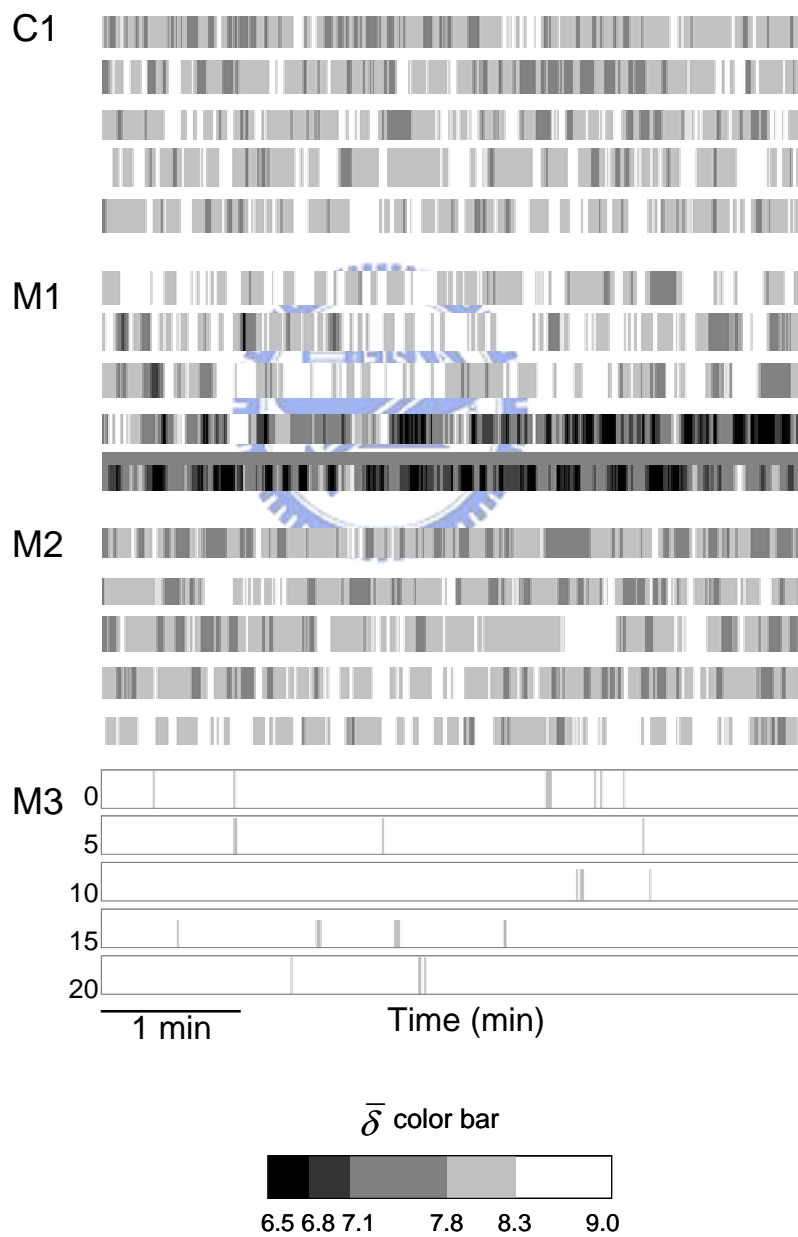


Fig. 5-3 The 25-minute running  $\bar{\delta}$  charts (channel O2) for the representatives in the control group (C1) and experimental groups (M1, M2, and M3).



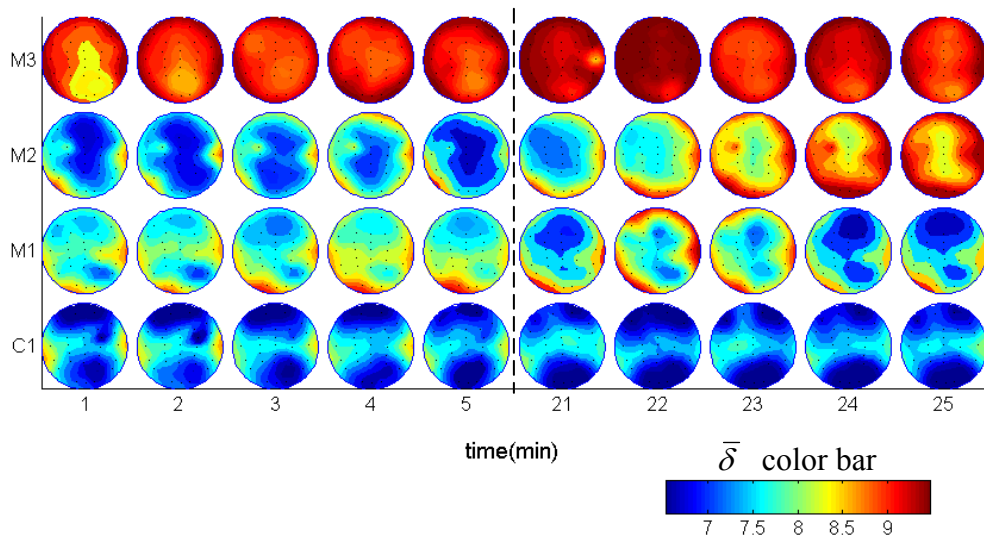


Fig. 5-4 The brain mappings of  $\bar{\delta}$  averaged over one minute for the control group C1 and the experimental groups M1, M2, and M3. The  $\bar{\delta}$  mappings for the first and the last five minutes are shown.

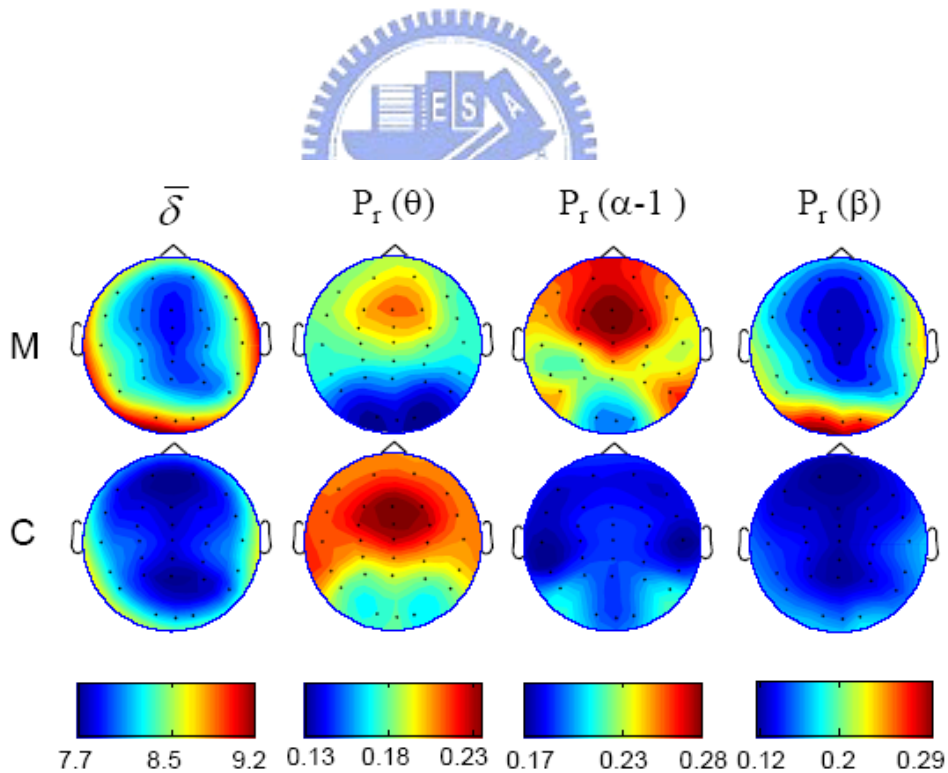


Fig. 5-5 Brain mappings of  $\bar{\delta}$ 's (leftmost column) and power spectra  $P_r()$ 's for meditators (M, top) and control subjects (C, bottom), with EEG signals selected from the mid-5min segments of main 40min meditation/relaxation sessions.

In Fig. 5-4, we further present the brain mappings of one-minute averaging  $\bar{\delta}$  reconstructed from the 30-channel EEGs. The  $\Phi/\beta$ -dominated EEG of groups M2 and M3 is evident in the brain mapping. Group M2 shows higher  $\bar{\delta}$ 's in the occipital and parietal regions, indicating the occurrence of significant  $\Phi/\beta$ . Group-M3 subjects have an extraordinary EEG during the entire meditation session—— consistent  $\Phi/\beta$  activities spread all over the scalp. Brain dynamics of high dimension and high complexity might be referred to the *transcendental* state of consciousness. After a twenty-minute recording, the  $\bar{\delta}$  charts differ a lot among the four groups (right side of Fig. 5-4). The brain mapping for the group-C1 control subjects remains about the same. Group-M1 EEG basically is composed of the same rhythmic patterns, yet with an increasing proportion of  $\alpha$  rhythms on the parietal and frontal regions. Group-M2 subjects enter into the high-complexity brain dynamics ( $\Phi/\beta$ ), as in group M3, all over the scalp during the last few minutes.



### V-1-3 Spatio-temporal resolution of experienced meditators

According to the preliminary findings, we speculated that the deep meditation state was accompanied by an increase of beta activity which correlated positively with complexity. Consequently, we mainly investigated the long-term Chan-meditation practitioners because, compared with novices, advanced practitioners might experience different physiological and psychological states and traits. This paper presents the further study of the Chan-meditation brain dynamics varying with the meditation process based on the complexity evaluation and spectral analysis.

In order to explore topological features of meditation-EEG  $\bar{\delta}$ , we analyzed statistical significance of average  $\bar{\delta}$ 's based on two-way ANOVAs involving two factors: Group (meditation, rest) and Site (30 recording electrodes). The average  $\bar{\delta}$ 's were derived by averaging the results of all epochs for each subject. ANOVAs revealed significant effects

of Group and Site (both  $P < 0.0001$ ). While compared with the control group, meditation group exhibited higher  $\bar{\delta}$ , especially at occipital, temporal and anterior regions (for the post t-test,  $P < 0.01$  for O1, O2, Oz, T8, FT8, F8, F7 and Fp1;  $P < 0.05$  for Pz, TP8, P3, TP7, FT7, Fp2 and T7). Brain mappings in Fig. 5-5 were reconstructed from the 30-channel results of analyzing the mid-5min segments (M: meditators, C: control subjects). The leftmost column shows the group average  $\bar{\delta}$ , that is, average of  $\bar{\delta}$ 's estimated from all the 23 subjects in the experimental and control group. The other three columns display the mappings of relative power. Note that, in meditation group, their  $\bar{\delta}$ 's increased progressively from frontal to posterior region and reached a high at centro-occipital Oz, while the control had a low average  $\bar{\delta}$  at Pz (see Fig. 5-5). To further investigate intra-group differences, a paired, two-sided t-test was performed.  $\bar{\delta}$  values for the two groups revealed no significant hemispheric asymmetry (except the pairs  $P3 > P4$  and  $P7 > P8$  for the experimental group and  $P7 > P8$  for the control group, all  $P < 0.01$ ).

Next, we discuss long-term evolution of EEG dynamics during meditation course. Since differences between the right and left hemisphere were not significant, we focused our investigation on EEG's mainly for sites on the midline regions (Fz, FCz, Cz, CPz, Pz, Oz). Spectral power values and complexity index were further analyzed in subjection to three-way ANOVAs: Group (meditators, non-meditators)  $\times$  Site (6 midline electrodes)  $\times$  Session (the first-, mid- and the last-5min). Significant results are showed in Table 5-3. To demonstrate the differences between sessions in each group, Fig. 5-6 displays the amount of the change of  $\theta$  and  $\beta$  power (in percentage) from one session to the other.

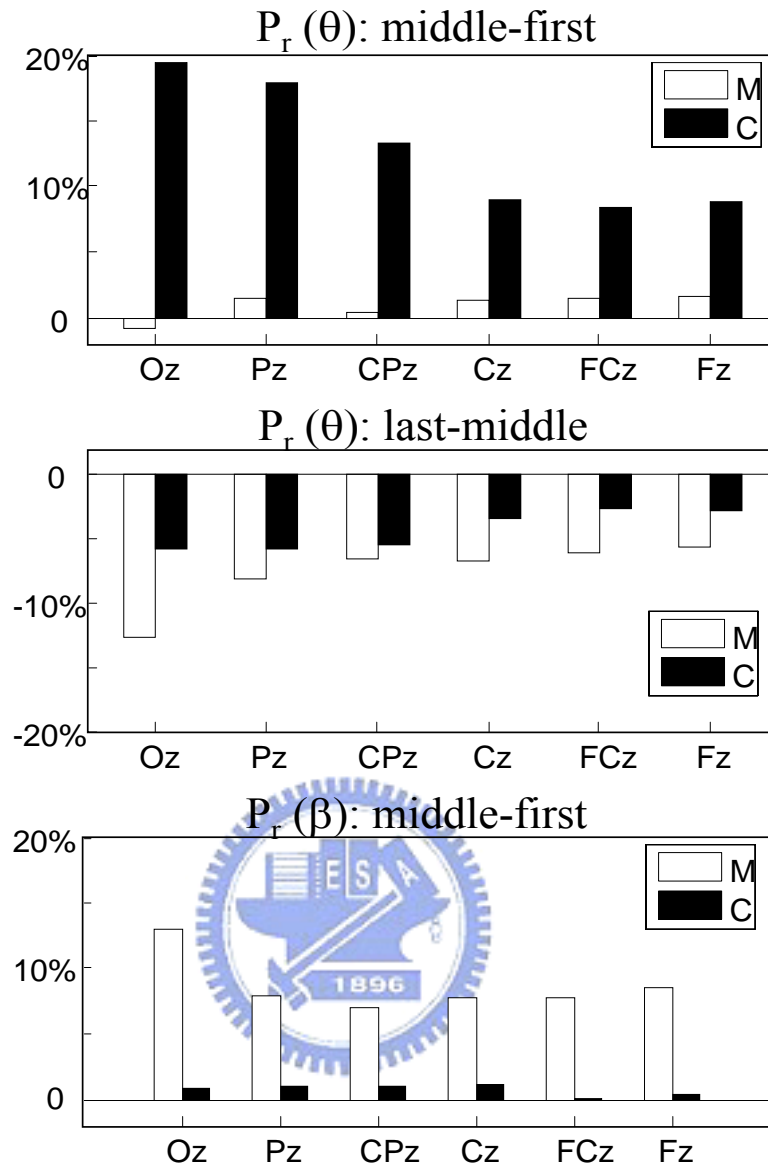


Fig. 5-6 Percentage of power differences between sessions derived by: (top) subtracting the first-5min  $P_r(\theta)$  from the mid-5min's; (middle) subtracting the mid-5min  $P_r(\theta)$  from the last-5min's and (bottom) subtracting the first-5min  $P_r(\beta)$  from the mid-5min's.

Table 5-3. ANOVA Results of Spectral Powers

Factor	<i>d.f.</i>	$P_r(\theta)$		<i>d.f.</i>	$P_a(\theta)$	
		<i>F</i>	<i>P</i>		<i>F</i>	<i>P</i>
Group	1	28.68	0.0000	1	18.00	0.0000
Session	2	2.56	NS	2	4.81	0.0084
Site	5	20.84	0.0000	5	33.72	0.0000
Factor	<i>d.f.</i>	$P_r(\alpha-1)$		<i>d.f.</i>	$P_a(\alpha-1)$	
		<i>F</i>	<i>P</i>		<i>F</i>	<i>P</i>
Group	1	31.57	0.0000	1	17.13	0.0000
Session	2	0.39	NS	2	2.67	0.0697
Site	5	2.89	0.0135	5	12.09	0.0000
Factor	<i>d.f.</i>	$P_r(\beta)$		<i>d.f.</i>	$P_a(\beta)$	
		<i>F</i>	<i>P</i>		<i>F</i>	<i>P</i>
Group	1	31.37	0.0000	1	0.43	NS
Session	2	1.22	NS	2	3.37	0.0347
Site	5	42.42	0.0000	5	4.21	0.0009

NS = not significant

*d.f.* = the degrees of freedom associated with each factor

*F* = F statistics

*P* = significance associated with F and *d.f.*

ANOVAs revealed significant effects of Group  $\times$  Site interaction ( $F_{5,264} = 4.89$ ,  $P < 0.0003$ ) only for relative beta power ( $P_r(\beta)$ ).  $P_r(\beta)$  was shown to be higher in the meditation state and attain highest value at Oz. Greatest differences ( $P < 0.05$ ) of  $P_r(\beta)$  between two groups were found for last-5min and for the Oz electrode (as the bottom panel of Fig. 5-6). Significant differences of  $P_a(\beta)$  revealed a higher power in last-5min compared to first-5min, especially for the meditation group ( $P < 0.05$ ).

Relative alpha-1 power ( $P_r(\alpha-1)$ ) and absolute alpha-1 power ( $P_a(\alpha-1)$ ) were higher in meditation state, especially at frontal electrode sites (Fz and FCz,  $P < 0.05$ ). Temporally,  $P_a(\alpha-1)$  increased as meditation progressed; while the control group did not reveal such a tempo during rest. Differences between groups were distinguished for the mid-5min and last-5min sessions ( $M > C$ ,  $P < 0.05$ ). Relative theta power ( $P_r(\theta)$ ) and absolute theta power ( $P_a(\theta)$ ) were lower during meditation as compared to that of control group at rest. There

appeared a general higher value of theta power during the last-5min session of non-meditating, rest state at all the recording sites ( $P < 0.05$ ), especially the frontal Fz and FCz. On the other hand, theta level of meditators appeared to be quite constant between different sessions. Tendency of  $Pr(\theta)$  was somewhat different. In experimental group,  $Pr(\theta)$  exhibited an overall decrease, especially pronounced over occipital regions, as the meditating session continued (as the top and middle panels of Fig. 5-6).

Differences between various meditation stages can also be traced by the nonlinear measures. Similarly with  $Pr(\beta)$ ,  $\bar{\delta}$  was larger in the later stages than in the earlier stage for the experimental group, but not for the control group. Finally, we investigated the relationship between  $\bar{\delta}$  and  $P_r$  for different frequency bands. A negative correlation between  $\bar{\delta}$  and  $P_r$  was observed for the delta ( $r = -0.33$ ) and theta band ( $r = -0.44$ ). On the other hand,  $\bar{\delta}$  correlates positively with alpha band ( $r = 0.21$ ). Notice that a clear positive correlation ( $r = 0.84$ ) was observed between  $\bar{\delta}$  and relative beta power. On the basis of a number of empirical studies, the threshold for beta level is selected to be  $> 8.3$ . Detailed spatio-temporal variations of three sessions in each group are displayed in Fig. 5-7 as the time percentage of  $\bar{\delta}$ . As the index  $\bar{\delta} > 8.3$  can reliably reflect the emergence of beta wave, we thus investigated, for each 5 min recording period, the amount of time within which  $\bar{\delta} > 8.3$ . Time percentage of highly complex EEG activities in the meditation period helps us explore the quality and consistency of meditation stage.

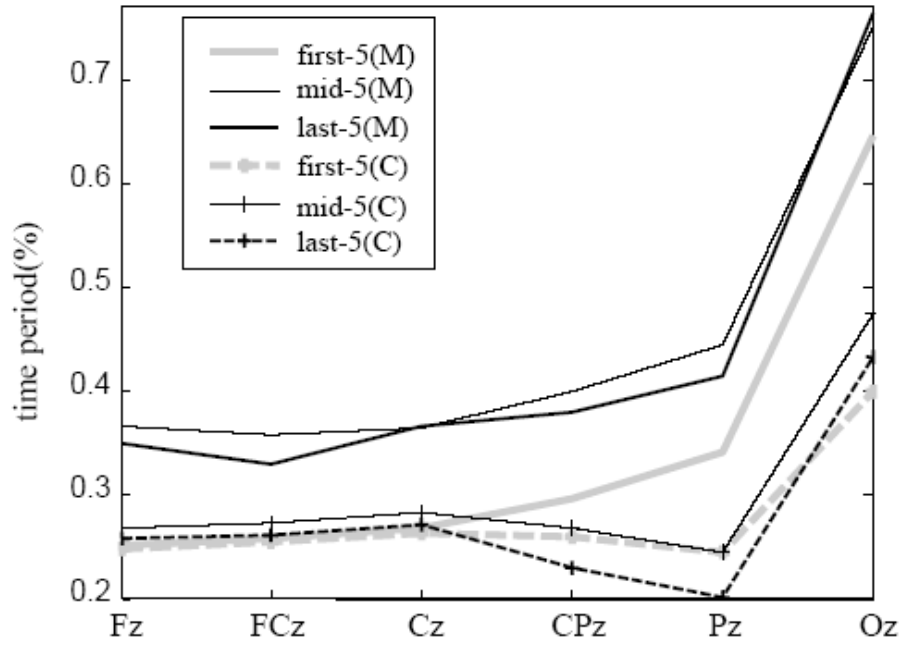


Fig. 5-7 The percent time during which  $\bar{\delta} > 8.3$  was present within each 5-min recording period for the meditation group (M) and the control group (C).



## V-2 Synchronization in Different Meditative Phases

This section shows the results of EEG coherence and  $S$  measure during different meditating phases. The aims of the study are to obtain if there are changes of EEG interdependence between left versus right hemispheres and frontal versus occipital cortex during meditation, to evaluate whether short-distance or long-distance interaction is more affected.

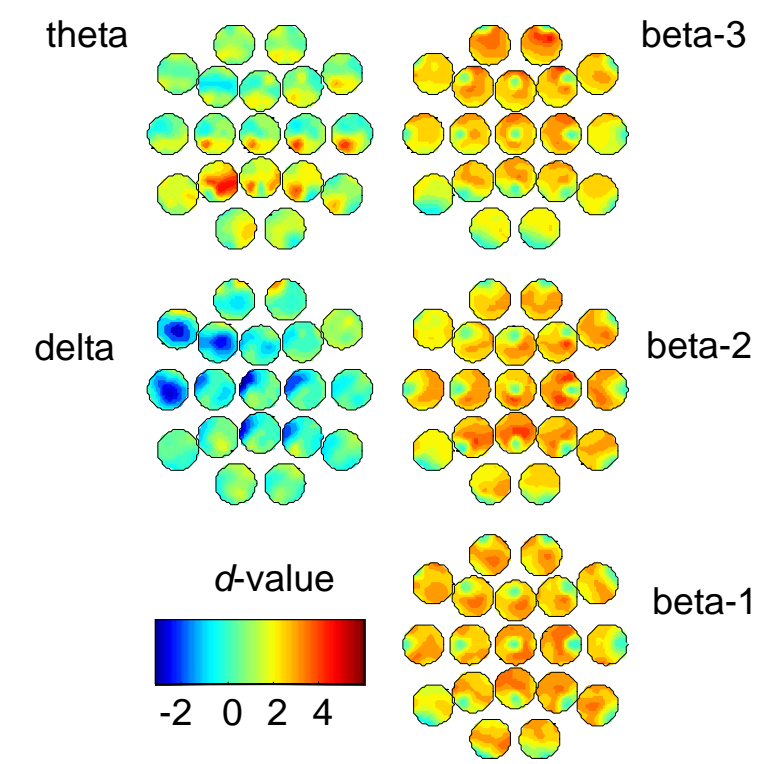
### V-2-1 Coherence function analysis

For each meditator, coherences for the different bands showed a similar topographical distribution, without significant side asymmetries, decreasing as distance increased. The differences between coherence ( $d$ -value) are displayed using a series of 19 brain maps to present the results of all 171 electrode-pair combinations. Each map shows the  $d$  values between the selected electrode and the remaining 18 electrodes. The position of a single map in the series is the position of the electrode taken into account: for example, the first map in the series is the position of the electrode taken into account: for example, the first map on the top left series of Fig. 5-8 shows the differences of theta coherence between Fp1 and the remaining electrodes in the M session compared with R.

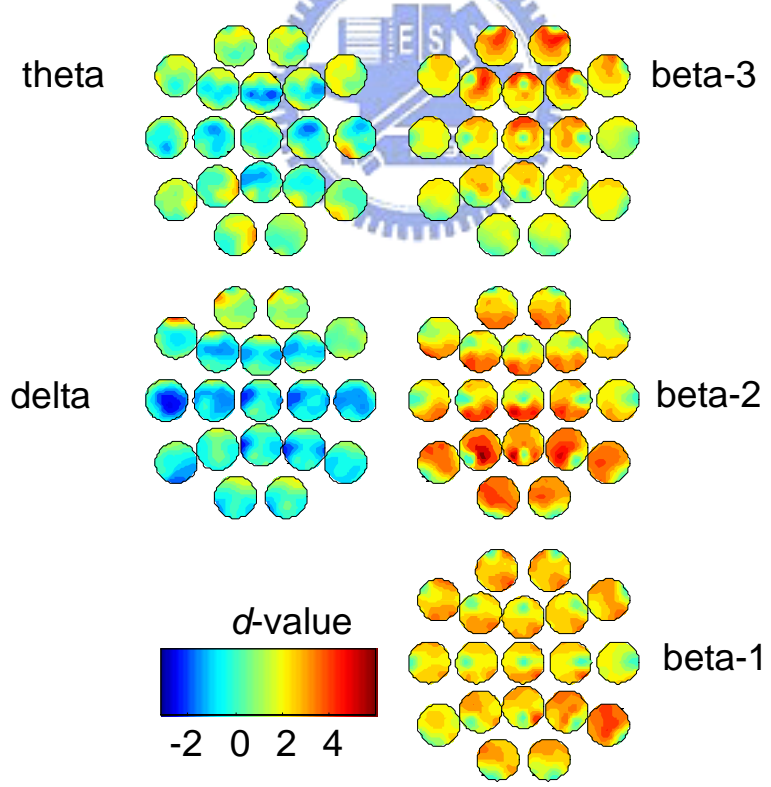
All our subjects showed coherence alterations. We found that many alterations are charged to beta band while no apparent modifications are present in slow frequency band as showed in Fig. 5-8. Coherence value was significantly higher for M and Z states compared with R state over a broad frequency band; the increase was more accentuated for the beta-1, beta-2 and beta-3 coherences.

Lines indicate electrode pairs with significantly different coherences (Fig. 5-9). The strength of beta-1 coherence in the Z state significantly exceeded that in the R state in a half of electrode pairs (95pairs,  $p < 0.05$ ). Most of the networks with increased coherences during the Z stage were formed between the left anterior and right posterior electrodes. Similar with beta-1, beta-2 coherence in the Z state was significantly higher than in the R state in





(a) M-R



(b) Z-R

Fig. 5-8 Differences of coherence ( $d$ -values) for meditation (M) and Zen chakra (Z) stages in compared with baseline rest (R)

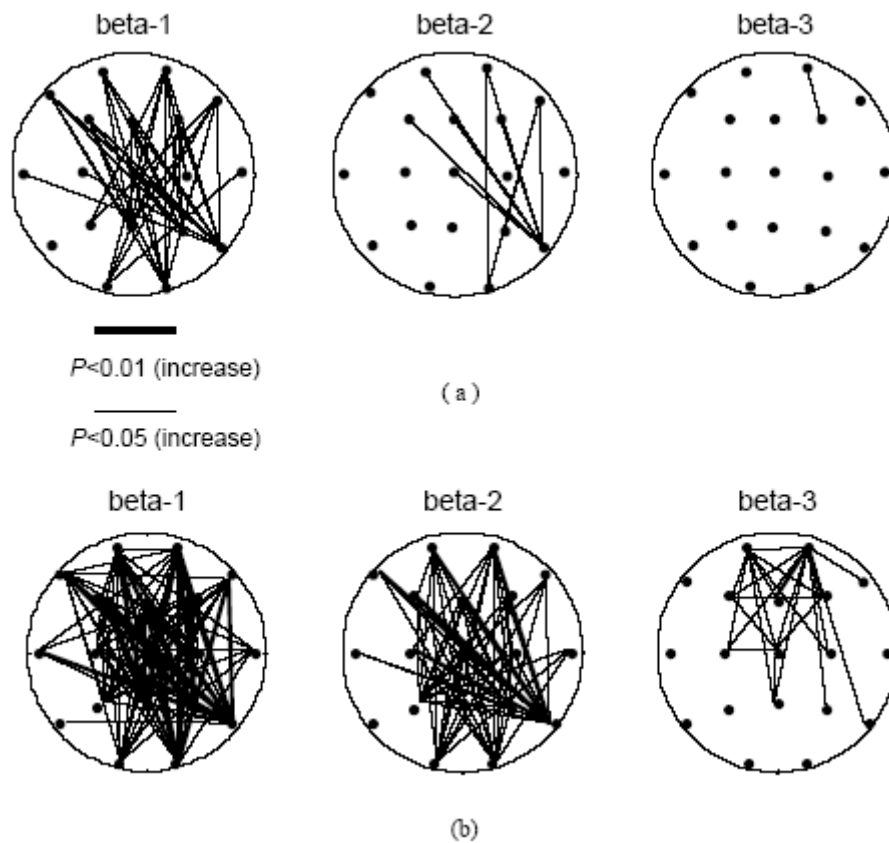


Fig.5-9 Significant probability mapping showing the comparison between (a) M and R states and (b) Z and R states. It is evident that Z and M states showed significantly higher synchronization over multiple cortical areas as compared with baseline rest.

one-third of electrode pairs (60 pairs,  $p < 0.05$ ). This increase was evident between electrodes over inter-hemispheric frontal- posterior regions and right intra-hemispheric anterior-posterior directions. As for beta-3 band, coherences tended to increase in the anterior and central electrodes in Z state compared with R state. Examining the difference between M state with R state (as showed in Fig. 5-9 (a)), an increase of beta coherence in the same brain area is also present.

Table 5-4 Regional mean coherence ( $\pm$  standard deviation) in different frequency bands for the free meditation (M), guarding Zen Chakra (Z) and the eye-closed rest (R) sessions (A: anterior; P: posterior; P-A: posterior to anterior; A-P: anterior to posterior; R-L: right to left)

	Mean $\pm$ SD						Mean $\pm$ SD					
	R	M	Z	M>R	Z>R		R	M	Z	M>R	Z>R	
$\delta$	A	0.66 $\pm$ 0.06	0.66 $\pm$ 0.08	0.68 $\pm$ 0.06	—	—	A	0.62 $\pm$ 0.1	0.69 $\pm$ 0.1	0.69 $\pm$ 0.09	**	**
	P	0.62 $\pm$ 0.06	0.62 $\pm$ 0.06	0.61 $\pm$ 0.08	—	—	P	0.51 $\pm$ 0.09	0.55 $\pm$ 0.1	0.55 $\pm$ 0.1	*	*
	P-A	0.39 $\pm$ 0.05	0.4 $\pm$ 0.05	0.4 $\pm$ 0.07	—	—	$\beta$ -1 P-A	0.3 $\pm$ 0.07	0.36 $\pm$ 0.1	0.36 $\pm$ 0.1	*	*
	A-P	0.43 $\pm$ 0.04	0.43 $\pm$ 0.05	0.44 $\pm$ 0.03	—	*	A-P	0.39 $\pm$ 0.08	0.46 $\pm$ 0.09	0.47 $\pm$ 0.09	**	**
	R-L	0.58 $\pm$ 0.05	0.59 $\pm$ 0.04	0.58 $\pm$ 0.05	—	—	R-L	0.45 $\pm$ 0.1	0.5 $\pm$ 0.1	0.5 $\pm$ 0.1	**	**
$\theta$	A	0.71 $\pm$ 0.08	0.71 $\pm$ 0.08	0.72 $\pm$ 0.05	—	—	A	0.63 $\pm$ 0.1	0.69 $\pm$ 0.1	0.68 $\pm$ 0.1	**	*
	P	0.55 $\pm$ 0.05	0.57 $\pm$ 0.07	0.56 $\pm$ 0.07	—	—	P	0.51 $\pm$ 0.09	0.55 $\pm$ 0.1	0.56 $\pm$ 0.09	*	**
	P-A	0.34 $\pm$ 0.03	0.35 $\pm$ 0.04	0.34 $\pm$ 0.05	—	—	$\beta$ -2 P-A	0.32 $\pm$ 0.07	0.37 $\pm$ 0.1	0.38 $\pm$ 0.1	*	**
	A-P	0.45 $\pm$ 0.04	0.46 $\pm$ 0.05	0.46 $\pm$ 0.03	—	—	A-P	0.42 $\pm$ 0.08	0.48 $\pm$ 0.1	0.49 $\pm$ 0.1	**	**
	R-L	0.54 $\pm$ 0.06	0.56 $\pm$ 0.05	0.56 $\pm$ 0.05	*	*	R-L	0.47 $\pm$ 0.1	0.52 $\pm$ 0.1	0.53 $\pm$ 0.1	**	**
$\alpha-1$	A	0.82 $\pm$ 0.1	0.82 $\pm$ 0.1	0.82 $\pm$ 0.06	—	—	A	0.59 $\pm$ 0.1	0.68 $\pm$ 0.2	0.69 $\pm$ 0.1	**	**
	P	0.52 $\pm$ 0.07	0.53 $\pm$ 0.08	0.54 $\pm$ 0.09	—	—	P	0.58 $\pm$ 0.1	0.63 $\pm$ 0.1	0.63 $\pm$ 0.1	*	*
	P-A	0.37 $\pm$ 0.1	0.39 $\pm$ 0.08	0.4 $\pm$ 0.1	—	—	$\beta$ -3 P-A	0.4 $\pm$ 0.1	0.46 $\pm$ 0.2	0.46 $\pm$ 0.1	*	—
	A-P	0.56 $\pm$ 0.09	0.57 $\pm$ 0.09	0.57 $\pm$ 0.08	—	—	A-P	0.43 $\pm$ 0.1	0.53 $\pm$ 0.2	0.54 $\pm$ 0.1	**	**
	R-L	0.62 $\pm$ 0.1	0.63 $\pm$ 0.1	0.62 $\pm$ 0.08	—	—	R-L	0.48 $\pm$ 0.1	0.55 $\pm$ 0.2	0.56 $\pm$ 0.1	**	**

Tests of spatial homogeneity of EEG coherence were conducted by comparing EEG coherence as a function of different interelectrode distances. The group means for EEG coherence in two meditation sessions and baseline rest are presented in Table 5-4. In comparison with baseline rest, both meditation stages present significant increase in beta coherence in every spatial connection. For the low frequency band, significant differences between states are presented for interhemispheric right-left theta and anterior-to-posterior delta band (Table 5-4).

Since the coherence decreases as the distance between the two electrodes increase, the values of local and long-distance coherence are in a different range. For each kind of regional coherence, the amount of the change is expressed as a percentage. As showed in

Fig. 5-10, consistent increases are seen in beta band for both meditation states compared with rest. For low frequency coherences the changes did not reach statistical significance. Higher increases ( $P<0.01$ ) were more apparent for long distance than for short distance. In connectivity between anterior-to-posterior cortex the increase are 20.24 % (beta-1), 19.19% (beta-2) and 30.08% (beta-3) for Z compared with R. For posterior-to-anterior coherences the increase is 19.36% (beta-1), 20.44% (beta-2) and 18.26% (beta-3). Both meditation stages also show stronger interhemispheric connectivity with 13.92% (beta-1), 14.47% (beta-2) and 19.47% (beta-3) increases for right-left coherences. For short-distance coherences, the changes on anterior region are more apparent where the increase is 11.34% (beta-1) and 17.61% (beta-3).

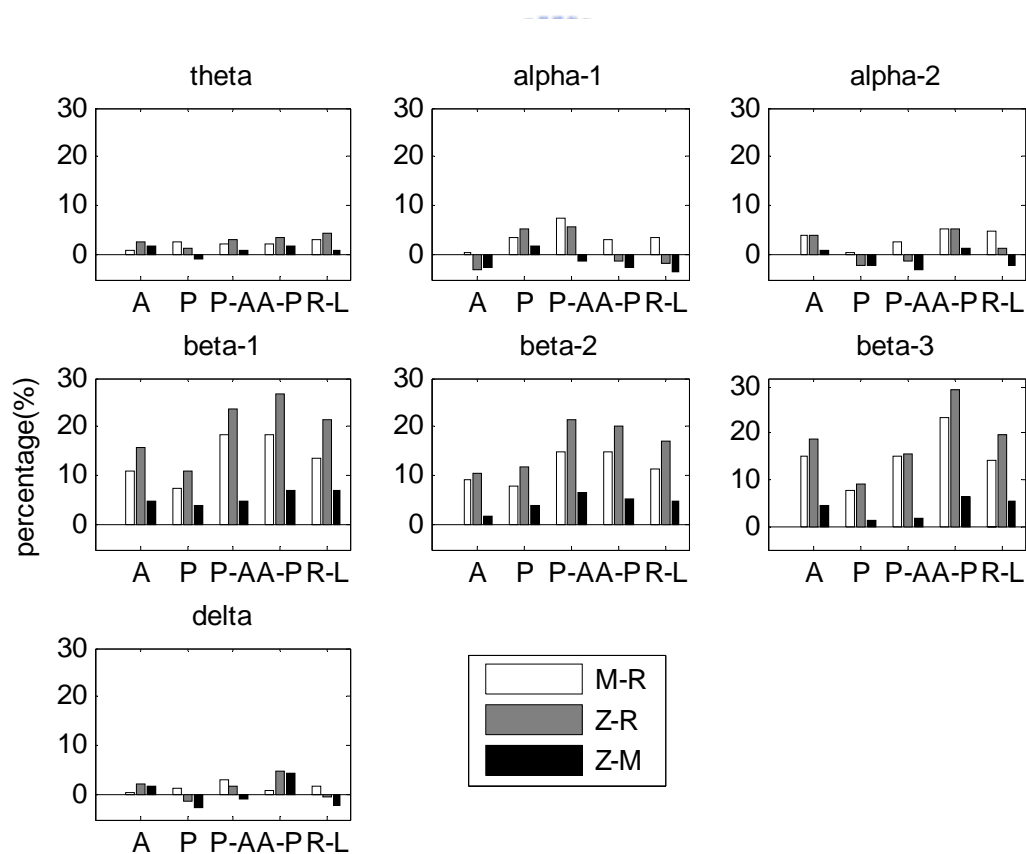


Fig. 5-10 Percentage of regional and far coherence change between stages

## V-2-2 Interdependence measure analysis

### *Interdependence matrix of Meditating EEG*

The results were expressed by a  $19 \times 19$  interdependence matrix  $S_{ij} = S(\mathbf{X}_i | \mathbf{X}_j)$ .  $S_{ij}$  represents the coupling strength of the interaction of a given source, signal  $\mathbf{X}_j$ , with respect to signal  $\mathbf{X}_i$ . As shown in Fig. 5-11, the result of a 9-year meditation practitioner during Z stage is encoded by an array of  $19 \times 19$  colored boxes. The horizontal (vertical) electrode denotes the  $\mathbf{X}_j$  ( $\mathbf{X}_i$ ). For example, the lower-left box shows the effect of conditioning O2 channel on channel Fp1. This figure is a typical example in showing stronger interdependence within the adjacent cortex and weaker interaction as inter-electrode distance increase. It is evident that S measure is asymmetric, i.e. box  $(i, j)$  and its partner box  $(j, i)$  are generally unequal. According to Fig. 5-11, we can assume that influence of occipital and posterior regions on anterior regions is weaker than influence of anterior regions on occipital and posterior regions.

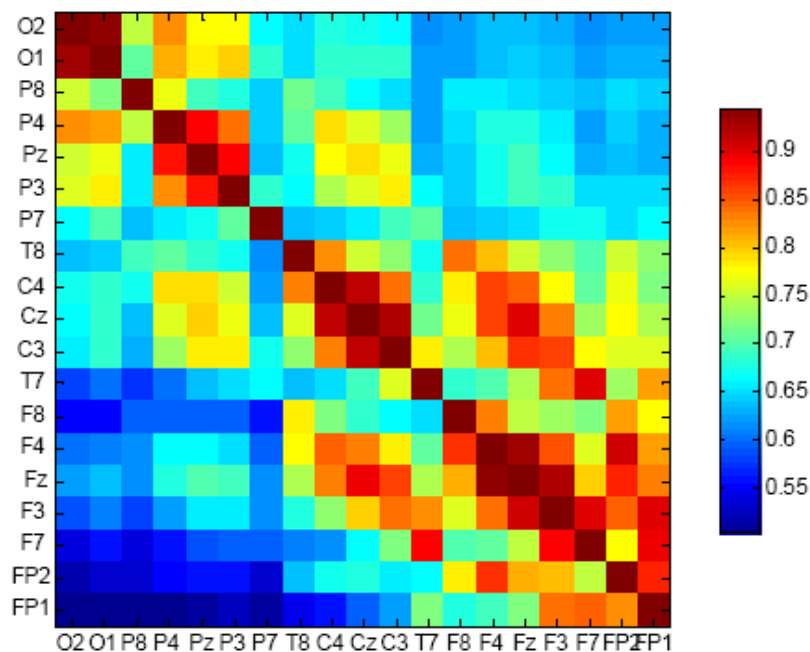


Fig. 5-11 Example for a  $19 \times 19$   $S$ -matrix of a 9-year meditator recorded during Z stage. For example, the leftmost bottom pixel represents  $S(\text{Fp1} | \text{O2})$ .

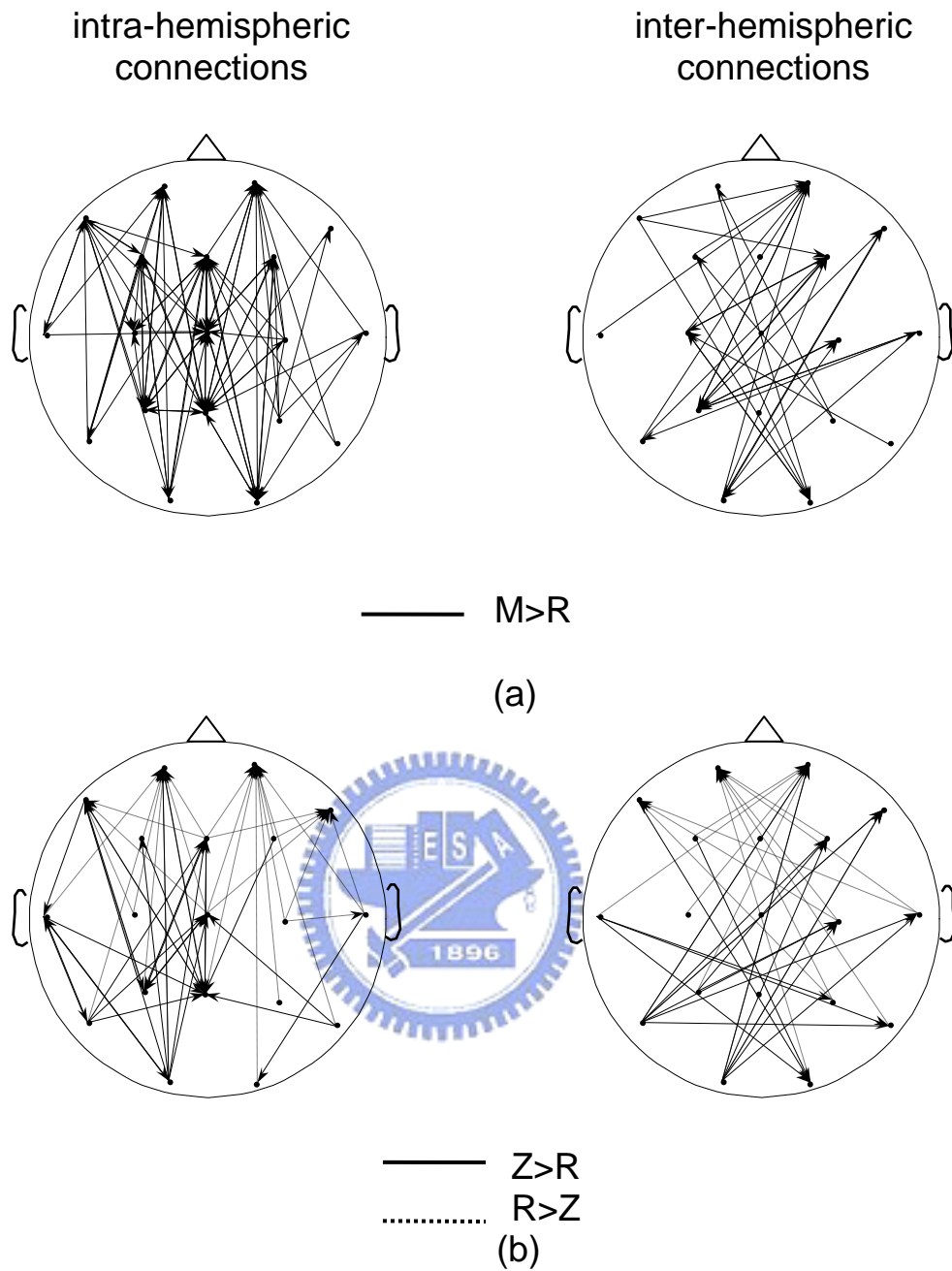
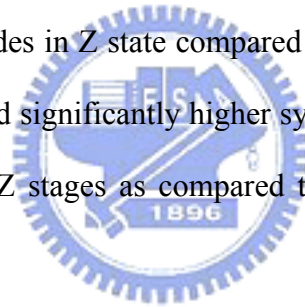


Fig. 5-12 A significant change of interdependence measure ( $P < 0.01$  or better) with respect to the baseline condition is mapped by a connection between the two electrodes of a pair, for the M state (a) and Z state (b). An arrow represents a sink site. For better visual clarity, intra- and inter-hemispheric connections are displayed separately. Solid line indicates an increase and dashed line indicates a decrease of  $S$  measure.

To obtain an idea of the overall topographic pattern of changes with stages, we applied paired *t*-test between different stages of each subject. Those electrode pairs with significant differences in synchronization ( $P < 0.01$ ) are indicated by arrowheaded lines (Fig. 5-12). Apparently, the strength of nonlinear synchronization (abbreviated to “NL-Syn”) in M state was significantly higher than the strength in R state in one-third electrode pairs (117 pairs,  $P < 0.01$ ). The increased networks during M stage were mainly formed between anterior and posterior electrodes, including both intra- and inter-hemispherical connections (Fig. 5-12 (a)). However, *S* value was much higher for Z state compared with R state in which only 46 pairs of significant difference ( $P < 0.01$ ). The increase was more evident for the left anterior-to-posterior connections and the inter-hemispheric posterior connections (Fig. 5-12 (b)). On the other hand, we observed a significant decrease in the coupling of the other regions with the frontal electrodes in Z state compared with R state (dash lines in Fig 5-12 (b)). Overall, meditators showed significantly higher synchronization over multiple cortical areas during meditation M or Z stages as compared to resting R. The enhancement was even greater for the M stage.



#### *Asymmetric property of the meditation EEG*

As mentioned in the previous session, another important property of nonlinear interdependence measure *S* is its asymmetric behavior. For each electrode  $\mathbf{X}_i$ , we obtained the average value of *S* as a sink ( $S_p(\mathbf{X}_i) = \frac{1}{n-1} \sum_j S(\mathbf{X}_i | \mathbf{X}_j)$ , where  $\mathbf{X}_j$  stands for all the other electrodes, *n* is the number of channels) and as a source ( $S_a(\mathbf{X}_i) = \frac{1}{n-1} \sum_j S(\mathbf{X}_j | \mathbf{X}_i)$ ). In this way, we aimed at outlining a general portrait of the overall dependencies of each site as influencing other regions or being influenced by other regions. Frontal electrodes Fp1, Fp2, F7 and F8 played likely active roles in all the stages ( $P < 0.01$ ). The opposite (i.e.  $S_p(\mathbf{X}_i) > S_a(\mathbf{X}_i)$ ) held for midline electrodes Fz, Cz and Pz, and the nearby electrodes C3, C4, P3 and P4 in all the stages ( $P < 0.01$ ). Occipital

electrodes O1, O2 and left posterior P7 were also more passive during M and R ( $P < 0.01$  in both cases) and only O1 was significantly passive during Z ( $P < 0.01$ ).

In order to illustrate the results of all 342 electrode-pair combinations, values of  $S$  difference ( $d$ -value) are displayed by a series of 19 brain maps. Each map shows the  $d$  values between the selected electrode (*target*) and the remaining 18 electrodes. The *target* plays the role of a *sink* (*source*) on the maps of left (right) column. Maps on the upper row display the differences between Z state and baseline R state, while the lower maps plot the changes from R state to M state. Considering the electrode as a sink (left column, Fig. 5-13), the topographic differences were greater at posterior P3, P4, and Pz. That is, these electrodes tended to be influenced more by the remaining electrodes during Z ( $P < 0.05$ ). During M, this difference was even greater for almost the whole brain, especially at frontal region ( $P < 0.001$ ). In addition, there existed stronger interaction between multiple cortex regions. When each electrode was considered as a source (right column, Fig. 5-13), we observed quite different patterns of the topographic change. Firstly, significant differences between Z and R appeared at the temporal and occipital locations T7, P7, and O1 ( $P < 0.01$ ,  $Z > R$ ), while such differences between M and R states were observed over the entire brain ( $P < 0.01$ ,  $M > R$ ), especially at posterior electrodes. There existed stronger influence from the *target* site to the others electrodes.

We also studied the problem of pairwise asymmetry in these three stages. It turned out that, at both R and M states, significantly more pairs exhibited asymmetrical synchronization ( $P < 0.01$ ); substantially,  $S_{ij} \neq S_{ji}$  in 81 pairs (R state) and 79 pairs (M state). However, Z state only induced significant asymmetry ( $P < 0.01$ ) in 62 electrode pairs. Therefore, the result raises a possible signature of higher synchronization with dense reciprocal and symmetric interactions between multiple cortical areas during guarding Zen Chakra as compared with baseline state.



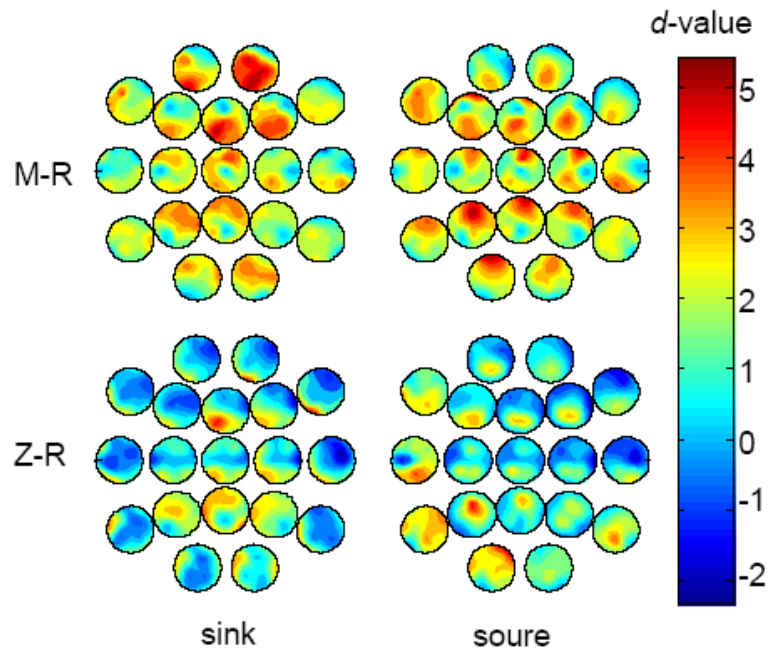


Fig. 5-13 The overall topographic differences of  $S$  ( $d$ -values) when the selected electrode was considered as a sink (left) and as a source (right) ( $d > 1.80$ ,  $P < 0.05$ ). The upper row shows the differences between Z state and baseline R state and the bottom row shows the changes for the M state versus R state.

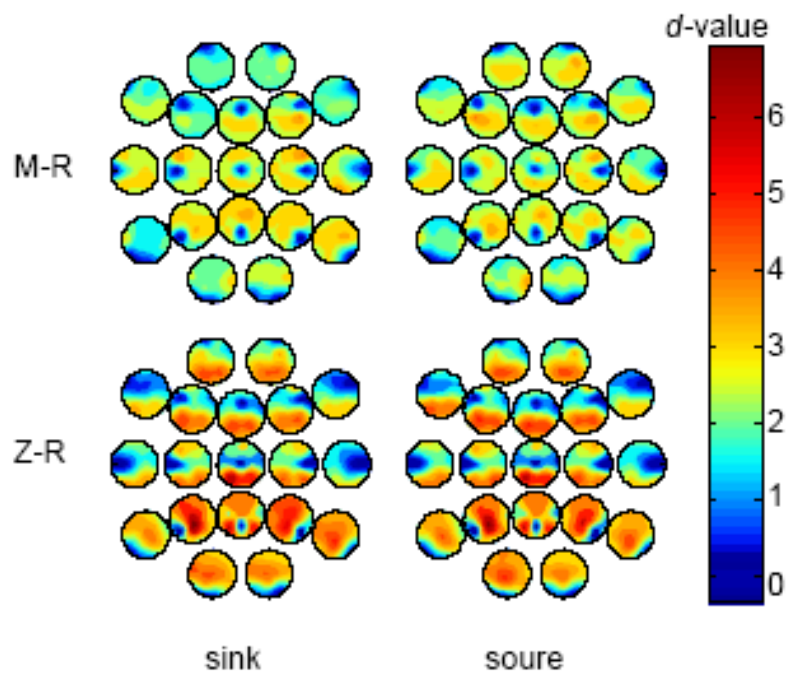


Fig. 5-14 The same expressions as Fig. 5-13 but for high frequency EEG data

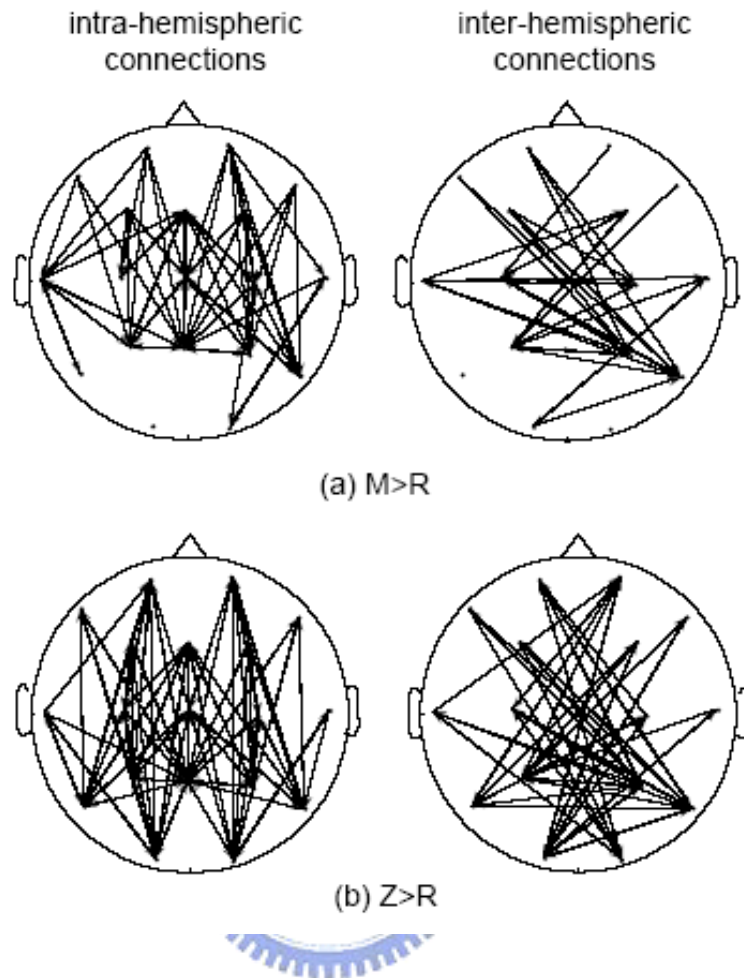


Fig. 5-15 The same expressions as Fig. 5-12 but for high frequency EEG data

*Nonlinear interdependence measure for high-frequency band*

As addressed in (Lo & Huang, 2007), EEG signals involve multi-rhythm patterns as well as the dimensional complexity with multimodal dynamics. Moreover, it is the high frequency band (>13Hz) that increases significantly during meditation (Lo & Huang, 2007). The detection of the fast band synchronization, therefore, becomes essential to the understanding and characterization of meditation brain functioning. In order to obtain the nonlinear interaction in the high-frequency band, meditation EEGs were pre-filtered before the interdependence analysis. In this study, we consider EEG signals filtered by sixth-order

Butterworth bandpass filter with low and high cutoff frequencies respectively at 13 and 45 Hz.

Corresponding to Fig. 5-13, Fig. 5-14 shows the brain mappings of the  $d$ -value for the high-frequency activity considering the *target* as either a source (right column) or a sink (left column). We noticed a number of differences between Figs. 5-13 and 5-14. Considering *target* electrode as a sink (left column, Fig. 5-14), the topographic differences between M and R increased at almost all electrodes. Nevertheless, the difference was even greater for Z state. Similar behavior was observed in the topographic change while considering *target* electrode as a source (right column, Fig. 5-14).

For each subject, paired  $t$ -test was applied for different stages. The result is illustrated in Fig. 5-15. The electrode pairs revealing significant difference ( $P<0.01$ ) of synchronization are connected by arrowheaded lines. Apparently, the NL-Syn strength in M state was significantly higher than the NL-Syn strength in R state at approximately one-third electrode pairs (115 pairs,  $P<0.01$ ). The meditation-modulated networks mainly reflected the effects in intra-hemispherical frontal and parietal regions (Fig. 5-15 (a)).  $S$  values were much higher in Z state compared with R state at even more electrode pairs (198 pairs,  $P<0.01$ ). The increases were more accentuated for the intra- and inter-hemispheric connections from anterior to posterior electrodes (Fig. 5-15 (b)).

As for the number of asymmetrical electrode pairs, i.e.  $S_{ij} \neq S_{ji}$ , it turned out that high frequency band presented less asymmetrical interaction. Significantly asymmetrical synchronization ( $P<0.01$ ) was observed at only 42 (R state), 32 (M state) and 21 (Z state) pairs of electrode connections. In consequence, degree of the high-frequency synchronization was significantly higher while guarding Zen Chakra that might suggest the possibility that a strong network with dense reciprocal and symmetric interactions between cortical regions was formed during this state.

Table 5-5 Regional mean  $S$  ( $\pm$  standard deviation) for the M, Z and R stages (A: anterior; P: posterior; P→A: posterior to anterior; A→P: anterior to posterior; R-L: right vs left side). \*  $p < 0.05$ , \*\*  $p < 0.01$

Mean $\pm$ SD	R	M	Z	M>R	Z>R
<b>A</b>	0.79 $\pm$ 0.04	0.82 $\pm$ 0.05	0.82 $\pm$ 0.05	**	*
<b>P</b>	0.73 $\pm$ 0.03	0.75 $\pm$ 0.05	0.75 $\pm$ 0.04	*	**
<b>P→A</b>	0.66 $\pm$ 0.02	0.68 $\pm$ 0.04	0.68 $\pm$ 0.03	*	**
<b>A→P</b>	0.71 $\pm$ 0.02	0.73 $\pm$ 0.03	0.74 $\pm$ 0.03	**	**
<b>R-L</b>	0.74 $\pm$ 0.04	0.76 $\pm$ 0.05	0.76 $\pm$ 0.04	*	*

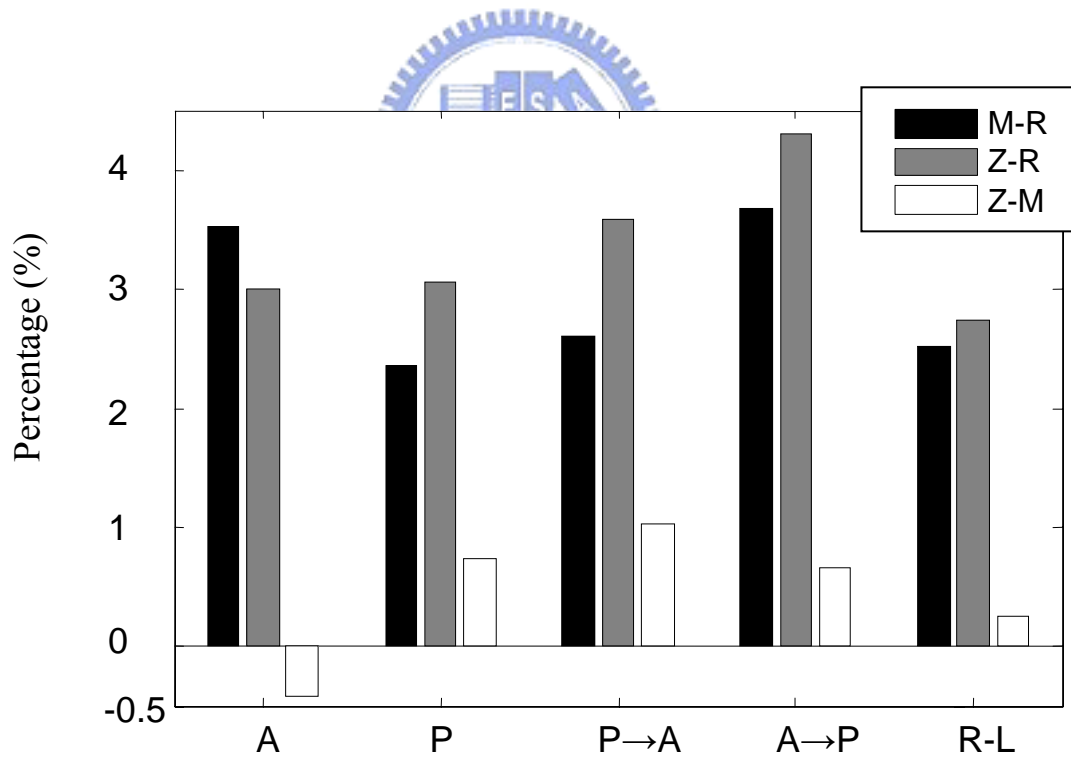


Fig. 5-16 Percentage of regional and far interdependence change between stages

We also studied the spatial characteristic of interdependence  $S$ . The same as coherence function, tests were conducted by comparing  $S$  measure as a function of different interelectrode distances in the local anterior and posterior connections as well as long anterior-to-posterior, posterior-to-anterior connections. Local anterior connectivity (A) was the averaged  $S$  between electrodes located in frontal and antero-temporal regions (Fp1–F7 (mean of  $S(\text{Fp1}|\text{F7})$  and  $S(\text{F7}|\text{Fp1})$ ), Fp2–F8, Fp1–F3, Fp2–F4, Fp1–C3 Fp2–C4, F7–C3, F8–C4, F3–C3, F4–C4, F3–F7 and F4–F8). Local posterior connectivity (P) was the average between temporo-parieto-occipital electrode pairs (O1–P3 (mean of  $S(\text{P3}|\text{O1})$  and  $S(\text{O1}|\text{P3})$ ), O2–P4, O1–P7, O2–P8, O1–C3, O2–C4, P3–C3, P4–C4, P7–C3, P8–C4, P3–P7, P4–P8 and). For posterior to anterior synchronization (P→A), we averaged indexes between pairs of electrodes: O1→Fp1 ( $S(\text{Fp1}|\text{O1})$ ), O2→Fp2, O1→F3, O2→F4, O1→C3, O2→C4, O1→P3 and O2→P4 and for anterior to posterior synchronization (A→P): Fp1→O1 ( $S(\text{O1}|\text{Fp1})$ ), Fp2→O2, Fp1→P3, Fp2→P4, Fp1→C3, Fp2→C4, Fp1→F3 and Fp2→F4, respectively. Since there is no significant side asymmetry for each meditator, interhemispheric connectivity of right-left interdependence (R-L) is derived from the average of homologous right-to-left and left-to-right electrode pairs as follows: Fp2-Fp1, F8-F7, F4-F3, T8-T7, C4-C3, P8-P7, P4-P3, O2-O1.

The group means of the three stages are presented in Table 5-5. Higher mean  $S$  was observed in frontal derivations than in posterior derivations while greater synchronization was presented in the posterior-to-anterior direction than in the anterior-to-posterior directions.

In comparison with baseline rest, we express the amount of the change as a percentage (Fig. 5-16) to obtain an idea of the regional pattern of changes. It is explicit that the degree of the high-frequency synchronization in both meditation stages was significantly higher in every spatial connection. In Z state, the stronger enhancement of interdependence is most related to posterior electrodes. On the contrary, higher increase is more apparent in the

connectivity from anterior electrodes in M state ( $p < 0.01$  for A and A→P). Both meditation stages show stronger interhemispheric connectivity for right-left synchronization.



## Chapter VI

### DISCUSSION and CONCLUSION

In the meditation research study, it is difficult to access changes of the consciousness state during meditation. Meditators once transcending the physiological and mental state cannot convey information outside. As a consequence, quantitative results together with the post-experimental, subjective narration may provide us with a glimpse of the meditation scenario. Scientific approach to the scope of Chan meditation provides insight into the mechanism in addition to the vague sketch of meditation sensation and its multiform benefits to human beings.

#### VI-1 Spatiotemporal Characteristics of Chan Meditation EEG

*Chan Meditation EEG scenarios*

In the beginning of this work, EEGs were measured and analyzed to study, as narrated by the meditators, the unique sensation during meditation or the changes of physiological conditions after years of practice. Based on the concept of fractional dimension estimation in nonlinear dynamic theory, running measurement of averaged complexity index ( $\bar{\delta}$ ) has been developed and implemented to measure long-time meditation EEGs to investigate the spatiotemporal Characteristics. Distinct differences were observed between the control and experimental groups. Of particular interest, we observed three different modes (scenarios) in the experimental (meditation) group according to the EEG evolution. These running  $\bar{\delta}$  charts somehow correlate with the subjective illustration of their meditation sensation.

Note that the group-M1 meditators were fully awake though a large amount of  $\theta$  and  $\Delta$  rhythms appeared. We attempt to hypothesize the occurrence of slow waves according to the quintessence and the ultimate aim of the orthodox Chan-Buddhist practice. Via the

practice, the human life system enters a unique status in harmony with nature and the universe. The meditators in group M3 are special. Their EEGs have been steady all the way through the meditation course. Particularly,  $\alpha$  rhythm has never even appeared since the beginning of meditation. The meditators in this particular group said that their brain and mentality had become totally different from what they were before practicing Chan-Buddhist meditation. They are now very calm, serene and peaceful when they are not in use. This status makes the meditators better preserve their mental power and body energy. In short, control subjects exhibit global  $\alpha$  activities in the first and last five-minute intervals.

#### *Spatio-temporal resolution of experienced meditators*

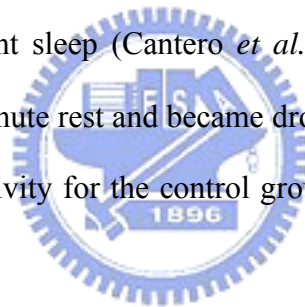
Since individual differences were showed in the meditation scenarios, it is conducted that the degree of change in EEG during Chan meditation is highly relevant to quality and length of the meditation practice. Professional meditators can produce relatively short-term states as well as long-term changes in traits and can perform deeper state of consciousness. Differing from the report on Chan-meditation studies dealt with novices practicing only the breath control (Takahashi *et al.*, 2005; Kubota *et al.*, 2001; Fumoto *et al.*, 2004), we restricted the subjects in this study to the experienced Chan meditators. In addition to the skill in breath control, the subjects focused on an aperture called Zen Chakra.

#### *Meditation EEG and alpha*

The second part of the study demonstrated that 40-min meditation resulted in such specific EEG changes as a significant increase of overall complexity index,  $P_a(\beta)$ ,  $P_r(\beta)$ ,  $P_a(\alpha-1)$  and a reduction of  $P_r(\alpha-1)$  and  $P_r(\theta)$ . Some of our findings are in agreement with results previously reported by other researchers. One consistent finding on meditation EEG involved the increase in alpha power and decrease in alpha frequency, particularly in the frontal area (Aftanas & Golocheikine, 2001; Banquet, 1973; Corby *et al.*, 1978; Travis &



Wallace, 1999). Our results showed that posterior alpha appeared predominantly in the beginning 5 minutes, and after twenty-minute meditation, slower alpha-1 or fast beta activity increased. On the other hand, control subjects at eye-closed resting exhibited no apparent change in the alpha band, instead, gradually dominated theta/delta rhythms were observed during the continuous resting. Enhancement of theta activity during meditation has been frequently reported (Kasamatsu & Hirai, 1966; Hebert & Lehmann, 1977; Corby *et al.*, 1978; Kubota *et al.*, 2001). This phenomenon was attributed to increased brain “idling” (Morse *et al.*, 1977) and subjective scores of mindfulness (Aftanas & Golocheikine, 2001; Takahashi *et al.*, 2005). However, we observed that relaxation state produced greater theta power than meditation’s over large regions of the cerebral cortex. Theta activity has been normally associated with little arousal and diminished information processing, and has been well observed during light sleep (Cantero *et al.*, 2002). Control subjects exhibited frontal  $\theta$  activities after five-minute rest and became drowsy in the midst relaxation session. Therefore, changes in theta activity for the control group can be interpreted as a reduction of alertness.



#### *Meditation EEG and beta*

One surprising finding was the emergence of beta rhythm during Chan meditation. Previous studies reported that beta activity demonstrated by proficient meditators was related to the deeper meditation like ‘samadhi’ or ‘transcendence’ state (Das & Gastaut, 1955; Banquet, 1973; Istratov *et al.*, 1996; Benson *et al.*, 1990; Lo *et al.*, 2003; Babloyantz *et al.*, 1985). Dunn *et al.* (1999) demonstrated that meditation produced greater mean amplitude of beta 1 (13-25Hz) activity than relaxation at central and posterior regions due to concentration and over the majority of the cerebral cortex due to mindfulness. Both meditations produced greater mean beta 2 (26-32Hz) power at posterior sites than relaxation (Dunn *et al.*, 1999). These results are compatible with our findings. In the beginning meditation,  $\alpha$  dominates the EEG, reflecting a relaxed, normal-consciousness

state of brain. As the meditation proceeded, however,  $\beta$ -rhythm occurred occasionally in the occipital (O1, O2 and Oz) regions. In other words, meditation induced an arousal state shifting to a higher frequency in EEG. An increase in behavioral arousal and attentive process is generally associated with an increase in beta power (Tzischinsky & Lavie, 1994). Note that Chan meditation induces transition from normal consciousness to inner mindful attention states. According to the subjective narration of meditators, the brain was subject to a wide, diffuse focus during the first- and mid-5min mediation, and gradually switched to a more concentrative focus on Chakra(s) (last-5-min mediation). It thus provides a possible explanation of why  $\alpha$ -1 and  $\beta$  activities alternately emerged. Meditation process may lead our brain into either peaceful relaxation, with more alpha-1 waves, or fully mindful awareness, associated with more beta activity.

According to Lo *et al.* (2003), increasing  $\beta$  power might probably correlate with a particular state of consciousness involving the inner-light perception. Thirteen meditators with profoundly deep Chan meditation had their EEG spectra shifting towards higher frequency band. Previous study (Lo *et al.*, 2003) has reported the observation of a significant correlation between perception of the inner light (spiritual energy inside the third ventricle, the Zen Chakra) and the alpha blocking on occipital channel EEG. Compatible with our present data, meditation sometimes caused either suppression of EEG amplitude down to almost null, or emergence of a large amount of  $\beta$ -rhythms.

#### *Meditation EEG and $\bar{\delta}$*

In nonlinear analyses, the beginning 5-min distribution of  $\bar{\delta}$  on the frontal-central brain region was pretty much the same for both groups (Fig. 5-7). The  $\bar{\delta}$  mappings revealed identifiable difference between two groups after 20 minutes. Topographical distribution for the control group remained about the same. Control EEG was basically composed of the same complicated rhythmic patterns during 40-minute rest. Together with

spectral analysis,  $\theta$  and  $\alpha$  rhythms dominated the EEG activities. Controls exhibited lower complexity in brain dynamics corresponding to the slow ( $\theta+\Delta$ ) activities, yet with increasing proportion of  $\theta$  rhythms on the frontal and central regions. As meditation session continued, however, experimental subjects entered into the high-complexity brain dynamics with fast  $\beta$  dominating occasionally. Evidently, time percentage of  $\bar{\delta} > 8.3$  showed that  $\beta$ -dominated EEG, characterized by higher  $\bar{\delta}$ 's, was significantly distributed over the occipital and parietal regions for meditation group in the later stages (Fig. 5-7).

Little is known about the meditation brain dynamics although nonlinear EEG analysis has been applied extensively to studying the brain dynamics underlying various cognitive processes and mental states. The only report relevant to brain dynamics under meditation was published by Aftanas and Golocheikine (2002). They reported, for Sahaja yoga meditators, the dimensional decline from frontal to occipital regions. And, during meditation, the estimated dimension decreased over midline frontal and central regions. In our study, however, lower indexes were obtained on midline frontal and central regions for Chan meditators. Furthermore, higher indexes correlated with beta power were more pronounced over occipital and temporal regions. What are the physiological effects and mechanisms that cause this phenomenon during meditation? EEG dimensional complexity may reflect the number of quasi-independent neuronal ensembles that are simultaneously active (Elbert *et al.*, 1994; Lutzenberger *et al.*, 1995; Lutzenberger *et al.*, 1997) and may also be associated with neural network excitability and the strength of neuronal connectivity (Bondarenko, 2005). According to our investigation of advanced Chan meditators with higher dimensional complexity somehow correlates with “strengthening of neural networks” that might be an internal mindful attention gradually switched to an extraordinary tranquil mind perceiving light inside.

According to published literatures, cortical activation of neuronal assemblies occurring in the high frequency range may be produced directly by ascending cholinergic and

serotonergic inputs to the neocortex (Dringenberg & Vanderwolf, 1998; Vanderwolf, 1988). Moreover, the serotonergic pathway from the midbrain raphe nuclei to cortex is a key component for the desynchronized, activated EEG activity consisting of high frequency, low amplitude waves (Dringenberg & Vanderwolf, 1998; Vanderwolf, 1988). Excitatory effects of serotonin (5-HT) on cortical neurons induce EEG activation by a direct, local action in the cortex (Neuman & Zebrowska, 1992). Serotonin is a neuromodulator that densely supplies the visual centers of the temporal lobe. Moderate increase of 5-HT appears to correlate with positive effect, while low 5-HT often signifies depression (Cohen & Brody, 1998; Walton et al., 1995). Previous experiments have indicated that practitioners showed higher levels of serotonin after meditation (Bujatti & Riederer, 1976; Walton & Levitsky, 2003; Newberg & Iverson, 2003). Although we cannot rule out other mechanisms or possibilities, it might be the effect of Chan meditation on 5-HT level, at least in part, giving rise to high-frequency EEG with more complexity. Further study in neurochemistry is required for verification. Our results, therefore, suggest that Chan meditation linked to the high state of consciousness is well justified by increasing high-frequency power and EEG complexity.

This work reports our investigation of electrophysiological and mental characteristics of individuals having been practicing Chan-Buddhist meditation for years. The averaged complexity index for characterizing brain dynamics revealed relatively higher beta power during meditation. We suggest that an increase of relative high-frequency power and complexity index over occipital cortex reflect the advanced states of consciousness during Chan-meditation practice. Most notably, our findings based on multi-channel EEG quantification provide scientific evidences and hypotheses for a great number of subjective reports on Chan-meditation benefit to health, in addition to the exploration of the merit of dimensional analysis in digging out small-power beta that signifies some important meditation stages.

## **VI-2 Synchronization in different meditative phases**

This work reports, for the first time, the nonlinear interdependence characteristics of brain interdependence of experienced Chan meditators based on multichannel EEG data recorded during three different phases R, M and Z. *S* indexes and coherence functions showed stage-related topographic differences in the interactions of EEGs from different cortical regions.

### *Coherence function of different meditative phases*

In this experiment, meditation sessions M and Z were characterized by significantly higher beta band coherence over the broad cortical area. The increases are mostly for the beta-1 band, and secondly, beta-2 band. Even if not so marked as the beta-1, beta-3 band coherences also tended to increase in Z state compared with R state.

Our results are different with those in earlier studies. Frontal and central alpha-1 power and frontal-central alpha-1 coherence have been reported during TM practice since 30 years ago. (Dillbeck & Bronson, 1981; Orme-Johnson & Haynes, 1981; Gaylord, Orme-Johnson, & Travis, 1989). Since that report, TM was characterized by significantly higher levels of alpha EEG coherence and has been reported to correlate with improvements in cognitive and emotional parameters such as moral reasoning, emotional stability and anxiety (Travis et al., 2004; Hebert et al., 2005). Dissimilar to their findings we have not seen the elevation of coherence reported in the above mentioned paper for the alpha frequency band in meditation. Instead, for low frequency band, coherence value was close to that obtained for the wakeful rest state.

We observed an increase in beta coherence in comparison with wakefulness for most electrode combinations. Higher levels beta power and coherence indicates cortical areas involved in task processing (Petsche et al., 1997) and functional coupling (Thatcher et al.,

1986) between brain regions. Also, transient synchronization of neuronal activity seems to be a key mechanism in the binding of anatomically distributed feature processing into coherent perceptual objects, where it is often associated with  $\beta$  or  $\gamma$  oscillations (Singer, 1999; Palva & Palva, 2007). Because Z state involves internal attention inside the third ventricle, enhancement of global, fast-band coherence may indicate the synchronization of massive distributive neural assemblies via the focusing process during Z state.

### *Coherence function and power spectral*

To make a general survey of topographical characteristics for band wave activities, topographic maps of relative power and coherence were made different frequency bands corresponding to EEG of R, M and Z stages. Fig. 6-1 shows average patterns across all meditators of topographical maps of relative power (upper row of each panel) and coherence (lower row of each panel). The gray bars on the right side of this panel indicate the level of relative band power while the gray bar on the bottom side indicates the coherence strength. To be simplification, only 35 electrode pairs (~20%) with the highest coherence were showed. In these stages (R, M, Z), there were no the remarkable changes of topographic characteristics in alpha-2 activities.

Topographic maps of theta and alpha-1 band demonstrated that the relative power increased as the function of meditation stages in the anterior-central areas of scalp but the changes of the coherence values are not significant. On the other hand, Topographic maps of coherence in beta-1 and beta-2 activities clearly demonstrated that the synchronous component in the anterior-central areas of scalp appeared to correspond with increasing relative power. Relative power of beta-3 band increased from occipital region to frontal region and coherence values were also high at those areas.

In general, increased alpha power over central and frontal cortices indicates cortical areas at rest or “cortical idling” and could indicate decreased motor and executive

processing during TM practice (Travis, 2001). Inspired by these results we thus propose that the meditators are more relaxed during M state with mental quiescence but full inner wakefulness. Even though power of fast rhythms is not so significantly different between two meditative states due to the low amplitude, the coherence estimate is. Coherence may be more sensitive than amplitude to distinguish Z state from the M and baseline R states. As a result, the increase of beta coherence was more relevant in Z state, and the increase of low frequency power was more relevant in the M state.

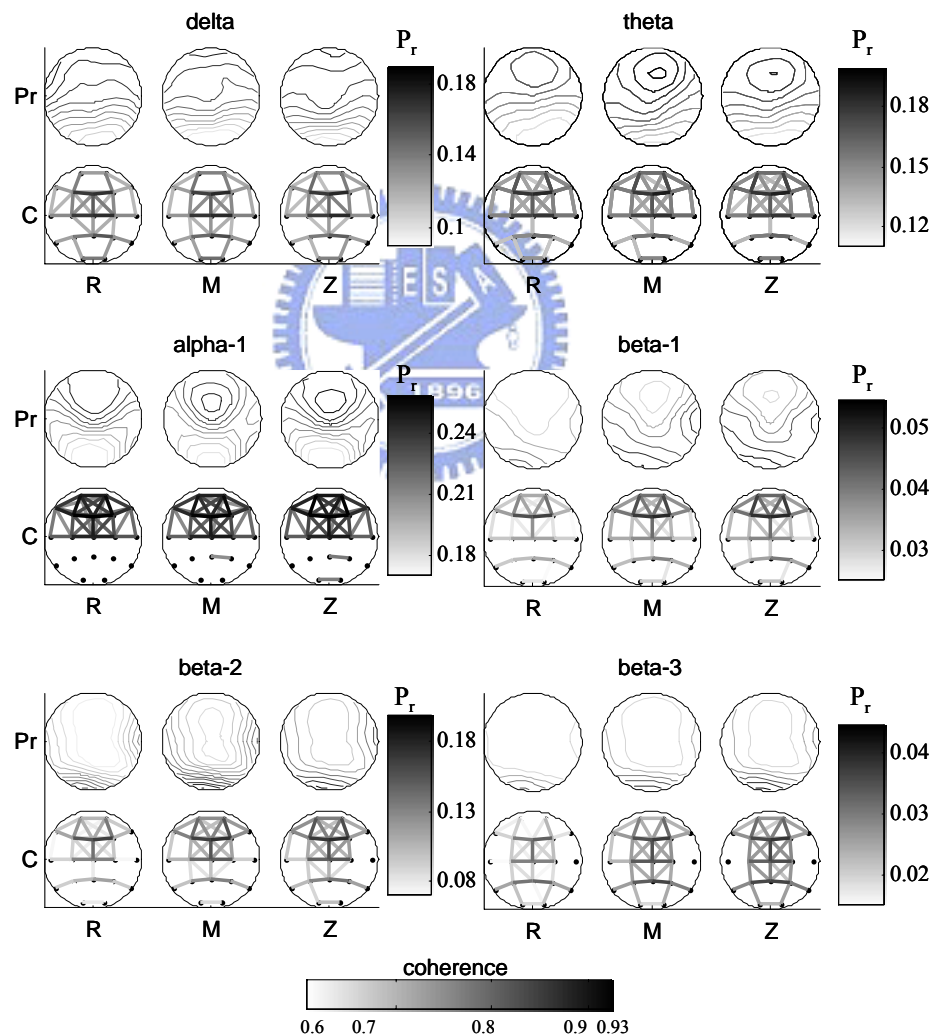


Fig. 6-1 Topographic maps of relative power (upper row of each panel) and coherence (lower row of each panel) for different frequency bands corresponding to EEG during R, M and Z stages. To be simplification, only 35 electrode pairs with the highest coherences were showed.

### *Nonlinear interdependence measure in different meditative phases*

Meditators showed significantly enhanced interactions between multiple cortical areas in both meditation stages M and Z. In addition, increased interdependence during M might be contributed by sinks at right frontal regions and sources at central, occipito-parietal regions. Z state reflected different EEG oscillatory behaviors. S value was higher for Z state in comparison with R state, but mainly in the left anterior-to-posterior connections and in posterior regions. Diversely, the coupling strength was found to decrease significantly along the direction from the other regions to the frontal electrodes in Z state compared with R state.

Nonlinear interdependence in meditation EEG might produce a stronger type of dynamical binding, with strong nonlinear coupling across broad band of frequency. Moreover, the increased interdependence from R to M state at the frontal regions somehow agrees with what was found in the previous studies. The predominant EEG findings in most meditation studies have indicated the increases of theta–alpha coherence, mostly in the frontal-central region (Cahn & Polich, 2006; Travis & Wallace, 1999; Travis *et al.*, 2002). Some of these studies further reported that high theta-alpha coherence was accompanied with thought-free, pure conscious experiences during meditation (Orme-Johnson & Haynes, 1981; Travis, 2001). In the present study, eight of 12 meditators reported that they experienced a state with little thought but full consciousness during M state. Such findings might imply that enhanced coupling in the frontal region related with low frequency band which is more pronounced during M state.

### *Nonlinear interdependence measure of high frequency band*

The degree of fast-band synchronization in both meditation stages was significantly



higher all over the scalp electrodes. The enhancement was greater in the Z state (Fig. 5-15 (b)). It was likely due the particular meditation practice and mental strategy that affected EEGs. Unlike other meditation skills emphasizing the concentration on a mantra or the breathing, Chan practitioners were asked to focus on their Zen Chakra inside the third ventricle in Z state. In Chan meditation practice, guarding chakra is a specific mental technique toward the ultimate Buddhahood state. According to the post-experimental interview, meditator experienced a particular state of consciousness involving mental quiescence with harmonic energy perception. These concentration techniques can be interpreted as a particular manner of top-down control where cortical processes are not determined by external stimuli but are driven by internal mental activity, mental imagery, etc. Evidences showed that top-down processing might induce changes in gamma frequency activity or synchronization (Tallon-Baudry et al., 1998; von Stein *et al.*, 2000). Moreover, neuronal oscillations and synchronization in the fast band play an important role in the higher brain functioning including consciousness (Lutz, 2002; Meador *et al.*, 2002) and attention etc (Bauer et al., 2006; Ayelet et al., 2007). Enhancement of cortical synchrony in gamma band has been proposed to be an integrative mechanism possibly bringing a widely distributed set of neurons together into a coherent ensemble underlying a conscious experience (Basar-Eroglu et al., 1996; Bertrand & Tallon-Baudry, 2000). Because Z state involves internal attention that induces inner light, a possible interpretation is that guarding Zen Chakra results in activation of attention-related networks and gives rise to a internal percept in visual cortex (Tallon-Baudry et al., 2005) that might also evoke fast-band EEG synchronization. In the situation, enhancement of global, fast-band interdependence may indicate the synchronization of massive distributive neural assemblies via the focusing process during Z state.

### *Asymmetric property of the meditation EEG*

In addition, nonlinear interdependence measures, as reported earlier, have the advantage of being asymmetric. Indeed, we found that  $S$  measures during the three states exhibit different patterns in regard to the direction of the interactions between each electrode pairs. Frontal electrodes Fp1, Fp2, F7 and F8 played active roles in all stages, whereas midline electrodes Fz, Cz and Pz, and the nearby electrodes C3, C4, P3 and P4 played likely passive roles in all stages. Occipital electrodes and left parietal regions were stage-dependent, with O1, O2 and P7 playing a role of sink during the M and R, and only O1 and F4 more likely as a sink during Z. Likewise, both the lateral regions showed the highest degree of independence in all the stages and remained neutral, i.e. they influenced in the same extent that they were influenced. On the other hand, asymmetries may also reflect different degrees of complexity of the two systems, such findings provide the implication that posterior electrodes are more complex with higher dimensional complexity while frontal electrodes has lower dimension, which is consistent with previous results (Lo et al., 2003; Chang & Lo, 2005).

In regard to asymmetrical properties, R and M states presented significantly more pairs of asymmetrical synchronization than Z state did, i.e.  $S_{ij} \neq S_{ji}$  in 81, 79 and 62 electrode pairs for R, M and Z states, respectively. Moreover, balance of mutual influence became even more apparent for high frequency band in the two meditative states (42, 32 and 21 pairs of connections for R, M and Z states, respectively). Topographic differences between states showed similar patterns despite sink or source in the high-frequency band. The results suggest that the degree of influence of one cortical region on the other region is comparable with vice versa. Therefore, the similarity possibly reflects stronger synchronization with dense reciprocal and mutual interactions between multiple cortical areas during meditation, especially for Z state in the high frequency band.

Finally, topographic differences (Fig. 5-16 and Table 5-5) showed that long-distance interaction ( $P \rightarrow A$  and  $A \rightarrow P$ ) is more affected by meditation. It is most likely consequent on more involvement in the information transfer from occipital to frontal cortical regions. Also, the changes were mostly related to the long axonal fibers which are the connections transmitted by the superior longitudinal fasciculus in both postero-anterior and antero-posterior directions (Locatelli, et al., 1998). Connectivity between near electrodes is particularly influenced by short connections while connectivity between distant electrodes is mainly due to long axon connections (Thatcher et al. 1986). Increased longitudinal interdependence must arise through long-range neural interconnections, presumably either pyramidal corticocortical projections or corticothalamic loops (Singer, 1999; Lutz et al., 2004). It is possible that the concentrating Z state with strong high frequency power is caused by the former, whereas M state with a strong alpha power arises through cortico-thalamic interactions. Thus, the increasing S in the frontal regions during free meditation was related to low frequency band and the increasing S in the posterior regions during guarding Zen Chakra was related to high frequency activity.

### **VI-3 Conclusion**

This work is devoted to the investigation of physiological and mental characteristics of individuals having been practicing the Chan-Buddhist meditation for years. The significance of the work is hard to overemphasize, especially since meditation practice has been proven to benefit mankind, including health, character, life outlook, social morality, etc. From the CAM instrument – ARDK, practitioners show a better health and physiological condition as a result of long term effect of Chan meditation.

These running  $\bar{\delta}$  charts somehow correlate with the subjective illustration of their meditation sensation. The averaged complexity index for characterizing brain dynamics

revealed relatively higher beta power during meditation. We suggest that an increase of relative high-frequency power and complexity index over occipital cortex reflect the advanced stage of consciousness during Chan-meditation practice. These findings suggest that Chan meditation practice leads to a state fundamentally different than eyes-closed rest. Most notably, our findings based on multi-channel EEG quantification provide scientific evidences and hypotheses for a great number of subjective reports on Chan-meditation benefit to health, in addition to the exploration of the merit of dimensional analysis in digging out small-power beta that signifies some important meditation stages.

Multichannel EEG patterns during R, M and Z periods were significantly different. Meditation sessions were characterized by significantly stronger nonlinear interdependence and higher beta coherence. In short, we have sketched the overall interdependence patterns in the EEG of experienced Chan meditators during different phases. Brain dynamics of meditation state were associated with high indexes of nonlinear interdependence. The use of the  $S$  index and  $\bar{\delta}$  makes it possible to determine that meditation exhibits dynamic nature different from baseline rest. Thus, the proposed index may provide more insights into the underlying dynamics and offer a promising tool to investigate the cognitive processes in Chan meditation.

Despite these findings, several questions need to be addressed. A concrete relationship between EEG activity and meditation states (or, various states of consciousness) is still inaccessible because of the fundamental problem of collecting information from the individual under meditation. Substantially speaking, the meditators cannot convey information by any means when they are meditating beyond the physiological and mental state. To report, they must return to the normal conscious state. Another issue encountered in the meditation EEG research is the effect of “ambiance”— meditators were not able to achieve good-quality meditation in the laboratory compared with meditation quality at the Chan-Buddhist meditation shrine where, described by the disciples, the sacred power of

Buddha is bestowed. Many factors involved in meditation study have been continuously disclosed since we began to investigate Chan-Buddhist meditation in 1999. Nevertheless, sophisticated experimental protocol is required to gain access to the myths of the spiritual realm without interfering with the meditation course.

The physiological effects and mechanisms that cause this phenomenon during meditation (the functional role of this phenomenon) have yet been determined. These questions relate to the origin and nature of microscopic properties of small group of neurons and their relationship to optimal information processing in the brain. Future research can be devoted to the analysis of Chan-meditation microstate.



## Appendix A

### Complexity Index

Derivation of eq. (3-2) was based on the concept that the probability of  $\mathbf{X}$  being inside the  $i$ th hypersphere is:

$$\mu = P(\mathbf{X}_i) \cong p(\mathbf{X}_i) \cdot v_{i,KNN} = p(\mathbf{X}_i) \cdot (\alpha \times d_{i,KNN}^n) \quad (\text{A-1})$$

where  $p(\mathbf{X}_i)$  is the probability density function and  $v_{i,KNN} = \alpha \times d_{i,KNN}^n$  is the volume of the  $i$ th hypersphere. The coefficient  $\alpha$  is the amending factor in computing the hyperspherical volume from the  $n$ th power of distance  $d_{i,KNN}$ . The probability density  $p(\mathbf{X}_i)$  depends on the distribution of  $\mathbf{X}$ . The first order moment of the  $K$ th NN distance of the  $i$ th hypersphere,  $E\{d_{i,KNN}\}$ , can be obtained by

substituting  $d_{i,KNN} = \mu^{1/n} (\alpha \cdot p(\mathbf{X}_i))^{-1/n}$ . Then the first moment of  $d_{KNN}$ ,  $E\{d_{KNN}\}$ , is computed by taking the expectation of  $E\{d_{i,KNN}\}$  with respect to  $\mathbf{X}_i$ . Detailed derivation can be found in (Fukunaga and Flick, 1984).

Fukunaga and Flick aimed at quantifying the pattern classification error in the  $KNN$  model. They hypothesized an  $n$ -dimensional space for the pattern vectors, where  $n$  is an integer. In order to quantify the waveform complexity of EEG signals, we apply the concept of fractional dimensionality of a strange attractor. Then the volume of the  $i$ th hypersphere can be estimated by

$$v_{i,KNN} = \frac{\mu}{p(\mathbf{X}_i)} \cong \alpha \times d_{i,KNN}^\delta \quad (\text{A-2})$$

where  $\delta$  is the complexity index of the trajectory to be evaluated in the EEG study.

And  $\delta$  may be a fractional number. The first-order moment of  $d_{i,KNN}$  for a given  $\mathbf{X}_i$  is

$$E\{d_{i,KNN}\} \cong E\left\{\left(\frac{\mu}{\alpha p(\mathbf{X}_i)}\right)^{1/\delta}\right\} = \int_0^1 \left(\frac{\mu}{\alpha p(\mathbf{X}_i)}\right)^{1/\delta} p(\mu) d\mu \quad (\text{A-3})$$

where the probability density function  $p(\mu)$  is (Fraser, 1957)

$$p(\mu) = \frac{N!}{(K-1)!(N-K)!} \mu^{K-1} (1-\mu)^{N-K} \quad (\text{A-4})$$

Substituting eq. (A-4) into eq. (A-3) leads to an estimate of  $E\{d_{i,KNN}\}$  as

$$\begin{aligned} E\{d_{i,KNN}\} &\cong (\alpha p(\mathbf{X}_i))^{-1/\delta} \frac{N!}{(K-1)!(N-K)!} \int_0^1 \mu^{K+1/\delta-1} (1-\mu)^{N-K} d\mu \\ &= (\alpha p(\mathbf{X}_i))^{-1/\delta} \frac{N!}{(K-1)!(N-K)!} \frac{\Gamma(K+1/\delta) \cdot \Gamma(N-K+1)}{\Gamma(N+1/\delta+1)} \end{aligned} \quad (\text{A-5})$$

where  $\Gamma(\cdot)$  is the gamma function. Since  $\Gamma(K) = (K-1)!$ , eq. (A-5) becomes

$$\begin{aligned} E\{d_{i,KNN}\} &\cong (\alpha p(\mathbf{X}_i))^{-1/\delta} \frac{\Gamma(N+1)}{\Gamma(K) \cdot \Gamma(N-K+1)} \frac{\Gamma(K+1/\delta) \cdot \Gamma(N-K+1)}{\Gamma(N+1/\delta+1)} \\ &= (\alpha p(\mathbf{X}_i))^{-1/\delta} \frac{\Gamma(N+1)}{\Gamma(K)} \frac{\Gamma(K+1/\delta)}{\Gamma(N+1/\delta+1)} \end{aligned} \quad (\text{A-6})$$

which can be further reduced to

$$E\{d_{i,KNN}\} \cong (\alpha p(\mathbf{X}_i))^{-1/\delta} \frac{\Gamma(K+1/\delta)}{\Gamma(K)} \quad (\text{A-7})$$

given that  $N \gg 1/\delta$ . Taking the first-order expectation, with respect to  $\mathbf{X}_i$ , of eq. (A-7)

results in

$$E\{d_{i,KNN}\} \cong \alpha^{-1/\delta} E\{p(\mathbf{X}_i)^{-1/\delta}\} \frac{\Gamma(K+1/\delta)}{\Gamma(K)} \quad (\text{A-9})$$

To eliminate the factor of  $p(\mathbf{X}_i)$  in computing  $\delta$ , the algorithm actually evaluates the

ratio of  $E\{d_{(K+1)NN}\}$  to  $E\{d_{KNN}\}$ . Since

$$\frac{E\{d_{(K+1)KNN}\}}{E\{d_{KNN}\}} \cong \frac{\Gamma(K+1+1/\delta)}{\Gamma(K+1)} \frac{\Gamma(K)}{\Gamma(K+1/\delta)} = \frac{K+1/\delta}{K} = 1 + \frac{1}{K\delta}, \quad (\text{A-10})$$

## REFERENCES

- Aftanas, L.I. and Golocheikine, S.A., 2001, "Human anterior and frontal midline theta and lower alpha reflect emotionally positive state and internalized attention: High-resolution EEG investigation of meditation," *Neuroscience Letters*, Vol. 310, No. 1, pp.57-60.
- Aftanas, L.I., and Golocheikine, S.A., 2002, "Non-Linear Dynamic Complexity of the Human EEG during Meditation," *Neuroscience Letters*, Vol. 330, No. 2, pp. 143-146.
- Anand, B. K., Chhina, G. S., and Singh, B., 1961, "Some Aspects of Electroencephalographic Studies in Yogis," *Electroencephalography and Clinical Neurophysiology*, Vol. 13, pp. 452-456.
- Andresen, J., 2000, "Meditation meets behavioural medicine: The story of experimental research on meditation," *Journal of Consciousness Studies*, Vol. 7, pp. 17-73.
- Arambula, P., Peper, E., Kawakami, M. and Gibney, K. H., 2001, "The Physiological Correlates of Kundalini Yoga Meditation: a Study of a Yoga Master," *Applied psychophysiology and biofeedback*, Vol. 26, No.2, pp. 147-53
- Arnhold, J., Grassberger, P., Lehnertz, K. and Elger, C., 1999, "A robust method for detecting interdependencies: application to intracranially recorded EEG," *Physica D*, Vol. 134, pp. 419-430.
- Ayelet N. L., Michael E., Lynn C. R., Shlomo B., and William P., 2007, "Different Effects of Voluntary and Involuntary Attention on EEG Activity in the Gamma Band," *The Journal of Neuroscience*, Vol. 27, pp. 11986-11990;
- Babloyantz A., Salazar, J. M., 1985, "Evidence of chaotic dynamics of brain activity during the sleep cycle." *Physics Letters A*, Vol. 111, pp. 152-156
- Babloyantz, A., and Destexhe, A., 1986, "Low-Dimensional Chaos in an Instance of Epilepsy," *Proceedings of the National Academy of Sciences of the United States of America*, Vol. 83, pp. 3513-3517.
- Bagchi, B. K., Wenger, M. A., 1957, "Electrophysiological correlates of some yogi exercise." *Electroencephalogr. Clin. Neurophysiol.* (Suppl)7, pp. 132-149
- Banquet, J. P., 1973, "Spectral analysis of the EEG in meditation," *Electroencephalography and Clinical Neurophysiology*, Vol. 35, pp. 143-151.
- Basar-Eroglu, C., Struber, D., Schurmann, M., Stadler, M., Basar, E., 1996, "Gamma-band responses in the brain: a short review of psychophysiological correlates and functional significance." *International Journal of Psychophysiology*, Vol. 24, pp. 101-112.
- Bauer, M., Oostenveld, R., Peeters, M. and Fries, P., 2006, "Tactile spatial attention enhances gamma-band activity in somatosensory cortex and reduces low-frequency activity in parieto-occipital areas," *J. Neurosci.*, Vol. 26, pp. 490-501



- Becker, D. E. and Shapiro, D., 1981, "Physiological Responses to Clicks during Zen, Yoga, and TM Meditation," *Psychophysiology*, Vol. 18, No. 6, pp. 694-699.
- Bennett, J. E. and Trinder, J., 1977, "Hemispheric Laterality and Cognitive Style Associated with Transcendental Meditation," *Psychophysiology*, Vol. 14, No., 3 pp. 293-296.
- Benson, H., Malhotra, M. S., Goldman, R. F., Jacobs, G. D., & Hopkins, P. J., 1990, "Three case reports of the metabolic and electroencephalographic changes during advanced Buddhist meditation techniques." *Behavioral Medicine*, Vol. 16, pp. 90-95.
- Berger, H. Über das, 1929, "Elektrenkephalogramm des Menschen." *Arch. Psychiat. Nervenkr.*, Vol. 87, pp. 527-570
- Bertrand, O., Tallon-Baudry, C., 2000, "Oscillatory gamma activity in humans: a possible role for object representation." *International Journal of Psychophysiology*, Vol. 38, pp. 211-223.
- Bhattacharya, J., Pereda, E. and Petsche, H., 2003, "Effective detection of coupling in short and noisy bivariate data," *IEEE Trans. Syst. Man Cybern. B*, Vol. 33 , pp. 85-95
- Bhattacharya, J., Petsche, H. and Pereda, E., 2001, "Interdependencies in the spontaneous EEG while listening to music," *Int. J. Psychophysiol.* Vol. 42, pp. 287-301.
- Bondarenko, V.E., 2005, "Information processing, memories, and synchronization in chaotic neural network with the time delay." *Complexity*, Vol. 11, pp. 39-52
- Braitenberg, V., 1978, Cortical architectonics: general and areal. In: M.A.B. Brazier and H. Petsche (Eds.), *Architectonics of the Cerebral Cortex*. Raven Press, New York.
- Breakspear M. and Terry J.R., 2002, "Detection and description of non-linear interdependence in normal multichannel human EEG data," *Clinical Neurophysiology*, Vol. 113, pp. 735-753
- Breakspear M. and Terry J.R., 2002, "Topographic organization of nonlinear interdependence in multichannel human EEG," *Neuroimage*, Vol. 16, pp. 822-835
- Bruske, J., and Sommer, G., 1998, "Intrinsic Dimensionality Estimation with Optimally Topology Preserving Maps," *IEEE Transactions on Pattern Analysis and Machine Intelligence*, Vol. 20, No. 5, pp. 572-575.
- Bujatti. M., Riederer, P., 1976, "Serotonin, noradrenaline, dopamine metabolites in Transcendental Meditation technique." *J Neural Transm*, Vol. 39, pp. 257-267.
- Cahn, B. R., Polich, J., 2006, "Meditation States and Traits: EEG, ERP, and Neuroimaging Studies." *Psychological Bulletin*, Vol. 132, pp. 180-211
- Cantero, J.L., Atienza, M., Salas, R.M., 2002, "Human alpha oscillations in wakefulness, drowsiness period, and REM sleep: different electroencephalographic phenomena within the alpha band." *Neurophysiol. Clin.*, Vol. 32, pp. 54-71.
- Chang, K. M., Lo, P. C., 2005, "Meditation EEG Interpretation Based on Novel Fuzzy-Merging Strategies and Wavelet Features." *Journal of Biomedical*

- Cohen, D., 1972, "Magnetoencephalography: detection of the brain's electrical activity with a superconducting magnetometer." *Science*, Vol. 175, pp. 664-66
- Cohen, M.L., Brody T.M., "5-Hydroxytryptamine (serotonin) and therapeutic agents that modulate serotonergic neurotransmission." Brody TM, Lerner J, Minneman KP: Human Pharmacology. Molecular to clinical. 3rd ed. St. Louis: Mosby, 1998; pp.157-67
- Coker, K.H., 1999, "Meditation and Prostate Cancer: Integrating a Mind/Body Intervention with Traditional Therapies," *Seminars in Urologic Oncology*, Vol. 17, No. 2, pp.111-118.
- Cooper, R, Osselton, J.W. and Shaw, J.C. 1980, EEG Technology. 3<sup>rd</sup> ed., Butterworth Inc., Woburn, MA.
- Corby, J. C., Roth, W. T., Zarcone, V. P., and Kopell, B. S., 1978, "Psychophysiological Correlates of the Practice of Tantric Yoga Meditation," *Arch Gen Psychiatry*, Vol. 35, pp. 571-577.
- Das, N. N. and Gastaut, H. C., 1955, "Variations of the electrical activity of the brain, heart, and skeletal muscles during yogic meditation and trance." *Electroencephalography and Clinical Neurophysiology*, Suppl. 6, pp. 211–219.
- De Carli F, Nobili L, Beelke M, Watanabe T, Smerieri A, Parrino L, Terzano MG and Ferrillo F., 2004, "Quantitative analysis of sleep EEG microstructure in the time-frequency domain." *Brain Research Bulletin*, Vol. 63, pp. 399-405.
- Delmonte, M.M., 1985, "Effects of expectancy on physiological responsivity in novice meditators," *Biol. Psychol.* Vol. 21, pp. 107–121.
- Destexhe, A., Sepulchre, J. A. and Babloyantz, A., 1988, "A comparative study of the experimental quantification of deterministic chaos," *Physics Letters A*, Vol. 132, pp.101-106.
- Dillbeck, M. C. and Bronson, E. C., 1981, "Short-term longitudinal effects of the transcendental meditation technique on EEG power and coherence." *International Journal of Neuroscience*, Vol. 14, 147–151.
- Dringenberg, H.C., Vanderwolf, C.H., 1998, "Involvement of direct and indirect pathways in electrocorticographic activation." *Neuroscience & Biobehavioral Reviews*, Vol. 22, pp. 243–257.
- Dunn, B. R., Hartigan, J. A. and Mikulas, W. L., 1999, "Concentration and mindfulness meditations: Unique forms of consciousness?" *Applied Psychophysiology and Biofeedback*, Vol. 24, pp. 147–165.
- Dvorak, I., 1990, "Takens Versus Multichannel Reconstruction in EEG Correlation Exponent Estimations," *Physics Letters A*, Vol. 151, pp.225-233.
- Eckmann, J.P. and Ruelle D., 1992, "Fundamental limitations for estimating dimensions and Lyapounov exponents in dynamical systems", *Physica D*, Vol. 56, pp.185-187

- Elbert, T.; Ray, W.J.; Kowalik, Z.J.; Skinner, J.E.; Graf, K.E. and Birbaumer, N. 1994, "Chaos and Physiology: Deterministic Chaos in Excitable Cell Assemblies," *Physiological Reviews*, Vol. 74, pp. 1–47.
- Elizabeth, M.-T., 2003, "The benefits of meditation: experimental findings," *The Social Science Journal*, Vol. 40, pp. 465-470
- Elson, B. D., Hauri, P., and Cunis, D., 1977, "Physiological Changes in Yoga Meditation," *Psychophysiology*, Vol. 14, No. 1, pp. 52-57.
- Feldmann U., Bhattacharya J., 2004, "Predictability improvement as an asymmetrical measure of interdependence in bivariate time series," *Int J Bifurcation Chaos*, Vol. 14, pp. 505--514
- Florian, G., Andrew, C. and Pfurtscheller, G., 1998, "Do changes in coherence always reflect changes in functional coupling?" *Electroencephalography and Clinical Neurophysiology*, Vol. 106, pp. 87–91.
- Fukunaga, K., and Flick, T. E., 1984, "Classification Error for a Very Large Number of Classes," *IEEE Transactions on Pattern Analysis and Machine Intelligence*, Vol. 6, No. 6, pp. 779-788.
- Fukunaga, K., and Olsen, D. R., 1971, "An Algorithm for Finding Intrinsic Dimensionality of Data," *IEEE Transactions on Computers*, Vol. 20, pp. 176-183.
- Gath, I., Feuerstein, C., Pham, D.T., Rondouin, G., 1992, "On the tracking of rapid dynamic changes in seizure EEG," *Biomedical Engineering, IEEE Transactions on*, Vol. 39, pp. 952-958
- Gaylord, C., Orme-Johnson, D. and Travis, F., 1989, "The effects of the transcendental meditation technique and progressive muscle relaxation on EEG coherence, stress reactivity, and mental health in black adults." *International Journal of Neuroscience*, Vol. 46, pp. 77–86.
- Grassberger, P. and Procaccia, I., 1983, "Characterization of strange attractors." *Phys. Rev. Lett.* Vol. 50, pp. 346-349.
- Grassberger, P. and Procaccia, I., 1983, "Measuring the strangeness of strange attractors." *Physica D*, Vol. 9, pp.189–208.
- Hebert, R. and Lehmann, D., 1977, "Theta Bursts: An EEG Pattern in Normal Subjects Practicing the Transcendental Meditation Technique," *Electroencephalography and Clinical Neurophysiology*, Vol.42, pp.397-405.
- Hebert, R., Lehmann, D., Tan, G., Travis, F. and Arenander, A., 2005, "Enhanced EEG alpha time-domain phase synchrony during Transcendental Meditation: Implications for cortical integration theory," *Signal Processing*, Vol. 85, pp. 2213-2232
- Heide, F. J., 1986, "Psychophysiological Responsiveness to Auditory Stimulation during Transcendental Meditation," *Psychophysiology*, Vol. 23, No. 1, pp. 71-75.
- Hentschel, H. G. E. and Procaccia, I., 1983, "The Infinite Number of Generalized Dimensions of Fractals and Strange Attractors," *Physica*, 8D, pp. 435-444.
- Hintz KJ, Yount GL, Kadar I, 2003, "Bioenergy definitions and research guidelines." *Alternative Therapies in Health and Medicine*. Vol. 9 (suppl 3):A13-A30.

- Holst, G.C., 1998, *Testing and Evaluation of Infrared Imaging Systems* (2<sup>nd</sup> ed.). Florida:JCD Publishing, Washington:SPIE
- Iasemedis, L.D., Sackellares, J.C., Zaveri, H.P. and Williams, W.J., 1990, *Brain Topogr.* Vol. 2, pp. 187
- Istratov, E. N., Lyubimov, N. N., and Orlova, T. V., 1996, "Dynamic Characteristics of Modified Consciousness During and After Transcendental Meditation," *Bulletin of Experimental Biology and Medicine*, Vol. 121, No. 2, pp.117-119.
- Jevning, R., Wallace, R. K., and Beidebach, M., 1992, "The Physiology of Meditation: A Review. A Wakeful Hypometabolic Integrated Response," *Neuroscience and Biobehavioral Reviews*, Vol. 16, pp. 415-424.
- Kalayci, T. and Özdamar, Ö., 1995, "Wavelet Preprocessing for Automated Neural Network Detection of EEG Spikes," *IEEE Engineering in Medicine and Biology Magazine*, Vol. 14 , No.2, pp.160-166.
- Kasamatsu, A. and Hirai, T., 1966, "An Electroencephalographic Study of the Zen Meditation (Zazen)," *Folia Psychiatrica et Neurologica Japonica*, Vol.20, pp.315-336.
- Katoh T, Suzuki A, Ikeda K. 1998, "Electroencephalographic derivatives as a tool for predicting the depth of sedation and anesthesia induced by sevoflurane." *Anesthesiology* Vol. 88, pp. 642–50.
- Korn, H. and Faure, P., 2003, "Is there chaos in brain? II. Experimental evidence and related methods," *C. R. Biol.* Vol. 326, pp. 787–840.
- Kubota, Y., Sato, W., Toichi, M., Murai, T., Okada, T., Hayashi, A., 2001, "Frontal midline theta rhythm is correlated with cardiac autonomic activities during the performance of an attention demanding meditation procedure," *Cognitive Brain Research*, Vol. 11, pp. 281–287
- Le Van Quyen, M., Adam, C., Baulac, M., Martenierie, J. and Varela, F. J., 1998, "Nonlinear interdependencies of EEG signals in human intracranially recorded temporal lobe seizures," *Brain Res.*, Vol. 792, pp. 24–40.
- Le Van Quyen, M., Martinerie, J., Adam, C. and Varela, F., 1999, "Nonlinear analyses of interictal EEG map the interdependencies in human focal epilepsy," *Physica D*, Vol. 127, pp. 250–266.
- Lehmann, D., Faber, P. L., Achermann, P., Jeanmonod, D., Gianotti, L. R. and Pizzagalli, D., 2001, "Brain sources of EEG gamma frequency during volitionally meditation-induced, altered states of consciousness, and experience of the self." *Psychiatry Research*, Vol. 108, pp. 111–121.
- Lehnertz, K. , Arnhold, J., Grassberger, P. and Elger, C.E., 2000, *Chaos in Brain?* World Scientific, Singapore.
- Lester, D., 1999, "Zen and Happiness," *Psychological Reports*, Vol. 84, No. 2, pp. 650-651.

- Levine, P. H., Hebert, J. R., Haynes, C. T. and Strobel, U., 1977, "EEG coherence during the Transcendental Meditation technique." In D. W. Orme-Johnson & J. T. Farrow (Eds.), *Scientific research on the TM program: Collected papers* (Vol. 1, pp. 187–207). Rheinweiler, Germany: MERU Press.
- Lo, P.-C. and Chung, W.-P., 2000, "An Approach to Quantifying the Multi-Channel EEG Spatial-Temporal Feature," *Biometrical Journal*, Vol. 42, No. 7, pp.21-34.
- Lo, P.-C. and Chung, W.-P., 2001, "An Efficient Method for Quantifying the Multi-Channel EEG Spatial-Temporal Complexity," *IEEE Transactions on Biomedical Engineering*, Vol. 48, No. 3, pp.394-397.
- Lo, P.-C. and Huang, H.-Y., 2007, "Investigation of Meditation Scenario by Quantifying the Complexity Index of EEG," *Journal of the Chinese Institute of Engineers*, Vol. 30, pp. 389-400.
- Lo, P.-C. and Principe, J. C., 1989, "Dimensionality Analysis of EEG Segments: Experimental Considerations," *Proceeding of International Joint Conference on Neural Network*, vol.1, pp.693-698.
- Lo, P.-C., Huang, M.-L., and Chang, K.-M., 2003, "EEG Alpha Blocking Correlated with Perception of Inner Light during Zen Meditation," *American Journal of Chinese Medicine*, Vol.31, No.4, pp.629-642.
- Locatelli, T., Cursi, M., Liberati, D., Franceschi, M. and Comi, G., 1998, "EEG coherence in Alzheimer's disease," *Electroencephalography and Clinical Neurophysiology*, Vol. 106, pp. 229-237
- Logothetis, N.K., 2001, "Neurophysiological investigation of the basis of the fMRI signal." *Nature*, Vol. 412, pp. 150.
- Lutz, A., Greischar, L. L., Rawlings, N. B., Ricard, M. and Davidson, R. J., 2004, "Long-term meditators self-induced high-amplitude gamma synchrony during mental practice." *Proceedings of the National Academy of Sciences, USA*, Vol. 101, pp.16369–16373.
- Lutz, A., Lachaux, J.-P., Martinerie, J. and Varela, F.J., 2002, "Guiding the study of brain dynamics by using first-person data: synchrony patterns correlate with ongoing conscious states during a simple visual task," *Proceedings of the National Academy of Sciences, USA*, Vol. 99, pp. 1586–1591
- Lutzenberger, W., Flor, H., Birbaumer, N., 1997, "Enhanced dimensional complexity of the EEG during memory for personal pain in chronic pain patients." *Neurosci. Lett.*, Vol. 226, pp. 167-170
- Lutzenberger, W., Preissl, H., Pulvermüller, F., 1995, "Fractal dimension of electroencephalographic time series and underlying brain processes." *Biological Cybernetics*, Vol. 73, pp.477-482
- MacLean, C.R., Walton, K.G., Wenneberg, S.R., Levitsky, D.K., Mandarino, J.P., Waziri, R., Hillis, S.L., and Schneider, R.H., 1997, "Effects of the Transcendental Meditation Program on Adaptive Mechanisms: Changes in Hormone Levels and Responses to Stress after 4 Months of Practice," *Psychoneuroendocrinology*, Vol. 22 , No.4, pp.277-295.

- Masaki, F., Ikuko, S.-S., Yoshinari, S., Yuko, M. and Hideho, A., 2004, "Appearance of high-frequency alpha band with disappearance of low-frequency alpha band in EEG is produced during voluntary abdominal breathing in an eyes-closed condition," *Neuroscience Research*, Vol. 50, pp. 307–317
- Matsumoto, K. and Tsuda, I., 1988, "Calculation of information flow rate from mutual information," *J. Phys. A*, Vol. 21, pp. 1405–1414.
- Meador, K.J., Ray, P.G., Echauz, J.R., Loring, D.W., Vachtsevanos, G.J., 2002, "Gamma coherence and conscious perception," *Neurology*, Vol. 59, pp. 847–854.
- Michel, O. and Flandrin, P., 1993, "Local Minimum Redundancy Representation of a System for Estimating the Number of Its Degrees of Freedom," *IEEE Signal Processing Workshop on Higher-Order Statistics*, pp.341-345.
- Milnor J., 1985, "On the concept of attractor," *Commun Math Phys*, Vol. 99, pp. 177–195.
- Mölle, M., Marshall, L., Wolf, B., Fehm, H.L., Born, J., 1999, "Enhanced dynamic complexity in the human EEG during creative thinking." *Psychophysiology*, Vol. 36, pp.95-104
- Morse, D. R., Martin, J. S., Furst, M. L. and Dubin, L. L., 1977, "A physiological and subjective evaluation of meditation, hypnosis, and relaxation," *Psychosomatic Medicine*, Vol. 39, pp. 304–324.
- Neuman, R.S., Zebrowska, G., 1992, "Serotonin (5-HT<sub>2</sub>) receptor mediated enhancement of cortical unit activity." *Can. J. Physiol. Pharm.*, Vol. 70, pp.1604–1609.
- Newberg, A.B., Iverson, J., 2003, "The neural basis of the complex mental task of meditation: neurotransmitter and neurochemical considerations." *Med Hypotheses*, Vol. 61, pp. 282–291.
- Newell, S. and Sanson-Fisher, R.W., 2000, "Australian Oncologists' Self-Reported Knowledge and Attitudes about Non-Traditional Therapies Used by Cancer Patients," *Medical Journal of Australia*, Vol. 172, No.3, pp. 110-113.
- Niedermeyer, E. and Lopes Da Silva, F.H. 1999, *Electroencephalography: Basic Principles, Clinical Applications, and Related Fields*. 4<sup>th</sup> ed., Williams & Wilkins, USA.
- Nunez, P.L., Silberstein, R.B., Shi, Z., Carpenter, M.R., Srinivasan, R., Tucker, D.M., Doran, S.M., Cadusch, P.J. and Wijesinghe, R.S., 1999. "EEG coherency. II. Experimental comparisons of multiple measures." *Clin Neurophysiol*, Vol. 110, pp. 469–486.
- Nunez, P.L., Srinivasan, R., Westdorp, A.F., Wijesinghe, R.S., Tucker, D.M., Silberstein, R.B. and Cadusch, P.J., 1997. "EEG coherency. I. Statistics, reference electrode, volume conduction, Laplacians, cortical imaging, and interpretation at multiple scales." *Electroencephalogr Clin Neurophysiol*, Vol. 103, pp. 499–515.
- Oohashi T, Kawai N, Honda M, Nakamura S, Morimoto M, Nishina E and Maekawa T. 2002, "Electroencephalographic measurement of possession trance in the field." *Clinical Neurophysiology*, Vol. 113, pp. 435-445.

- Orme-Johnson, D. W. and Haynes, C. T., 1981, "EEG phase coherence, pure consciousness, creativity, and TM-Siddhi experiences." *International Journal of Neuroscience*, Vol. 13, 211–217.
- Oschman, J.L., 2000, *Energy Medicine: The Scientific Basis of Bioenergy Therapies*. Philadelphia, PA: Churchill Livingstone.
- Pagano, R. R., Rose, R. M., Stivers, R. M., and Warrenburg, S., 1976, "Sleep during Transcendental Meditation," *Science*, Vol. 191, pp.308-310.
- Palva, S. and Palva, J. M., 2007, "New vistas for a-frequency band oscillations," *Trends in Neurosciences*, Vol. 30, pp. 150-158
- Passamante, A. and Farrell, M. E., 1991, "Characterizing Attractors Using Local Intrinsic Dimension via Higher-Order Statistics," *Physical Review A*, Vol. 43, No.10, pp.5268-5274.
- Pereda, E., Gamundi, A., Rial, R. and Gonzalez, J., 1998, "Non-linear behaviour of human EEG: fractal exponent versus correlation dimension in awake and sleep stages," *Neurosci. Lett.*, Vol. 250, pp. 91–94.
- Pereda, E., Mañas S., De Vera L., Garrido, J. M., López, S., González, J.J., 2003, "Non-linear asymmetric interdependencies in the electroencephalogram of healthy term neonates during sleep," *Neuroscience Letters*, Vol. 337, pp. 101–105
- Pereda, E., Quian Quiroga R. and Bhattacharya, J., 2005, "Nonlinear multivariate analysis of neurophysiological signals," *Progress in Neurobiology*, Vol. 77, pp. 1-37
- Pereda, E., Rial, R., Gamundi, A. and González, J., 2001, "Assessment of changing interdependencies between human electroencephalograms using nonlinear methods," *Physica D*, Vol. 148, pp. 147–158.
- Petsche, H., Kaplan, S., von Stein, A. and Filz, O., 1997, "The possible meaning of the upper and lower alpha frequency for cognitive and creative tasks: a probability mapping study." *Int. J. Psychophysiol.* Vol. 26, pp. 77–97.
- Pettis, K. W., Bailey, T. A., Jain, A. K., and Dubes, R. C., 1979, "An Intrinsic Dimensionality Estimator from Near-Neighbor Information," *IEEE Transactions on Pattern Analysis and Machine Intelligence*, Vol. 1, pp. 25-37.
- Pijn, J. P. M., Neerven, J. V., Noest, A., and Lopes da Silva, F. H., 1991, "Chaos or Noise in EEG Signals: Dependence on State and Brain Site," *Electroencephalography and Clinical Neurophysiology*, Vol.79 ,pp. 371-381.
- Pijn, J.P., 1990. "Quantitative evaluation of EEG signals in epilepsy," Ph.D. Thesis, Amsterdam University, Amsterdam.
- Pradhan, N., Sadasivan, P.K., Chatterji, S. and Narayana, D., 1995, "Patterns of attractor dimensions of sleep EEG," *Comput. Biol. Med.*, Vol. 25, pp. 455–462.
- Pritchard W.S., Duke D.W., 1992, "Dimensional analysis of no-task human EEG using the Grassberger-Procaccia method," *Psychophysiology*, Vol. 29, pp. 182--192
- Pritchard W.S., Duke D.W., 1992, "Measuring chaos in the brain: a tutorial review of nonlinear dynamical analysis," *Int. J. Neurosci.* Vol. 67, pp. 31–80.

- Quian Quiroga, R., Arnhold, J. and Grassberger, P., 2000, "Learning driver-response relationships from synchronization patterns," *Phys. Rev. E*, Vol. 61, pp. 5142–5148.
- Quian Quiroga, R., Kraskov, A., Kreuz, T. and Grassberger, P., 2002, "Performance of different synchronization measures in real data: a case study on electroencephalographic signals," *Phys. Rev. E*, Vol. 65, pp. 041903.
- Rapp, P. E. , Bashore, T. R., Martinerie, J. M., Albano, A. M., and Mees, A. I., 1989, "Dynamics of Brain Electrical Activity," *Brain Topography*, Vol. 2, pp. 99-118.
- Rappelsberger, P., 1989, "The reference problem and mapping of coherence: a simulation study." *Brain Topography*, Vol. 2, pp. 63-72
- Rey, M. and Guillemant, P., 1997, "Apport des mathématiques non-linéaires (théorie du chaos) à l'analyse de l'EEG," *Neurophysiol. Clin.*, Vol. 27, pp. 406–428.
- Rosenblum, M.G., Pikovsky, A.S. and Kurths, J., 1996, "Phase synchronization of chaotic oscillators," *Phys. Rev. Lett.*, Vol. 76, pp. 1804–1807
- Rulkov, N.F., Sushchik, M.M., Tsimring, L.S. and Abarbanel, H.D.I., 1995, "Generalized synchronization of chaos in directionally coupled chaotic systems," *Phys. Rev. E*, Vol. 51, pp. 980–994
- Russek, L., and Schwartz, G., 1996, "Energy cardiology: a dynamical energy systems approach for integrating conventional and alternative medicine." *The Journal of Mind-Body Health*. Vol. 12, pp. 4-24.
- Sancier, K.M. and Holman, D., 2004, "Commentary: multifaceted health benefits of medical qigong." *Journal of Alternative and Complementary Medicine*. Vol. 10, pp. 163-165.
- Schiff, S.J., So, P., Chang, T., Burke, R.E. and Sauer, T., 1996, "Detecting dynamical interdependence and generalized synchrony through mutual prediction in a neural ensemble," *Phys. Rev. E*, Vol. 54, pp. 6708–6715.
- Schneider, R.H., Nidich, S.I., Salerno, J.W., Sharma, H.M., Robinson, C.E., Nidich, R.J., Alexander, C.N., 1998, "Lower Lipid Peroxide Levels in Practitioners of the Transcendental Meditation Program," *Psychosomatic Medicine*, Vol. 60, No.1, pp.38-41.
- Schupp H.T., Lutzenberger W., Birbaumer N., Miltner W., Braun C., 1994, "Neurophysiological differences between perception and imagery." *Cogn Brain Res*, Vol. 2, pp. 77-86
- Segundo, J.P., 2001, "Nonlinear dynamics of point process systems and data," *Int. J. Bifurcation Chaos*, Vol. 13, pp. 2035–2116.
- Shapiro, S.L., Schwartz, G.E., and Bonner, G., 1999, "Effects of Mindfulness-Based Stress Reduction on Medical and Premedical Students," *Journal of Behavioral Medicine*, Vol. 21, No. 6, pp. 581-599.
- Singer, W., 1999, "Neuronal synchrony: a versatile code for the definition of relations?" *Neuron*. Vol. 24, pp. 49–65
- Singer, W., 2001, "Consciousness and the binding problem." *Ann NY Acad Sci*, 929, 123–146.



- Stam C.J., van Woerkom T.C.A.M., Pritchard W.S., 1996, Use of non-linear EEG measures to characterize EEG changes during mental activity," *Electroenceph Clin Neurophysiol*, Vol. 99, pp. 214--224
- Stam, C. J. and van Dijk, B. W., 2002, "Synchronization likelihood: an unbiased measure of generalized synchronization in multivariate data sets," *Physica D: Nonlinear Phenomena*, Vol. 163, pp. 236-251
- Stam, C. J., Breakspear M., van Walsum, A.-M. van C., and van Dijk, B. W. , 2003, "Nonlinear Synchronization in EEG and Whole-Head MEG Recordings of Healthy Subjects," *Human Brain Mapping*, Vol. 19, pp.63–78
- Stam, C.J. , 2005, "Nonlinear dynamical analysis of EEG and MEG: review of an emerging field," *Clin. Neurophysiol.* Vol. 116, pp. 2266–2301
- Stigsby, B., Rodenberg, J. C., and Moth, H. B., 1981, "Electroencephalographic Finding during Mantra Meditation (Transcendental Meditation). A Controlled, Quantitative Study of Experienced Meditators," *Electroencephalography and Clinical Neurophysiology*, Vol. 51, pp. 434-442.
- Takahashi, T., Murata,T., Hamada,T., Omori, M., Kosaka, H., Kikuchi, M., Yoshida, H., Wada, Y., 2005, "Changes in EEG and autonomic nervous activity during meditation and their association with personality traits," *International Journal of Psychophysiology*, Vol. 55, pp. 199-207
- Takens, F., 1981, "Detecting Strange Attractors in Turbulence," *Lecture Notes in Mathematics*, Springer, Berlin, Vol. 898, pp. 366-381.
- Tallon-Baudry, C., Bertrand, O., Hénaff M.-A., Isnard J. and Fischer C., 2005, "Attention Modulates Gamma-band Oscillations Differently in the Human Lateral Occipital Cortex and Fusiform Gyrus," *Cerebral Cortex*, Vol. 15, pp. 654—662
- Tallon-Baudry, C., Bertrand, O., Peronnet, F. and Pernier, J., 1998, "Induced gamma-band activity during the delay of a visual short-term memory task in humans," *J. Neurosci.* Vol. 18, pp. 4244–4254.
- Telles, S., Nagarathna, R. and Nagendra, H.R., 1995, "Autonomic Changes During "OM" Meditation." *Indian J Physiol Pharmacology* Vol. 39, pp. 418-420.
- Thatcher, R.W., Krause, P.J. and Hrybyk, M., 1986, "Cortico-cortical associations and EEG coherence: a two-compartmental model." *Electroenceph. clin. Neurophysiol.* Vol. 64, pp. 123–143
- Theiler, J. and Rapp, P., 1996, "Re-examination of the evidence for low dimensional, nonlinear structure in the human electroencephalogram," *Electroencephalogr. Clin. Neurophysiol.* Vol. 98, pp. 213–222.
- Theiler, J., Eubank, S., Longtin, A., Galdrikian, B. and Farmer, J. D., 1992, "Testing for nonlinearity in time series: the method of surrogate data, *Physica D*, Vol. 58, pp. 77–94.
- Tirsch, W. S., Stude, P., Scherb, H. and Keidel, M., 2004, "Temporal order of nonlinear dynamics in human brain", *Brain Research Reviews*, Vol. 45, pp. 79-95

- Tooley, G.A., Armstrong, S.M., and Norman, T.R., 2000, "Acute Increases in Night-Time Plasma Melatonin Levels Following a Period of Meditation," *Biological Psychology*, Vol. 53, No. 1, pp. 69-78.
- Travis, F. and Pearson, C., 2000, "Pure Consciousness: Distinct Phenomenological and Physiological Correlates of Consciousness Itself," *International Journal of Neuroscience*, Vol. 100, pp. 77-89
- Travis, F., 2001, "Autonomic and EEG patterns distinguish transcending from other experiences during transcendental meditation practice." *International Journal of Psychophysiology*, Vol. 42, pp. 1-9.
- Travis, F., Arenander, A. and Dubois, D., 2004, "Psychological and physiological characteristics of a proposed object-referral/self-referral continuum of self-awareness," *Conscious. Cogn.* Vol. 13, pp. 401-420.
- Travis, F., Tecce, J., Arenander, A. and Wallace, R. K., 2002, "Patterns of EEG coherence, power, and contingent negative variation characterize the integration of transcendental and waking states." *Biological Psychology*, Vol. 61, pp. 293-319
- Travis, F., Wallace, R. K., 1999, "Autonomic and EEG patterns during eyes-closed rest and transcendental meditation (TM) practice: The basis for a neural model of TM practice." *Consciousness and Cognition*, Vol. 8, pp.302-318.
- Trunk, G. V., 1976, "Statistical Estimation of the Intrinsic Dimensionality of a Noisy Signal Collection," *IEEE Transactions on Computers*, Vol. 25, pp. 165-171.
- Tzischinsky, O., Lavie, P., 1994, "Melatonin possesses time-dependent hypnotic effects," *Sleep*, Vol. 17, pp. 638-645.
- van den Broek, P.L.C., van Egmond, J., van Rijn, C.M., Takens, F., Coenen, A.M.L. and Booij, L., 2005, "Feasibility of real-time calculation of correlation integral derived statistics applied to EEG time series," *Physica D*, Vol. 203, pp. 198-208.
- van Gils, M., Rosenfalck, A., White, S. , Prior, P. , Gade, J. , Senhadji, L. , Thomsen, C. , Ghosh, I. R., Langford, R. M., and Jensen, K., 1997, "Signal Processing in Prolonged EEG Recordings during Intensive Care," *IEEE Engineering in Medicine and Biology Magazine*, Vol. 16, No.6, pp.56-63.
- van Putten, M. J. A. M. and Stam, C. J., 2001, "Is the EEG Really 'Chaotic' in Hypsarrhythmia?" *IEEE Engineering in Medicine and Biology Magazine*, Vol. 20, No. 5, pp. 72-79.
- Vanderwolf, C.H., 1988, "Cerebral activity and behavior: control by central cholinergic and serotonergic systems." *Int. Rev. Neurobiol.*, Vol. 30, pp. 225-340.
- Verveer, P. J. and Duin, P. W., 1995, "An Evaluation of Intrinsic Dimensionality Estimators," *IEEE Transactions on Pattern Analysis and Machine Intelligence*, Vol. 17, No. 1, pp. 81-86.
- von Stein, A., Chiang, C. and Konig, P., 2000, "Top-down processing mediated by interareal synchronization," *Proc. Natl. Acad. Sci. USA* 97, Vol. 26, pp. 14748-14753.

- Wackermann, J., Lehmann, D., Dvorak, I., and Michel, C. M., 1993, "Global Dimensional Complexity of Multi-Channel EEG Indicates Change of Human Brain Functional State after a Single Dose of a Nootropic Drug," *Electroencephalography and Clinical Neurophysiology*, Vol. 86, pp. 193-198.
- Wallace, R. K., 1970, "Physiological Effects of Transcendental Meditation," *Science*, Vol. 167, pp. 1751-1754.
- Walton K.G., D.K. Levitsky, 2003, "Effects of the Transcendental Meditation program on neuroendocrine abnormalities associated with aggression and crime." *J Offender Rehab*, Vol. 36, pp. 67–88.
- Walton, K.G., Pugh, N.D., Gelderloos, P., Macrae, P., 1995, Stress Reduction and Preventing Hypertension: Preliminary Support for a Psychoneuroendocrine Mechanism. *J Altern Complement Med*, Vol. 1, pp. 263-83
- Welch, P.D., 1967, "The Use of Fast Fourier Transform for the Estimation of Power Spectra: A Method Based on Time Averaging Over Short, Modified Periodograms." *IEEE Trans. Audio Electroacoust.* Vol. AU-15, pp. 70-73.
- West, M. A., 1980, "Meditation and the EEG," *Psychological Medicine*, Vol. 10, pp. 369-375.
- Widman, G., Schreiber, T., Rehberg, B., Hoefft, A. and Elger, C. E., 2000, "Quantification of depth of anesthesia by nonlinear time series analysis of brain electrical activity," *Phys. Rev. E*, Vol. 62, pp. 4898–4903.
- Williams, P. and West, M., 1975, "EEG Responses to Photic Stimulation in Persons Experienced at Meditation," *Electroencephalography and Clinical Neurophysiology*, Vol. 39, pp. 519-522.
- Wolf, A., Swift, J. B., Swinney, H. L., Vastano, J. A., 1985, *Physica D*, Vol. 16, pp. 285.
- Woolfolk, R. L., 1975, "Psychophysiological Correlates of Meditation," *Arch Gen Psychiatry*, Vol. 32, pp. 1326-1333.
- Yaylali, I., Koçak, H., and Jayakar, P., 1996, "Detection of Seizures from Small Samples Using Nonlinear Dynamic System Theory," *IEEE Transactions on Biomedical Engineering*, Vol. 43, No. 7, pp. 743-751.
- Young J.D. and Taylor E., 1998, "Meditation as a voluntary hypometabolic state of biological estivation," *News Physiol. Sci.* Vol. 13, pp. 149–153.
- Young, H., Baum, R. and Cremerius, U., 1999, "Measurement of clinical and subclinical tumour response using [18F]-fluorodeoxyglucose and positron emission tomography: review and 1999 EORTC recommendations." *European Journal of Cancer*, Vol. 35, pp. 1773–1782.
- Yu, T., Tsai, H.-L., and Hwang, M.-L., 2003, "Suppressing Tumor Progression of In Vitro Prostate Cancer Cells by Emitted Psychosomatic Power through Zen Meditation," *American Journal of Chinese Medicine*, Vol. 31, pp. 499-507

## Vita and Publication List

**Hsuan-Yung Huang** was born in Taiwan, on January 5, 1975. She received her M.S. degree in electronic engineering from National Tsing-Hua University, Taiwan in 1999 and Ph D. degree in Electrical and Control Engineering from National Chiao-Tung University, Taiwan in 2008. Her research interests include biomedical signal processing and electrophysiological phenomenon.

### Journal:

1. H.-Y. Huang and P.-C. Lo, "EEG Nonlinear Interdependence Measure of Brain Interactions under Zen Meditation" *Journal of Biomedical Engineering Research* (Accepted).
2. H.-Y. Huang and P.-C. Lo, "EEG Dynamics of Experienced Zen-Meditation Practitioners Probed by Complexity Index and Spectral Measure", *Journal of Medical Engineering & Technology* (Accepted)
3. P.-C. Lo and H.-Y. Huang, "Investigation of Meditation Scenario by Quantifying the Complexity Index of EEG," *Journal of the Chinese Institute of Engineers*, Vol. 30, no. 3, pp. 389-400, 2007.
4. H.-Y. Huang, Y.-Y. Lee and P.-C. Lo, "A Novel Algorithm for Computing the 2D Split-Vector-Radix FFT," *Signal Processing*, Vol. 84, pp. 561-570, 2004.

### Conference:

1. H.-Y. Huang and P.-C. Lo, "Investigation of the meditation EEG by analyzing the complexity index," *Proc. Annual symposium Biomedical Engineering Society ROC.*, Dec. 17-18, 1999.
2. H.-Y. Huang and P.-C. Lo, "Description of the dynamic state in meditation EEG by analyzing the complexity index," *Conf. Health and Management*, Yuanpei University of Science and Technology, Oct. 2002.